Electron paramagnetic resonance studies of low-spin d^5 transition metal complexes

Philip H. Rieger
Department of Chemistry, Brown University, Providence, RI 02912 (USA)

(Received 11 January 1993)

CONTENTS

Abstract 204
1. Introduction 205
2. Theoretical background 206
   2.1 Electronic structure 206
      2.1.1 Octahedral complexes 206
      2.1.2 Monosubstituted and trans-disubstituted complexes 206
      2.1.3 Complexes with three-fold or pseudo-three-fold symmetry 207
      2.1.4 Metallocenes and bis-arene complexes 208
      2.1.5 Complexes of lower symmetry 209
   2.2 Jahn–Teller distortions 209
3. Interpretation of EPR parameters 212
   3.1 Perturbation theory approach 212
      3.1.1 The *g* matrix 212
      3.1.2 The nuclear hyperfine matrix 213
      3.1.3 Non-coincident *g* and hyperfine matrix principal axes 216
   3.2 "Exact" calculation of *g* matrix components 218
      3.2.1 Distorted octahedral complexes 218
      3.2.2 A more general approach 219
   3.3 The dipole–dipole coupling parameter, *P* 223
4. Survey of experimental results 224
   4.1 Titanium(−I) and zirconium(−I) 225
      4.1.1 Tris-bipyridyl complexes 225
      4.1.2 Bis-arene complexes 225
   4.2 Vanadium(0), niobium(0) and tantalum(0) 225
      4.2.1 Carbonyl complexes 225
      4.2.2 Tris-bipyridyl complexes 229
      4.2.3 Nitrosyl complexes 229
      4.2.4 Bis-arene complexes 231
   4.3 Chromium(I), molybdenum(I) and tungsten(I) 231
      4.3.1 Carbonyl complexes 231
      4.3.2 Tris-bipyridyl complexes 233
      4.3.3 Nitrosyl complexes 234
      4.3.4 Bis-arene complexes 237
      4.3.5 "Piano-stool" complexes 241

Correspondence to: P.H. Rieger, Department of Chemistry, Brown University, Providence, RI 02912, USA.

0010-8545/94/$26.00
SSDI 0010-8545(93)00986-3

4.4 Manganese(II), technetium(II) and rhenium(II) 245
4.4.1 Manganese(II) complexes 245
4.4.2 Nitrosyl complexes 247
4.4.3 "Sandwich" complexes 248
4.4.4 "Piano-stool" complexes 249
4.5 Iron(III), ruthenium(III) and osmium(III) 251
4.5.1 High-spin and low-spin configurations 251
4.5.2 Halide complexes 252
4.5.3 Cyanide complexes 253
4.5.4 Tris-bipyridyl and related N_6 complexes 255
4.5.5 Ammine complexes 257
4.5.6 Porphyrin and other N_4X_2 complexes 258
4.5.7 O_6 and S_6 complexes 262
4.5.8 Bidentate and tridentate (N, O, S) complexes 264
4.5.9 Dithiolene complexes 267
4.5.10 Sandwich complexes 267
4.5.11 "Piano-stool" complexes 269
4.6 Cobalt(IV), rhodium(IV) and iridium(IV) 271
4.6.1 Halide complexes 271
4.6.2 Aquo and hydroxo complexes 271
4.6.3 Dithiolene complexes 272
4.6.4 Organometallic complexes 272
References 274

ABSTRACT

A discussion of the connection between EPR parameters and the electronic structures of mononuclear low-spin d^5 complexes, including systems with orbitally degenerate ground states which undergo Jahn–Teller distortions. EPR experimental results are critically surveyed for complexes of Ti(−I), V(0), Cr(I), Mn(II), Fe(III), Co(IV), and their heavier congeners. A review with 426 references.

ABBREVIATIONS

acac	acetylacetonate
bpy	2,2′-bipyridyl
Bz	η^6-C_6H_6
Ch	η^7-C_7H_7
Cp	η^5-C_5H_5
Cp*	η^5-C_5Me_5
DMA	*N*,*N*-dimethylacetamide
DME	dimethoxyethane
DMF	*N*,*N*-dimethylformamide
dmg	dimethylglyoxime
dmpe	$Me_2PCH_2CH_2PMe_2$
DMSO	dimethylsulfoxide

dppe	$Ph_2PCH_2CH_2PPh_2$
dppm	$Ph_2PCH_2PPh_2$
dtc	dithiocarbamate
en	1,2-diaminoethane
ENDOR	electron-nuclear double resonance
EPR	electron paramagnetic resonance
HMPA	hexamethylphosphoramide
Im	imidazole
LCAO	linear combination of atomic orbitals
mnt	maleonitriledithiolate
MO	molecular orbital
NMR	nuclear magnetic resonance
phen	1,10-phenanthroline
sacsac	dithioacetylacetonate
SOMO	singly occupied molecular orbital
THF	tetrahydrofuran
Tp	tris(pyrazolyl)borate
Tp*	tris(3,5-dimethylpyrazolyl)borate

1. INTRODUCTION

It has been over 20 years since the comprehensive review of EPR studies of transition metal complexes by Goodman and Raynor [1] was published. More limited discussions of the applications of EPR spectroscopy to transition metal chemistry have appeared since then [2–6], and the field has been reviewed nearly every year by the Specialist Periodicals Report *Electron Spin Resonance* [7]. Other reviews, focussed on the chemistry or electrochemistry of odd-electron organometallics and coordination complexes [8,9], deal with some aspects of EPR spectroscopy. Nonetheless, it is long past time for a more comprehensive update of the Goodman–Raynor review. The field has grown so much, however, that a monograph would now be necessary. Accordingly, the present review will be limited to EPR studies of low-spin d^5 complexes, a topic which occupied nine pages in the 1970 review.

This review includes both classical coordination complexes and organometallic molecules and is not limited to work which has appeared since 1970; the major areas are traced back to the seminal work regardless of date. However, the scope is limited by several exclusions: (i) for the most part, attention is confined to mononuclear complexes; (ii) with only a few exceptions, we will not discuss EPR studies of d^5 ions substituted in ionic crystal lattices; and (iii) we will not discuss EPR studies of Fe(III) in biological systems (this topic was reviewed most recently by Smith and Pilbrow [10]), although Fe(III) porphyrin complexes designed as heme or cytochrome models are covered.

There is a great temptation in a review of this type to discuss results from related techniques, most notably Mössbauer spectroscopy, or to digress into the often fascinating chemistry and electrochemistry of 17- and 19-electron systems. Although the focus will be kept squarely on EPR theory and experimental results, a major contribution of EPR spectroscopy is to our understanding of molecular electronic structure. In particular, the components of the g matrix can provide information on the ligand-field splittings of the d orbitals and nuclear hyperfine coupling matrices can be deconvoluted to provide a map of the singly occupied molecular orbital (SOMO). Thus, we begin with a discussion of the electronic structures of d^5 systems and the interpretation of EPR parameters.

2. THEORETICAL BACKGROUND

In this section, we will review the electronic structures of representative d^5 metal complexes, focusing on the effects of π-bonding (π-acceptor vs. π-donor ligands) and nuclear charge. High-symmetry low-spin d^5 complexes often have orbitally degenerate ground states and are thus subject to Jahn–Teller distortions. Accordingly, the section concludes with a brief discussion of the Jahn–Teller theorem and the Epikernel Principle.

2.1 Electronic structure

2.1.1 Octahedral complexes

For an MA_6 complex with O_h symmetry, the d-orbitals split into a t_{2g} set (d_{xy}, d_{xz}, and d_{yz}) and an e_g set ($d_{x^2-y^2}$ and d_{z^2}), separated by energy Δ_{oct}, as shown in Fig. 1. When Δ_{oct} is large compared with the pairing energy, e.g. in $V(CO)_6$, $Fe(CN)_6^{3-}$, $Ru(NH_3)_6^{3+}$, and $IrCl_6^{2-}$, the five electrons occupy the t_{2g} set, giving a nominal $^2T_{2g}$ ground state, the low-spin configuration. According to the Jahn–Teller theorem, such a complex will distort so as to remove the orbital degeneracy. Jahn–Teller distortions are often small, so that thermally accessible excited states provide an efficient spin-lattice relaxation mechanism. Accordingly, EPR spectra of octahedral complexes are usually observable only at liquid helium temperature.

2.1.2 Monosubstituted and trans-disubstituted complexes

Monosubstitution or trans-disubstitution is equivalent to a tetragonal distortion from octahedral symmetry. In MA_5B (C_{4v} symmetry) or *trans*-MA_4B_2 (D_{4h} symmetry), the t_{2g} orbitals split to b_2 or $b_{2g}(d_{xy})$ and e or $e_g(d_{xz}, d_{yz})$, as shown in Fig. 1. If B is a stronger π-acceptor (or a weaker π-donor) than A, the e orbitals generally are more bonding (or less anti-bonding) than b_2, and, in either case, lower in energy; b_2 is then singly occupied (the SOMO) and the ground state is $^2B_2$. Examples are the nitrosyl complexes, e.g. $[Cr(NO)(CN)_5]^{2-}$. Conversely, if B is a weaker π-acceptor or a stronger π-donor than A, a ^2E ground state (and a Jahn–Teller

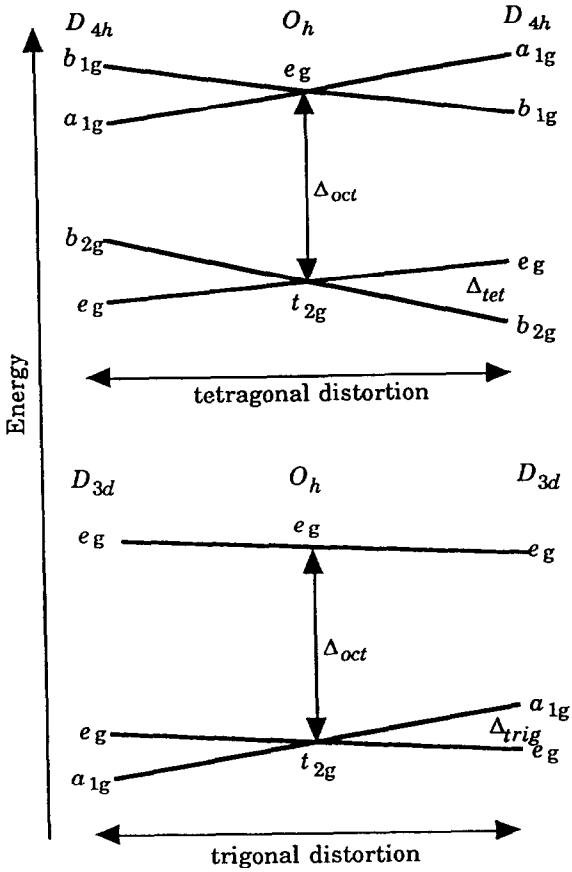

Fig. 1. Schematic representation of the effect of tetragonal and trigonal distortions on the orbital energies of an octahedral complex.

distortion) is expected; examples include *trans*-$V(CO)_4(PMe_3)_2$ and most axial adducts of Fe(III) porphyrin complexes.

2.1.3 *Complexes with three-fold or pseudo-three-fold symmetry*

In complexes with a three-fold axis, tris-chelates or *fac*-MA_3B_3, the coordinate system is redefined with z taken as the C_3 axis. The t_{2g} set splits into $a_1(|d_{z^2}\rangle)$ and

$$e\left(\sqrt{\frac{2}{3}}|d_{x^2-y^2}\rangle - \frac{1}{\sqrt{3}}|d_{xz}\rangle, \sqrt{\frac{2}{3}}|d_{xy}\rangle + \frac{1}{\sqrt{3}}|d_{yz}\rangle\right),$$

as shown in Fig. 1. The a_1 orbital is largely non-bonding, whereas the e

orbitals interact with the ligands via π-bonding. Thus, for π-acceptor ligands, the e-pair is stabilized and a $^2A_1$ ground state is expected. For π-donor ligands, the ground state is ^2E, and a Jahn–Teller distortion is expected.

Most of the metals between titanium and osmium are known to form tris(2,2'-bipyridyl) complexes with formal d^5 configurations [11]. EPR spectra of low-spin $[Ti(bpy)_3]^-$, $V(bpy)_3$, $[Cr(bpy)_3]^+$, and $[Mo(bpy)_3]^+$ are easily detected in solution at room temperature [12]. $[Fe(bpy)_3]^{3+}$, $[Ru(bpy)_3]^{3+}$, and $[Os(bpy)_3]^{3+}$ are also low-spin, but EPR spectra can only be observed at low temperatures [13]. $[Mn(bpy)_3]^{2+}$ is high-spin [14].

Hanazaki and Nagakura [15] have discussed the electronic structure of the tris-bipyridyl complexes in some detail. For the early transition metals, the bpy π^* orbitals are close in energy to the t_{2g} orbitals and π-back-bonding leads to a relatively large energy gap between the e and a_1 orbitals. As the nuclear charge increases, the metal orbitals fall in energy and the degree of π-back-bonding decreases until, for iron, the gap is small. Spin-lattice relaxation is then efficient so that room-temperature spectra are no longer detectable.

In the limit of fast ring rotation, "piano-stool" complexes such as $CpCr(CO)_3$ resemble *fac*-MA_3B_3 with pseudo-C_{3v} symmetry, and the t_{2g} set splits to a_1 and e. When the Cp ring is taken into account, the symmetry drops to C_s($a_1 \rightarrow a'$ and $e \rightarrow a' + a''$). Strictly speaking, piano-stool complexes are not Jahn–Teller active, but the $^2A'$ and $^2A''$ states are often sufficiently close that spectra can only be observed at low temperatures. MO calculations, constrained to C_s symmetry, on $CpCr(CO)_3$ and $CpCr(CO)_2PH_3$ by Fortier et al. [16], found two closely spaced potential minima, corresponding to $^2A'$ and $^2A''$ ground states, as shown in Fig. 2. In agreement with experiment (see Sect. 4.3.5), the $^2A'$ state is lowest for $CpCr(CO)_3$ but phosphine substitution reverses the order.

2.1.4 Metallocenes and bis-arene complexes

The paramagnetic metallocenes and bis-arenes have received a great deal of attention from EPR spectroscopists. The field has been reviewed by Warren [17], who discussed the application of ligand-field theory and molecular orbital theory to the interpretation of EPR, electronic, photoelectron, and charge-transfer spectra and magnetic susceptibilities, and by Ammeter [18], who dealt with EPR studies of orbitally degenerate compounds such as $[Fe(Cp)_2]^+$.

Ligand-field theory or molecular orbital theory treatments of metallocenes and bis-arenes [17,19,20] show that the frontier orbitals are primarily metal in character and fall in the order d_{xy}, $d_{x^2-y^2}$(e_{2g} or δ) $\sim d_{z^2}$(a_{1g} or σ) $\ll d_{xz}$, d_{yz}(e_{1g} or π) where the symmetry designations refer to D_{5d} (or D_{6h}) or to pseudo-cylindrical symmetry; the detailed order of the e_{2g} and a_{1g} levels depends on the metal and ligand as well as the oxidation state. The a_{1g} orbital is essentially non-bonding, e_{2g} weakly bonding, and e_{1g} strongly antibonding. For $[Fe(Cp)_2]^+$, $a_{1g} < e_{2g}$ so that the ground state is $^2E_{2g}$. For $Mn(Cp)_2$, $a_{1g} < e_{2g}$, but the σ–δ splitting is comparable with the pairing

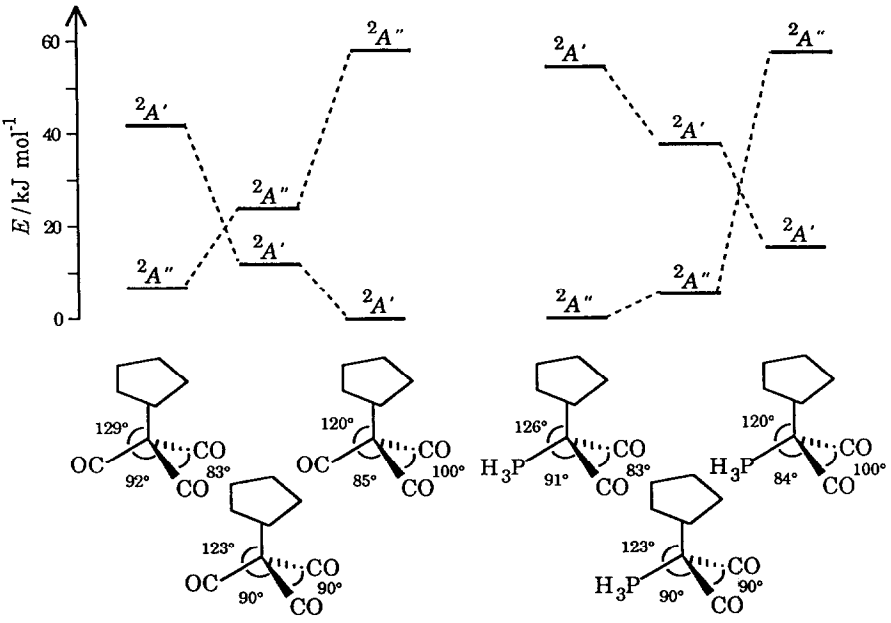

Fig. 2. Relative energies of the $^2A'$ and $^2A''$ states of $CpCr(CO)_3$ and $CpCr(CO)_2PH_3$ for the idealized conformation with 90° OC–Cr–CO bond angles and for two minimum-energy conformations retaining C_s symmetry. From Fortier et al. [16].

energy; thus both $^2E_{2g}$ or $^6A_{1g}$ states are observed depending on the molecular environment. For $V(Bz)_2$ and $[Cr(Bz)_2]^+$, on the other hand, $e_{2g} < a_{1g}$ and the ground state is $^2A_{1g}$. An important factor in the $a_{1g}-e_{2g}$ order is the degree of π-back-bonding which depends on the relative energies of the metal d and ligand π^* orbitals. The early transition metals have d energies well matched to arene π^* energies. With increasing nuclear charge, the metal orbitals fall in energy, and for decreasing ring size, the lowest π^* rises, resulting in substantially reduced π-back-bonding for $Mn(Cp)_2$ and $[Fe(Cp)_2]^+$.

2.1.5 Complexes of lower symmetry

In C_{2v}, e.g. *cis*-MA_4B_2 or *mer*-MA_3B_3, or lower symmetries, the degeneracy of the t_{2g} orbitals is completely lifted. The identity of the SOMO depends on the nature of the ligands, but a non-degenerate ground state is expected in any case.

2.2 Jahn–Teller distortions

We have identified several structural types for which orbitally degenerate ground states are expected. According to the first-order Jahn–Teller theorem, such

a complex will distort along one or more of the vibrational normal mode coordinates Q_i to lower the energy by ΔE [21].

$$\Delta E = \sum_i \langle \psi_0 | H_{1i} | \psi_0 \rangle Q_i \tag{1}$$

In eqn. (1), H_{1i} is the linear term in a Taylor series expansion of the Hamiltonian in Q_i and ψ_0 is the (degenerate) ground state wave function. Since $H_{1i}Q_i$ must belong to the totally symmetric representation of the group, H_{1i} and Q_i belong to the same representation. If the ith term of eqn. (1) is non-zero, Q_i must be contained in the direct product $\Gamma(\psi_0) \times \Gamma(\psi_0)$. Thus, in general, only a few of the normal mode coordinates are Jahn–Teller active.

In the case of *trans*-MA_4B_2 with a ^2E_g ground state, the only Jahn–Teller active coordinates are the b_{1g} stretch and the b_{2g} bend (see Fig. 3(a)). If only the b_{1g} distortion were to take place, the symmetry would be reduced from D_{4h} to D_{2h} with the C_2 axes along the metal–ligand bonds; if only the b_{2g} distortion were important, the symmetry would again drop to D_{2h}, but with the C_2 axes along the M–B bonds and midway between the M–A bonds. If the two distortions were energetically equivalent, a "Mexican hat" potential surface would result (Fig. 4(a)) and, in general, the symmetry would be C_{2h}. In practice, however, since force constants for bends are significantly smaller than for stretches, warping of the potential surface is expected, as shown in Fig. 4(b), to give two minima corresponding to positive and negative

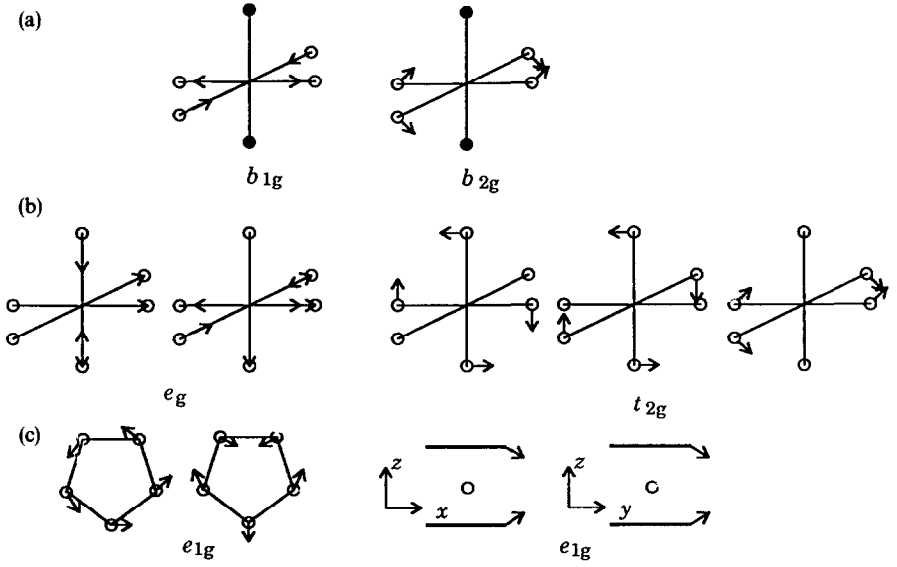

Fig. 3. Jahn–Teller active vibrational modes for (a) *trans*-MA_4B_2 complex (^2E_g state in D_{4h} symmetry), (b) ML_6 complex ($^2T_{2g}$ state in O_h symmetry) and (c) Cp_2M complex ($^2E_{2g}$ state in D_{5d} symmetry).

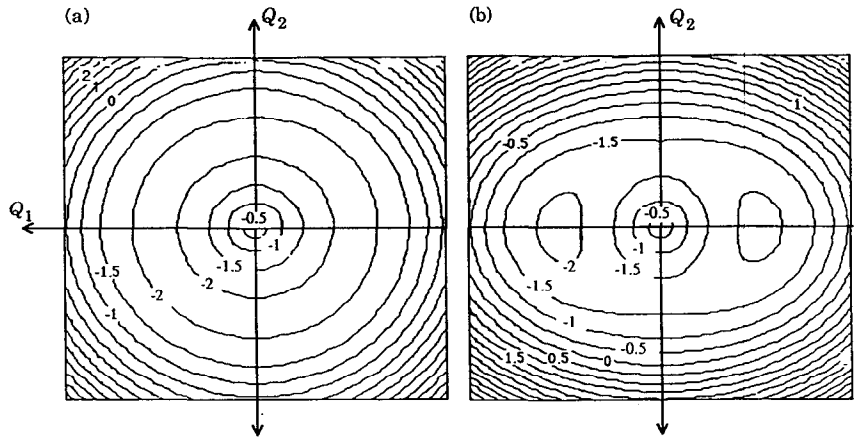

Fig. 4. Schematic energy contours for Jahn–Teller distortion of *trans*-MA_2B_4 along vibrational coordinates Q_1 and Q_2 for force constants (a) $k_1 = k_2$, and (b) $k_1 < k_2$.

bending coordinates. At sufficiently low temperatures, a molecule should be trapped in one of these minima.

The above analysis is equivalent to an application of the Epikernel Principle [22]. An epikernel is an intermediate subgroup in the decomposition scheme of a point group. In the $E_g \times (b_{1g} + b_{2g})$ problem just discussed, for example, distortion of a D_{4h} molecule passes through either of two D_{2h} epikernels to the general distortion limit (the kernel) of C_{2h}. Thus, in the potential surfaces shown in Fig. 4, the symmetry at the origin is D_{4h}, distortion along the $Q_1(b_{1g})$ coordinate lowers the symmetry to $D_{2h}(C_4^2, 2C_2)$ (i.e. the equatorial C_2 axes are along the M–B bonds), and distortion along $Q_2(b_{2g})$ lowers the symmetry to D_{2h} $(C_4^2, 2C_2')$ (i.e. the equatorial C_2 axes bisect the B–M–B bond angles). A general point on the potential surface corresponds to C_{2h} symmetry. The Epikernel Principle states that the distortion of Jahn–Teller molecules tends to stop at an epikernel symmetry rather than continuing to the kernel symmetry. When several epikernels are available, higher ranking epikernels are preferred over lower ranking ones.

The above arguments apply to isolated complexes. For an isolated complex, distortion along $+Q_2$ and $-Q_2$ are equivalent and we expect equal numbers of complexes with d_{xz} and d_{yz} SOMOs. Complexes in dilute single crystals are subject to crystal packing effects which will generally favor one direction over the other so that only d_{xz} or d_{yz} unpaired electrons are observed. Similarly, when the complex is in a glass or frozen solution, random solvation effects will generally favor one distortion direction over the other, although here the experimental distinction between d_{xz} and d_{yz} SOMOs is lost.

For an octahedral complex MA_6 with a $^2T_{2g}$ ground state, only the e_g stretching and t_{2g} bending modes are Jahn–Teller active (see Fig. 3(b)). Symmetry analysis of the $O_h \times (e_g + t_{2g})$ problem shows that the kernel symmetry is C_i, but there are

intermediate epikernel symmetries of $D_{2h}(C_4^2, 2C_2)$, $C_{2h}(C_2)$ and $C_{2h}(C_4^2)$. The Epikernel Principle then says that the most likely symmetry is D_{2h}, analogous to the expected symmetry for *trans*-MA_4B_2. Multiple equivalent potential minima are expected so that the SOMO could be d_{xz}, d_{yz} or d_{xy}, but again crystal packing effects are likely to favor one of these over the others.

For a D_{5d} metallocene with $^2E_{2g}$ ground state, the Jahn–Teller-active modes are of e_{1g} symmetry: a ring C–C stretch mode and the ring tilt mode (Fig. 3(c)). Again, we would expect the bending mode to dominate so that minimum energy corresponds to C_{2v} symmetry. Jahn–Teller distortions of metallocenes have been explored extensively, both theoretically and experimentally [18,23].

3. INTERPRETATION OF EPR PARAMETERS

To a first approximation, orbital angular momentum is quenched in three-dimensional molecules. Indeed, when the SOMO can be described accurately by a single real p or d orbital, the expectation value of L_z is zero, and the magnetic moment results from electron spin only. In this idealized situation, the Kramers doublet states are separated by $\Delta E = g\mu_B B$ where $g = g_e = 2.0023$ and μ_B is the Bohr magneton. In practice, however, spin–orbit coupling reinstates an orbital contribution to the magnetic moment. For example, if $d_{xy} = (-i/\sqrt{2})(|2\rangle - |-2\rangle)$ and $d_{x^2-y^2} = (1/\sqrt{2})(|2\rangle + |-2\rangle)$ are mixed, the combination in general will have an excess of the $|2\rangle$ or $|-2\rangle$ function and thus a non-zero expectation value for L_z. The orbital and spin angular momenta add vectorially so that the magnetic moment may be either larger or smaller than the spin-only value. The effective g value then differs from g_e and, in general, will be different in different directions; g then becomes a 3×3 matrix (colloquially referred to as the g tensor) and the Zeeman Hamiltonian term is written $\mu_B \vec{B} \cdot \mathbf{g} \cdot \vec{S}$ where $\vec{S}$ is the effective electron spin.

When the d-orbital energy splittings are sufficiently large, spin–orbit coupling can be treated by second-order perturbation theory to find the g matrix components. For many low-spin d^5 molecules, however, spin–orbit coupling is comparable with or even larger than the splitting of the t_{2g} orbitals, and a more exact calculation is required. Although a third-order treatment is possible [24], most workers have used a method equivalent to exact diagonalization of the Hamiltonian matrix.

3.1 Perturbation theory approach

3.1.1 The g matrix

For a system in which the unpaired electron is largely confined to the central metal, the g matrix components are given by eqn. (2) [25]

$$g_{ij} = g_e \delta_{ij} + 2\lambda \sum_{m \neq 0} \frac{\langle m|L_i|0\rangle \langle 0|L_j|m\rangle}{E_0 - E_m} \tag{2}$$

where δ_{ij} is the Kronecker delta ($\delta_{ij}=1$ if $i=j$, $\delta_{ij}=0$ if $i\neq j$), λ is the spin–orbit coupling parameter, i and j refer to molecular coordinate axes (x, y, z), L_i and L_j are orbital angular momentum operators, E_0 is the energy of the SOMO, and m sums over the other MOs with energies E_m.

If, for example, the metal contribution to the SOMO is purely d_{xy} with LCAO coefficient c_{xy}, spin–orbit coupling mixes in d_{xz}, d_{yz}, and $d_{x^2-y^2}$ character such that the g matrix components are given by eqns. (3a–c) where, for example, c^m_{xz} is the

$$g_{xx}-g_e=2\lambda\sum_{m\neq 0}\frac{(c_{xy})^2(c^m_{xz})^2}{E_0-E_m}=\frac{2\lambda(c_{xy})^2}{\delta_{xz}} \tag{3a}$$

$$g_{yy}-g_e=2\lambda\sum_{m\neq 0}\frac{(c_{xy})^2(c^m_{yz})^2}{E_0-E_m}=\frac{2\lambda(c_{xy})^2}{\delta_{yz}} \tag{3b}$$

$$g_{zz}-g_e=8\lambda\sum_{m\neq 0}\frac{(c_{xy})^2(c^m_{x^2-y^2})^2}{E_0-E_m}=\frac{8\lambda(c_{xy})^2}{\delta_{x^2-y^2}} \tag{3c}$$

LCAO coefficient of d_{xz} in the mth MO and $1/\delta_{xz}$ is the weighted average reciprocal energy difference. For many low-spin d^5 systems with a d_{xy} SOMO, d_{xz} and d_{yz} lie just below the SOMO (δ_{xz}, δ_{yz} small and positive); $d_{x^2-y^2}$ is empty and much higher in energy ($\delta_{x^2-y^2}$ large and negative). Thus we expect g_{xx} and g_{yy} to be significantly greater than g_e and g_{zz} to be slightly less than g_e. Table 1 summarizes the results when one of the other d orbitals is singly occupied.

Even in cases where the SOMO is nearly a pure d_{xy} orbital, π- and σ-delocalization may spread d_{xz}, d_{yz} and $d_{x^2-y^2}$ character over several MOs, both filled and unfilled, so that $1/\delta_{xz}$, $1/\delta_{yz}$, and $1/\delta_{x^2-y^2}$ are the sum of two or more terms of opposite sign. The pentacyanonitrosyl complexes $[M(CN)_5(NO)]^{n-}$, provide a good example of this effect. As shown in Table 9 (see below), $g_\parallel$ increases from 1.974 to 2.014 and $g_\perp$ increases from 2.007 to 2.072 as M is changed from V to Fe. Symons and co-workers [26] suggest that this progression arises from the strong nuclear charge dependence of the energy of the (largely) metal-based SOMO and the relatively weaker dependence of the more delocalized MOs (see Fig. 5). Thus for V, $\delta_{x^2-y^2}$ is negative because the SOMO is closer to $3b_1$ (the anti-bonding MO with $d_{x^2-y^2}$ character) whereas for Fe, it is closer to $1b_1$. Similarly, as the nuclear charge increases, the SOMO drops closer to the filled π-bonding orbitals (5e and 6e) and further from the anti-bonding counterpart (7e), thus increasing $\delta_{xz,\,yz}$.

3.1.2 *The nuclear hyperfine matrix*

The isotropic part of the hyperfine coupling can be expressed by eqn. (4). A_s, the Fermi contact contribution, includes both a direct contribution from the metal $(n+1)$s component of the SOMO (if any) and an indirect contribution from polarization of inner-shell s orbitals by metal nd spin density (eqn. (5)). In general, there is also a spin–orbit coupling contribution to the isotropic hyperfine coupling, propor-

TABLE 1

g and A matrices for single d-electron SOMOs to second order in perturbation theory

SOMO	Δg_x	Δg_y	Δg_z	$(A_x - A_s)/P$	$(A_y - A_s)/P$	$(A_z - A_s)/P$
d_{z^2}	$\frac{6\lambda}{\delta_{xy}}$	$\frac{6\lambda}{\delta_{xz}}$	0	$-\frac{2}{7}(c_{z^2})^2 + \Delta g_x + \frac{1}{14}\Delta g_y$	$-\frac{2}{7}(c_{z^2})^2 + \Delta g_y + \frac{1}{14}\Delta g_x$	$\frac{4}{7}(c_{z^2})^2 - \frac{1}{14}(\Delta g_x + \Delta g_y)$
d_{xz}	$\frac{2\lambda}{\delta_{xy}}$	$\frac{2\lambda}{\delta_{x^2-y^2}} + \frac{6\lambda}{\delta_{z^2}}$	$\frac{2\lambda}{\delta_{yz}}$	$\frac{2}{7}(c_{xz})^2 + \Delta g_x - \frac{3}{14}\Delta g_z + \frac{3}{7}\left(\frac{\lambda}{\delta_{x^2-y^2}} - \frac{\lambda}{\delta_{z^2}}\right)$	$-\frac{4}{7}(c_{xz})^2 + \Delta g_y + \frac{3}{14}(\Delta g_x + \Delta g_z)$	$\frac{2}{7}(c_{xz})^2 + \Delta g_z - \frac{3}{14}\Delta g_x - \frac{3}{7}\left(\frac{\lambda}{\delta_{x^2-y^2}} - \frac{\lambda}{\delta_{z^2}}\right)$
d_{yz}	$\frac{2\lambda}{\delta_{x^2-y^2}} + \frac{6\lambda}{\delta_{z^2}}$	$\frac{2\lambda}{\delta_{xy}}$	$\frac{2\lambda}{\delta_{xz}}$	$-\frac{4}{7}(c_{yz})^2 + \Delta g_x + \frac{3}{14}(\Delta g_y + \Delta g_z)$	$\frac{2}{7}(c_{yz})^2 + \Delta g_y - \frac{3}{14}\Delta g_z + \frac{3}{7}\left(\frac{\lambda}{\delta_{x^2-y^2}} - \frac{\lambda}{\delta_{z^2}}\right)$	$\frac{2}{7}(c_{yz})^2 + \Delta g_z - \frac{3}{14}\Delta g_y - \frac{3}{7}\left(\frac{\lambda}{\delta_{x^2-y^2}} - \frac{\lambda}{\delta_{z^2}}\right)$
d_{xy}	$\frac{2\lambda}{\delta_{yz}}$	$\frac{2\lambda}{\delta_{xz}}$	$\frac{8\lambda}{\delta_{x^2-y^2}}$	$\frac{2}{7}(c_{xy})^2 + \Delta g_x - \frac{3}{14}\Delta g_y$	$\frac{2}{7}(c_{xy})^2 + \Delta g_y - \frac{3}{14}\Delta g_x$	$-\frac{4}{7}(c_{xy})^2 + \Delta g_z + \frac{3}{14}(\Delta g_x + \Delta g_y)$
$d_{x^2-y^2}$	$\frac{2\lambda}{\delta_{xz}}$	$\frac{2\lambda}{\delta_{yz}}$	$\frac{8\lambda}{\delta_{xy}}$	$\frac{2}{7}(c_{x^2-y^2})^2 + \Delta g_x - \frac{3}{14}\Delta g_y$	$\frac{2}{7}(c_{x^2-y^2})^2 + \Delta g_y - \frac{3}{14}\Delta g_x$	$-\frac{4}{7}(c_{x^2-y^2})^2 + \Delta g_z + \frac{3}{14}(\Delta g_x + \Delta g_y)$

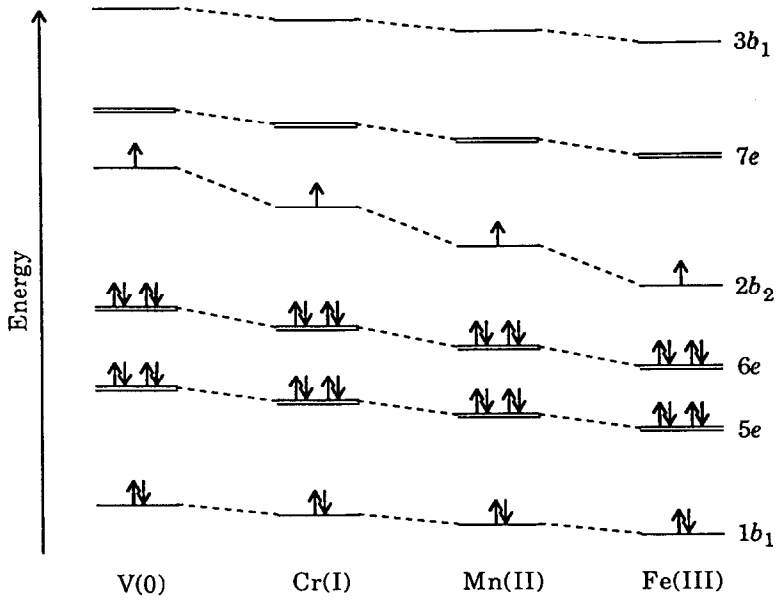

Fig. 5. Schematic representation of the effect of nuclear charge on the energies of the frontier MOs in a pentacyanonitrosyl complex (after Bloom et al. [26]) based on MO calculations by Manoharan and Gray [203].

tional to $\langle g\rangle - g_e$. The proportionality constant, P, is given by eqn. (6), where g_N is the nuclear g-value, μ_N is the nuclear magneton and $\langle r^{-3}\rangle$ is an average over the atomic orbital wavefunction. P and Q_s have the same sign as the nuclear magnetic moment, but the spin–polarization contribution, Q_d, is usually (but not necessarily) of opposite sign.

$$\langle A\rangle = A_s + P\langle \Delta g\rangle \tag{4}$$

$$A_s = Q_s\rho_s + Q_d\rho_d \tag{5}$$

$$P = g_e g_N \mu_B \mu_N \langle r^{-3}\rangle \tag{6}$$

The anisotropic part of A has contributions from spin–orbit coupling and from the electron–nuclear dipolar interaction, the latter given by eqn. (7), where the l_{ij} are given by eqns. (8a–f) [27].

$$(A_d)_{ij} = \frac{2}{7} P l_{ij} \tag{7}$$

$$l_{xx} = -(c_{z^2})^2 - 2(c_{yz})^2 + (c_{xz})^2 + (c_{x^2-y^2})^2 + (c_{xy})^2 - 2\sqrt{3}(c_{z^2})(c_{x^2-y^2}) \tag{8a}$$

$$l_{yy} = -(c_{z^2})^2 + (c_{yz})^2 - 2(c_{xz})^2 + (c_{x^2-y^2})^2 + (c_{xy})^2 + 2\sqrt{3}(c_{z^2})(c_{x^2-y^2}) \tag{8b}$$

$$l_{zz} = 2(c_{z^2})^2 + (c_{yz})^2 + (c_{xz})^2 - 2(c_{x^2-y^2})^2 - 2(c_{xy})^2 \tag{8c}$$

$$l_{xy} = -2\sqrt{3}(c_{z^2})(c_{xy}) + 3(c_{yz})(c_{xz}) \tag{8d}$$

$$l_{yz} = \sqrt{3}(c_{z^2})(c_{yz}) + 3(c_{xz})(c_{xy}) - 3(c_{yz})(c_{x^2-y^2}) \tag{8e}$$

$$l_{xz} = \sqrt{3}(c_{z^2})(c_{xz}) + 3(c_{yz})(c_{xy}) + 3(c_{xz})(c_{x^2-y^2}) \tag{8f}$$

The spin–orbit contributions to hyperfine coupling can be computed by methods described by Atherton [28] and McGarvey [29]. The contribution to A_i is usually on the order of $P\Delta g_i$; detailed results for unhybridized d orbitals are given in Table 1.

If the metal contribution to the SOMO is d_{xy}, the components of the dipolar matrix are given by eqns. (9a–c). Thus the hyperfine coupling is expected to be largest in magnitude when the molecule is oriented with the magnetic field along z.

$$(A)_{xx} = A_s + P\left[\frac{2}{7}(c_{xy})^2 + \Delta g_x - \frac{3}{14}\Delta g_y\right] \tag{9a}$$

$$(A)_{yy} = A_s + P\left[\frac{2}{7}(c_{xy})^2 + \Delta g_y - \frac{3}{14}\Delta g_x\right] \tag{9b}$$

$$(A)_{zz} = A_s + P\left[-\frac{4}{7}(c_{xy})^2 + \Delta g_z + \frac{3}{14}(\Delta g_x + \Delta g_y)\right] \tag{9c}$$

3.1.3 Non-coincident g and hyperfine matrix principal axes

When the metal contribution to the SOMO is a single d orbital, the principal axes of the g and hyperfine matrices are necessarily coincident. However, in low-symmetry molecules, it is often found that the metal contribution is a hybrid of two or more of the t_{2g} orbitals [6]. Consider, for example, the elements of the g and hyperfine matrices when the SOMO is a d_{xy}/d_{yz} hybrid (eqn. (10)). Neglecting spin–orbit coupling to d_{z^2} and $d_{x^2-y^2}$, the components of g are given by eqns. (11a–d).

$$|\mathrm{SOMO}\rangle = c_{xy}|d_{xy}\rangle + c_{yz}|d_{yz}\rangle \tag{10}$$

$$\Delta g_{xx} = (c_{xy})^2\delta_{xz} \tag{11a}$$

$$\Delta g_{yy} = (c_{xy})^2\delta_{yz} + (c_{yz})^2\delta_{xy} \tag{11b}$$

$$\Delta g_{zz} = (c_{yz})^2\delta_{xz} \tag{11c}$$

$$g_{xz} = -c_{xy}c_{yz}\delta_{xz} \tag{11d}$$

The matrix is diagonalized by rotation about the y axis by the angle β_g (eqn. (12)) to give the principal values represented by eqns. (13a–c).

$$\tan 2\beta_g = \frac{2c_{xy}c_{yz}}{(c_{yz})^2-(c_{xy})^2} \tag{12}$$

$$\Delta g_X = [(c_{xy})^2+(c_{yz})^2]\delta_{xz} \tag{13a}$$

$$\Delta g_Y = (c_{xy})^2\delta_{yz}+(c_{yz})^2\delta_{xy} \tag{13b}$$

$$\Delta g_Z = 0 \tag{13c}$$

The dipolar interaction matrix (eqns. (14a–d)) is diagonalized by rotation about the y axis by the angle β_A (eqn. (15)) to give the principal values shown in eqns. (16a, b).

$$(A_d)_{xx} = \frac{2}{7}P[(c_{xy})^2-2(c_{yz})^2] \tag{14a}$$

$$(A_d)_{yy} = \frac{2}{7}P[(c_{xy})^2+(c_{yz})^2] \tag{14b}$$

$$(A_d)_{zz} = \frac{2}{7}P[-2(c_{xy})^2+(c_{yz})^2] \tag{14c}$$

$$(A_d)_{xz} = \frac{6}{7}P(c_{xy})(c_{yz}) \tag{14d}$$

$$\tan 2\beta_A = -\frac{2c_{xy}c_{yz}}{(c_{yz})^2-(c_{xy})^2} \tag{15}$$

$$(A_d)_{X'} = (A_d)_{Y'} = \frac{2}{7}P[(c_{xy})^2+(c_{yz})^2] \tag{16a}$$

$$(A_d)_{Z'} = -\frac{4}{7}P[(c_{xy})^2+(c_{yz})^2] \tag{16b}$$

Thus the angle β_g, which transforms from the molecular x, y, z axes to the g matrix X, Y, Z axes, is equal, but of opposite sign, to the angle β_A, which transforms to the A matrix X', Y', Z' axes. The g matrix axes then differ from the A matrix axes by $\beta_g+\beta_A \approx 2\beta_g$.

This somewhat surprising result can be rationalised by reference to the schematic diagram shown in Fig. 6. When the SOMO contribution is solely d_{xy} or d_{yz}, the largest component of Δg is along the x or z axes, respectively. Thus we have a counter-clockwise rotation of the principal axes in the xz plane for intermediate hybridizations. For A, the largest component is along the z and x axes when the SOMO contribution is solely d_{xy} or d_{yz}, respectively, requiring a clockwise rotation in the xz frame for intermediate hybridizations. The same result is obtained for the

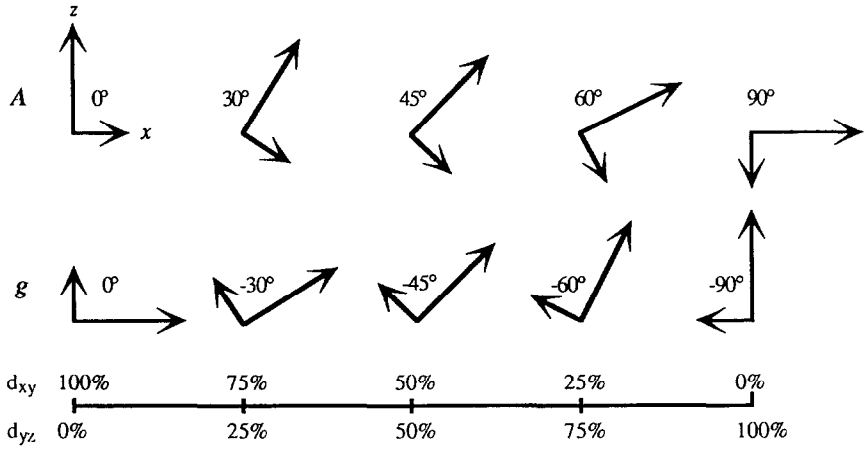

Fig. 6. Schematic representation of the orientation of the g and A principal axes in the xz plane as a function of d_{xy}/d_{yz} hybridization.

other binary hybrids except that for d_{xy}/d_{xz} combinations, the rotation is in the yz plane and for d_{xz}/d_{yz} combinations, the rotation is in the xy plane.

3.2 *"Exact" calculation of g matrix components*

3.2.1 *Distorted octahedral complexes*

When the symmetry is known, an exact calculation of the g matrix is relatively straightforward [30–32]. The problem is simplified by treating an electron hole in the t_{2g} shell. The *hole formalism* avoids dealing with a properly antisymmetrized five-electron function (with 5! terms), but it implies sign changes for λ, the spin–orbit coupling parameter, and for the energy splitting terms.

For a tetragonally distorted octahedral complex with d_{xy} singly occupied and a $d_{xy}-d_{xz}$, d_{yz} energy difference of Δ_{tet}, the g matrix is axial with components given by eqns. (17a, b).

$$g_{\parallel} = -1 + \frac{3(1-\eta/2)}{\Lambda} - 4\varepsilon\left[1 + \frac{1-3\eta/2}{\Lambda}\right] \tag{17a}$$

$$g_{\perp} = 1 + \frac{1+3\eta/2}{\Lambda} + 2\sqrt{2}\varepsilon\left[1 - \frac{1+3\eta/2}{\Lambda}\right] \tag{17b}$$

In these equations, $\eta = \lambda/\Delta_{tet}$, $\varepsilon = \lambda/\Delta_{oct}$, $\Lambda = \sqrt{1-\eta+(9/4)\eta^2}$. For small η, $g_{\parallel} \approx 2-8\varepsilon$, $g_{\perp} \approx 2+2\eta$ (the result obtained by perturbation theory), but, as shown in Fig. 7, for increasing η (and negligible ε), $g_{\parallel}$ decreases through zero and approaches -2 for large η; $g_{\perp}$ increases with increasing η and then decreases, approaching $+2$ for large η.

For a trigonally distorted octahedral complex, the g matrix components

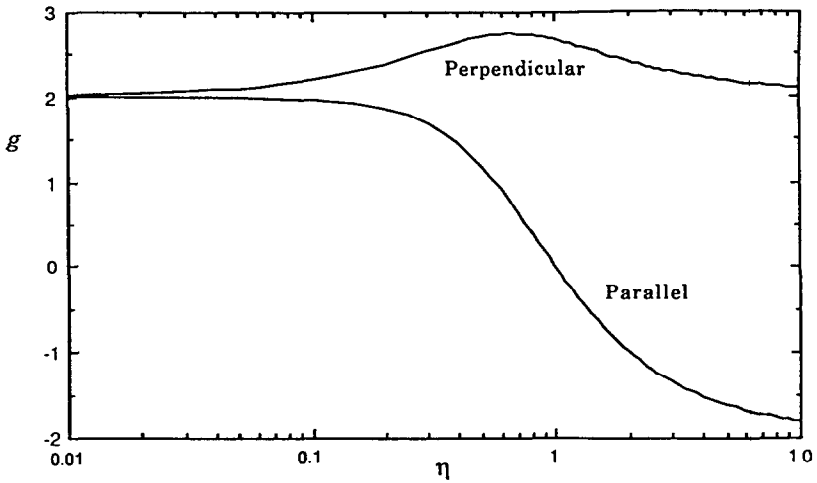

Fig. 7. Predicted g-tensor components for a tetragonally or trigonally distorted octahedral complex as a function of the ratio of the spin–orbit coupling parameter to the distortion splitting, $\eta = \lambda/\Delta$.

(eqns. (18a, b)) [31], are similar to those for a tetragonal distortion except that the limiting values for small η are $g_\parallel = 2$, $g_\perp = 2 + 2\eta - 4\varepsilon$.

$$g_\parallel = -1 + \frac{3(1-\eta/2)}{\Lambda} + 2\varepsilon\left[1 - \frac{1+3\eta/2}{\Lambda}\right] \tag{18a}$$

$$g_\perp = 1 + \frac{1+3\eta/2}{\Lambda} - 2\varepsilon\left[1 + \frac{1-3\eta/2}{\Lambda}\right] \tag{18b}$$

It is at first startling to see that $g_\parallel$ becomes negative for $\eta > 1$. The effect arises because spin–orbit coupling mixes $|-1, -\frac{1}{2}\rangle$ and $|1, \frac{1}{2}\rangle$, respectively, into the nominal $|+\frac{1}{2}\rangle$ and $|-\frac{1}{2}\rangle$ functions. For $\eta = 1$, the expectation value of S_z is $\pm 1/6$, that of L_z is $\mp 1/3$, and the sum $\langle L_z + g_e S_z \rangle$ is zero. For $\eta > 1$, the admixtures dominate and the effective g value becomes negative for the magnetic field aligned along z.

3.2.2 A more general approach

The preceding section exemplifies one strategy for the analysis of experimental data: A model is assumed and ligand-field or MO theory calculations are performed in an attempt to match the g components.

Another more general approach was introduced many years ago by Bleaney and O'Brien [33] and elaborated by Griffith [34], Taylor [35] and Bohan [36]. In this method, the three possible Kramers doublets arising from the t_{2g}^5 configuration are written as linear combinations of the d_{xy}, d_{xz} and d_{yz} functions with undetermined coefficients. These coefficients, which are related formally to the ligand-field splittings and the spin–orbit coupling, are used to compute the g components. The coefficients

are evaluated using the experimental g components and used to obtain the ligand-field splittings which are then used to construct a model for the system.

As before, the t_{2g}^5 system is thought of as an electron hole in a closed t_{2g}^6 shell. Distortion from octahedral symmetry is assumed to result in three energy states:

ξ: $E=\Delta/3+V/2$ $\quad d_{xy}^2 d_{xz}^2 d_{yz}^1$

η: $E=\Delta/3-V/2$ $\quad d_{xy}^2 d_{xz}^1 d_{yz}^2$

ζ: $E=-2\Delta/3$ $\quad d_{xy}^1 d_{xz}^2 d_{yz}^2$

where V and Δ are defined in Fig. 8, following Taylor [35]. The method explicitly assumes that the d_{xz}, d_{yz} and d_{xy} orbitals are not hybridized by the ligand-field splitting. The lowest-energy Kramers doublet is then written as a linear combination of the three states (eqns. (19a, b)). If we associate the functions Ψ^+ and Ψ^- with the spin functions α and β, respectively, in a spin Hamiltonian with effective spin $S=1/2$, the matrix elements of the Zeeman operators $k_j L_i + g_e S_i$, $i=x, y, z$, $j=\xi, \eta, \zeta$, give the components of the effective g matrix (eqns. (20a–c)).

$$\Psi^+ = a|\xi, \alpha\rangle - ib|\eta, \alpha\rangle - c|\zeta, \beta\rangle \tag{19a}$$

$$\Psi^- = -a|\xi, \beta\rangle - ib|\eta, \beta\rangle - c|\zeta, \alpha\rangle \tag{19b}$$

$$g_x = 2[(a+b)^2 - c^2 - (2-k_\xi - k_\eta)ab] \tag{20a}$$

$$g_y = 2[(a+c)^2 - b^2 - (2-k_\xi - k_\zeta)ac] \tag{20b}$$

$$g_z = 2[(a^2 - (b+c)^2 + (2-k_\eta - k_\zeta)bc] \tag{20c}$$

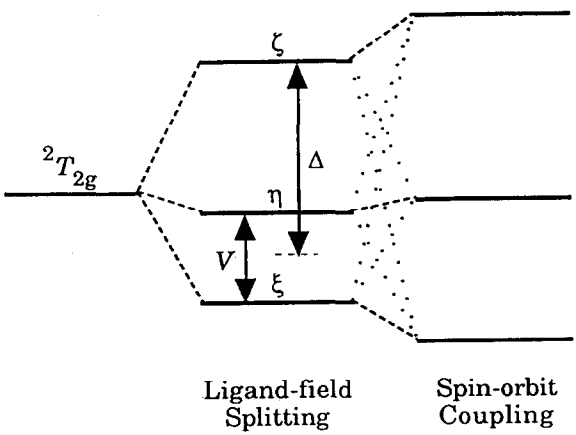

Fig. 8. General splitting of the $^2T_{2g}$ state of a d^5 complex by the ligand field to give the states ξ, η and ζ and further mixing resulting from spin orbit coupling.

In these equations, k_j is an orbital reduction factor intended to account for covalent mixing of ligand orbital character into the electron hole functions. For approximately octahedral complexes such as $Fe(CN)_6^{3-}$, $k_\xi \approx k_\eta \approx k_\zeta$. For porphyrins and related complexes, $k_\zeta \approx 1$, $k_\xi \approx k_\eta$, but it is common practice to set all three parameters to one.

With the $k_j = 1$, eqns. (20a–c) are easily inverted to obtain the coefficients.

$$a = \frac{g_z + g_y}{2\sqrt{2(g_x + g_y + g_z)}} \tag{21a}$$

$$b = \frac{g_z - g_x}{2\sqrt{2(g_x + g_y + g_z)}} \tag{21b}$$

$$c = \frac{g_y - g_x}{2\sqrt{2(g_x + g_y + g_z)}} \tag{21c}$$

When an orbital-reduction parameter is included in the fit of the g components, it is necessary to include the normalization condition

$$a^2 + b^2 + c^2 = 1 \tag{22}$$

The 6×6 spin-orbit coupling matrix factors into two identical 3×3 matrices (eqn. (23)).

	$\lvert\xi,\alpha\rangle$ or $-\lvert\xi,\beta\rangle$	$\lvert\eta,\alpha\rangle$ or $\lvert\eta,\beta\rangle$	$\lvert\zeta,\beta\rangle$ or $\lvert\zeta,\alpha\rangle$
$\lvert\xi,\alpha\rangle$ or $-\lvert\xi,\beta\rangle$	$\Delta/3 + V/2$	$i\lambda/2$	$-\lambda/2$
$\lvert\eta,\alpha\rangle$ or $\lvert\eta,\beta\rangle$	$-i\lambda/2$	$\Delta/3 - V/2$	$i\lambda/2$
$\lvert\zeta,\beta\rangle$ or $\lvert\zeta,\alpha\rangle$	$-\lambda/2$	$-i\lambda/2$	$-2\Delta/3$

(23)

Equations (19a, b) are eigenfunctions of the Hamiltonian matrix, so that V and Δ can be obtained (in units of λ) in terms of the coefficients a, b and c

$$\frac{V}{\lambda} = \frac{a+c}{2b} - \frac{b+c}{2a} \tag{24a}$$

$$\frac{\Delta}{\lambda} = \frac{a+b}{2c} - \frac{a+c}{4b} - \frac{b+c}{4a} \tag{24b}$$

If necessary, the energies of the excited states can be found by diagonalizing eqn. (23), knowing V/λ and Δ/λ.

EPR studies of Fe(III) porphyrins, hemes, cytochromes, etc. have usually been

summarized in terms of the ligand-field parameters Δ/λ, the tetragonal splitting, and V/Δ, the "rhombicity". With the help of model systems, these parameters have been used to infer the nature of the axial ligands in Fe(III) porphyrin-containing biological proteins (see Sect. 4.5.6).

For $|V|, |\Delta| \gg |\lambda|$, the g components must approach g_e. This behavior is predicted by eqns. (20a–c) for $a \gg b, c$, i.e. for V and Δ positive and d_{yz} half-occupied (the ξ state). However, when the hole is in d_{xy} (the ζ state, $\Delta < 0$, $c \gg a, b$), eqns. (20a–c) lead to negative g_x and g_z; this problem can be corrected by interchanging the association of ψ^+ and ψ^- with α and β and changing the sign of ψ^- (note that this changes the signs of b and c in eqns. (24a, b)). The signs of the g components are a considerable source of confusion in the literature. Although DeSimone [37] and Bohan [36] have discussed the problem, most workers have reported the g component signs which result from a fit of data to eqns. (20a–c) without consideration of the appropriate limiting case.

Since the signs of the g components are unknown, there are eight possible assignments which must be considered; unless the experiment used a dilute single crystal, the orientations of the g axes are also unknown, so that in general there are 48 possible combinations of sign and x, y, z labels. A computer program is usually used to search for solutions [38]. Not all solutions lead to real values of a, b and c or realistic values of Δ/λ and V/λ, and usually only one or two of the solutions make physical sense. The options can be further reduced by comparison with other data, e.g. magnetic susceptibilities, optical spectra, or Mössbauer spectra.

Consider, for example, the application of this method to $[Fe(CN)_6]^{3-}$. Using the experimental g components [39], $|g_x| = 2.35$, $|g_y| = 2.10$, $|g_z| = 0.915$ and eqns. (20a–c) (ignoring orbital reduction), only two of the eight possible choices of sign give sensible results: $g_x, g_z < 0$, $g_y > 0$ or $g_x < 0$, $g_y, g_z > 0$. In both cases, $c^2 > a^2$, b^2, suggesting that the ζ state (d_{xy}) lies lowest. Furthermore, the coefficients do not satisfy the normalization condition (eqn. (22)), suggesting significant covalency. Including a single orbital reduction factor and changing the signs of eqns. (20a) and (20c), we obtain: for $g_x, g_y, g_z > 0$, $a = -0.298$, $b = 0.351$, $c = 0.888$, $k = 0.564$; and for $g_x, g_y > 0$, $g_z < 0$, $a = -0.484$, $b = 0.522$, $c = 0.702$, $k = 0.877$. The second solution, which is in better agreement with susceptibility measurements [33], leads to the energy level diagram shown in Fig. 9. According to this analysis, the ion undergoes a very small distortion from octahedral symmetry, $|\Delta/\lambda| = 0.48$, $|V/\lambda| = 0.27$. Since the tetragonal splitting is smaller than the spin–orbit coupling parameter, there is substantial scrambling of the d orbitals and a highly anisotropic g matrix.

In principle, this method extracts a lot of information from the measured g components, but there are some serious drawbacks which suggest caution in its use. Since three parameters are computed from three pieces of experimental data and the fitting problem is very non-linear, experimental errors may propagate in unexpected ways, leading to a real danger of overinterpretation. Taylor [35] has discussed the

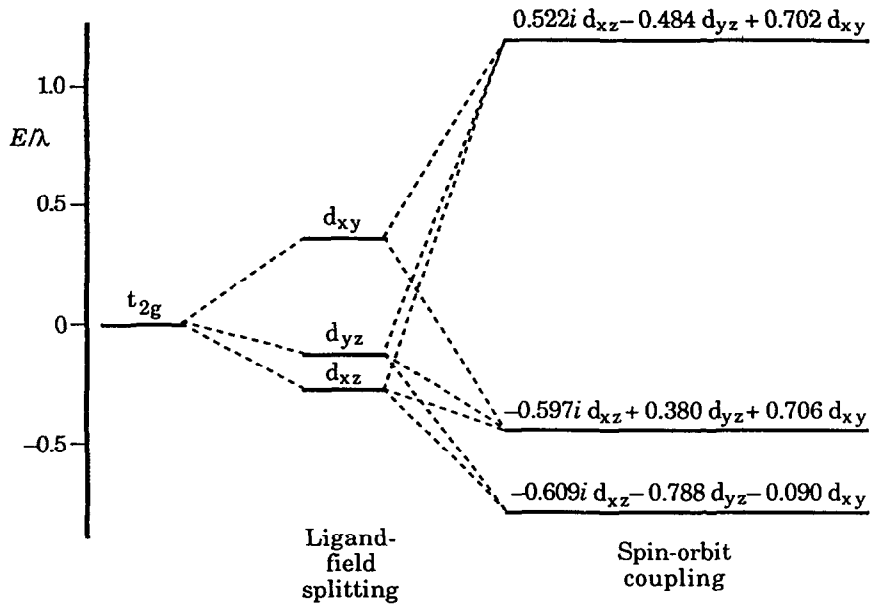

Fig. 9. Energy level diagram for $[Fe(CN)_6]^{3-}$ in $K_3Co(CN)_6$ derived from the g matrix by the method of Bleaney and O'Brien [33].

error propagation problem and gives equations for the variances of the derived parameters.

The theory itself is deficient in several ways. (i) It is assumed at the outset that the only mixing of d_{xy}, d_{xz} and d_{yz} is through spin–orbit coupling; in low-symmetry systems with significant covalency, this may not be true. (ii) Spin–orbit coupling to the e_g levels is ignored; when the octahedral splitting is large, as in $[Fe(CN)_6]^{3-}$, this may be acceptable, but there are cases where serious errors occur. (iii) Since the data can support the determination of at most one orbital reduction parameter, most applications in the literature tacitly assume that all orbitals are equally delocalized; in general, this is simply not true. (iv) Configuration interaction with $t_{2g}^4e_g^1$ excited states has been shown to make small, but significant, contributions [40–42].

3.3 The dipole–dipole coupling parameter, P

Estimation of spin densities using the anisotropic part of the electron–nuclear hyperfine coupling relies on a value for the parameter P (eqn. (6)). There have been several attempts to generate tables of P for use in spin density estimation. The tabulation of Goodman and Raynor [1] was based largely on Hartree–Fock atomic orbitals computed by Froese [43]; that by Morton and Preston [44] employed

TABLE 2
Analysis of anisotropic hyperfine data for $[Cr(CN)_5NO]^{3-}$

Nucleus	Goodman–Raynor[a]		Morton–Preston[b]		Koh–Miller[c]	
	$P/10^{-4}$ cm^{-1}	ρ	$P/10^{-4}$ cm^{-1}	ρ	$P/10^{-4}$ cm^{-1}	ρ
^{53}Cr	−29.9	0.75	−34.4	0.65	−29.9	0.75
^{14}N (NO)	39.1	0.10	46.3	0.08	40.1	0.10
^{13}C (CN_{ax})	74.6	0.03	89.6	0.02	75.5	0.03
^{13}C (CN_{eq})	74.6	0.06	89.6	0.05	75.5	0.06
Total		1.12		0.95		1.12

[a] Ref. 1.
[b] Ref. 44.
[c] Ref. 46.

Hartree–Fock–Slater functions computed by Herman and Skillman [45]; and that by Koh and Miller [46] employed Hartree–Fock functions computed by the methods of Clementi and Roetti [47,48]. As Morton and Preston have pointed out, spin densities computed using P derived from the Froese wavefunctions are often too large; in cases where hyperfine coupling is observed for most or all of the atoms of a radical species, the sum of computed spin densities often exceeds unity. The Koh–Miller parameters are very similar to those of Goodman and Raynor and thus lead to similar problems. For example, analysis of the hyperfine data for $[Cr(CN)_5(NO)]^{3-}$ [49] leads to the spin densities given in Table 2. The Morton–Preston parameters lead to total computed spin density comfortably less than unity, allowing for the unsampled spin densities on the cyanide nitrogen and nitrosyl oxygen atoms, whereas the Koh–Miller and Goodman–Raynor parameters lead to totals significantly greater than unity. For this reason, we will employ the Morton–Preston parameters exclusively in this review. A selection of those parameters used here is given in Table 3.

In evaluating spin densities derived from this or any application of anisotropic hyperfine data, it should be remembered that the results have an absolute accuracy of $\pm 10\%$ at best; they are most valuable in comparing spin densities in homologous series where the errors in P are (hopefully) all in the same direction.

4. SURVEY OF EXPERIMENTAL RESULTS

In the following sections, we will examine the EPR results for low-spin d^5 complexes of titanium, vanadium, chromium, manganese, iron, cobalt and their heavier congeners. EPR parameters for representative examples are collected in Tables 4–9 and 12–27. Note that all hyperfine couplings are in units of 10^{-4} cm^{-1}.

TABLE 3
Parameters for analysis of EPR hyperfine data[a]

Isotope	I	Percent Abund.	A (ns)	P
^{13}C	1/2	1.11	1260 (2s)	89.6 (2p)
^{14}N	1	99.6	604 (2s)	46.3 (2p)
^{31}P	1/2	100.0	4438 (3s)	305.9 (3p)
^{51}V	7/2	99.8	1389 (4s)	146.0 (3d)
^{53}Cr	3/2	9.5	−249.6 (4s)	−34.4 (3d)
^{55}Mn	5/2	100.0	1680 (4s)	207.5 (3d)
^{57}Fe	1/2	2.24	249.2 (4s)	32.6 (3d)
^{59}Co	7/2	100.0	1984 (4s)	282.0 (3d)
^{93}Nb	9/2	100.0	2198 (5s)	152.5 (4d)
^{95}Mo	5/2	15.8	−662 (5s)	−50.3 (4d)
^{97}Mo	5/2	9.6	−676 (5s)	−51.4 (4d)
^{99}Tc	9/2	–	3150 (5s)	228.9 (4d)
^{99}Ru	5/2	12.8	−537 (5s)	−48.7 (4d)
^{101}Ru	5/2	17.0	−588 (5s)	−53.3 (4d)
^{103}Rh	1/2	100.0	−410 (5s)	−40.4 (4d)
^{181}Ta	7/2	100.0	5010 (6s)	148.6 (5d)
^{183}W	1/2	14.3	1927 (6s)	60.9 (5d)
^{185}Re	5/2	37.1	11718 (6s)	382.0 (5d)
^{187}Re	5/2	62.9	11838 (6s)	385.9 (5d)
^{189}Os	3/2	16.1	4403 (6s)	150.4 (5d)
^{191}Ir	3/2	38.5	1096 (6s)	38.6 (5d)
^{193}Ir	3/2	61.5	1165 (6s)	41.0 (5d)

[a] A and P are in units of 10^{-4} cm^{-1}, parameters from Morton and Preston [44].

4.1 Titanium(−I) and zirconium(−I)

4.1.1 Tris-bipyridyl complexes (see Table 4)

A single-line isotropic spectrum was reported for $[Ti(bpy)_3]^-$ by König [12], but no further work has been done. Although $[Zr(bpy)_3]^-$ is known [11], the EPR spectrum has not been reported.

4.1.2 Bis-arene complexes (see Table 5)

Green and co-workers [50] have reported an isotropic spectrum for $[Ti(Bz)_2]^-$ in THF solution, but the anisotropic parameters have not been determined.

4.2 Vanadium(0), niobium(0) and tantalum(0)

4.2.1 Carbonyl complexes (see Table 6)

An EPR spectrum of $V(CO)_6$ in pentane at 1.3 K was reported by Pratt and Myers [51] in 1967, but no hyperfine structure was resolved in the apparently axial

TABLE 4
EPR parameters for tris-(2,2'-bipyridyl) complexes

Complex	$\langle g \rangle$	$\langle A^M \rangle$[a]	$\langle A^N \rangle$[a]	Ref.
$[Ti(bipy)_3]^-$	2.0074			12
$V(bipy)_3$	1.9831	77.3	2.1	12
$Nb(bipy)_3$	1.974			63
$[Cr(bipy)_3]^+$	1.9971	20.3	2.8	12
$[Mo(bipy)_3]^+$	2.037	25		92

[a]In units of 10^{-4} cm^{-1}.

spectrum. A decade later, Rubinson [52] found that $V(CO)_6$ gave very broad lines in many solvents, but that an axial spectrum with ^{51}V hyperfine structure was obtained in cyclohexane or toluene at 90 K. The spectrum depended on the thermal history of the sample, broadened at higher temperatures and became undetectable above 130 K. Morton and co-workers [53] and Ammeter et al. [54] obtained spectra of $V(CO)_6$ in single crystals of $Cr(CO)_6$ and $M(CO)_6$ (M = Cr, Mo, W), respectively. The spectra become increasingly non-axial in the sequence W < Mo < Cr. Morton and Preston found that the anisotropic hyperfine coupling accounts for about half the spin, suggesting significant delocalization onto the carbonyl ligands, but there were some peculiarities. If, as Rubinson [52] assumed, $V(CO)_6$ undergoes a tetragonal distortion to D_{4h} symmetry with a $^2B_{2g}$ ground state (d_{xy} SOMO), the g and hyperfine matrices should have been axial with the minimum g component along the same axis as the maximum hyperfine component. In fact, the matrices are rhombic and the axis of the minimum g component is close to that for the *minimum* hyperfine component (the axes differ by about 15° in the yz plane). Symons and co-workers [55] repeated Rubinson's experiments and found that a lower concentration of $V(CO)_6$ in cyclohexane resulted in much better resolution and clearly rhombic g and hyperfine matrices (although the departure from axial symmetry was smaller than that observed in $Cr(CO)_6$). These authors found that their data were best interpreted in terms of a scissors distortion in the xy plane, leaving the unpaired electron in the $d_{x^2-y^2}$ orbital (^2A_g in D_{2h} symmetry; note that the x and y axes are rotated by 45° in this symmetry).

In order to shed further light on $V(CO)_6$, McCall et al. [56] obtained the EPR spectrum of *trans*-$V(CO)_4(PMe_3)_2$ in a single crystal of *trans*-$Cr(CO)_4(PMe_3)_2$. The g and hyperfine matrices again showed a large departure from axial symmetry and the spectrum could only be detected at low temperatures. Since PMe_3 is a much weaker π-acceptor than CO, a ^2E_g ground state is expected for the D_{4h} complex (Sect. 2.1.2). A Jahn–Teller distortion along the b_{2g} bending coordinate (a scissors distortion in the xy plane) leads to a $^2B_{2g}$ ground state in D_{2h} symmetry. This interpretation nicely fits the EPR parameters.

McCall et al. [56] point out that the X-ray structure [57] of $V(CO)_6$ shows

TABLE 5

EPR parameters for bis-arene complexes of Ti, V, Nb, Ta, Cr, Mo and W[a]

Species	Medium	T/K	$\langle g \rangle$	$g_\parallel$	$g_\perp$	$\langle A^M \rangle$	$A^M_\parallel$	$A^M_\perp$	A^H	Ref.
$[Ti(Bz)_2]^-$	THF	300	1.986			4.4			4.19 (12H)	50
$V(Bz)_2$	$Fe(Cp)_2$	4, 290	1.986	(2.001)	1.978	58.7	(5.9)	85.1	3.6 (12H)	66
	Toluene	130, 300	1.9860	(2.001)	1.978	59.2	(6.8)	85.4	3.7 (12H)	67
	Toluene	77		1.9857	1.981		9.46	86.4	4.0 (12H)	68
(Cp)V(Ch)	2-MeTHF	77, 290	1.987	(2.005)	1.978	63.7	(13.7)	88.7	4.4 (7H)	71
$V(Cot)_2$	2-MeTHF		1.983	(2.001)	1.974	79.5	(18)	110	<4	72
$V(C_5H_5P)_2$	[2.2]Para-cyclophane	38		2.002	1.9764		16.4	97.3		73
					1.9814			81.2		
		300		2.002	1.9801		21.5	86.8		
	DME	300	1.9874			65.2				
V(Bz)	Ar/C_6H_6	12		1.989	1.945		8.68	106.51	4.8 (‖) 4.9 (⊥) (6H)	76
$Nb(Bz)_2$	Toluene	77, 298	1.982	2.0010	1.9730	17	87.0	19.0	4.7 (12H)	78
$Ta(Bz)_2$	Toluene	77, 298	1.955	1.997	1.942	126	205	86.5	5.6 (12H)	78
$[Cr(Bz)_2]^+$	$DMF/CHCl_3$	120, 200	1.9865	2.0023	1.9785	16.8	(0.8)	24.8	3.21 (12H) 2.9 (‖) 3.4 (⊥)	141
(Cp)Cr(Bz)	$DMF/CHCl_3$[a]	140, 120	1.9885	2.0030	1.9787	13.6	(0.4)	20.6	2.18 (5H) 4.32 (6H)	141
$[(Cp)Cr(Ch)]^+$	$DMF/CHCl_3$	140, 220	1.9882	2.0001	1.9797	17.6	6.4	23.1	2.00 (5H) 3.36 (7H)	141
$[(Cp)Cr(MeCh)]^+$	$DMF/CHCl_3$	140, 220	1.9879	2.0006	1.9787	17.9			2.18 (5H) 3.54 (6H) 0.94 (3H)	143
$(Cp)Cr(\eta^6\text{-}C_7H_8)$	2-MeTHF	120, 170	1.9886	2.0009	1.9802	18.3			1.07 (5H) 4.60 (2H) 4.13 (2H) 3.42 (2H)	159
$[Cr(Pyridine)_2]^+$	Ethanol	126, 298	1.9820	1.9981	1.9742	15.8				157
$[(Bz)Cr(Pyridine)]^+$	Methanol	131, 173	1.9858	2.0024	1.9779	16.0				157
$[Cr(\eta^6\text{-}C_5H_5As)_2]^+$	$DMF/CHCl_3$	140, 300	1.9892	1.9730	1.9980	17.9	(16)	19		158
$[Mo(Bz)_2]^+$	Ethanol	110, 290	1.9845	1.998	1.977				4.12 (12H)	65
$[W(Bz)_2]^+$	Ethanol	110, 290	1.9707	1.991	1.960				5.2 (12H)	65

[a] Hyperfine couplings in units of 10^{-4} cm^{-1}.

TABLE 6

EPR parameters for vanadium carbonyl radicals[a]

Species	Medium	T/K	g_x	g_y	g_z	A_x^M	A_y^M	A_z^M	A_x^L	A_y^L	A_z^L	Ref.
$V(CO)_6$	$Cr(CO)_6$	4	2.135	2.108	1.976	43	52	23				53
$V(CO)_6$	Cyclohexane	77	2.066	2.055	1.984	50.7	49.1	14.5				55
trans-$V(CO)_4(PMe_3)_2$	$Cr(CO)_4(PMe_3)_2$	4	2.0419	2.0244	2.0002	28.0	72.8	30.6	30.4 (2P)	28.6 (2P)	27.1 (2P)	56
fac-$V(CO)_3(PMe_3)_3$	CH_2Cl_2	77	2.018	2.018	2.004	31	31	93	20 (3P)	20 (3P)	37 (3P)	58
$V(CO)_5$	Krypton	20	2.0898	2.0559	1.9877	37.3	34.4	88.3	–	4.6 (2C)	3.1 (2C)	59
										8.6 (2C)	11.9 (2C)	
$V(CO)_3$	Neon	4	2.102	2.102	1.992	50	50	18				60

[a]Hyperfine couplings in units of 10^{-4} cm^{-1}.

a tetragonal *compression* (not an elongation as assumed earlier) and that the EPR results for $V(CO)_6$ could be interpreted more consistently in terms of a model similar to that used for *trans*-$V(CO)_4(PMe_3)_2$. Such an interpretation is in accord with a prediction based on the Epikernel Principle (see Sect. 2.2).

McCall et al. [58] also obtained EPR spectra of *fac*-$V(CO)_3(PMe_3)_3$ in CH_2Cl_2. In this case, liquid solution spectra at 213 K showed coupling to three equivalent ^{31}P nuclei, confirming the *facial* stereochemistry ($\langle g \rangle = 2.013$, $\langle A^V \rangle = 45$, $\langle A^P \rangle = 25$). The appearance of a liquid solution spectrum indicates a long spin–lattice relaxation time and thus an orbitally non-degenerate ground state as expected (see Sect. 2.1.3). The axial frozen solution spectrum was interpreted in terms of a d_{z^2} SOMO, where z is the three-fold axis ($^2A_1$ in C_{3v} symmetry).

EPR spectra of all five $V(CO)_x$ fragments have been recorded. Morton and Preston [59] found spectra assignable to $V(CO)_5$ and $V(CO)_4$ when a sample of $V(CO)_6$ in a krypton matrix was UV-irradiated at 4 K. The signal assigned to $V(CO)_5$ has rhombic g and ^{51}V hyperfine matrices, and (in a ^{13}C-enriched sample) superhyperfine coupling to two pairs of carbon atoms. The spectrum was interpreted in terms of a distorted trigonal bipyramidal structure with the odd electron in d_{xy} ($^2B_2$ in C_{2v} symmetry, derived from $^2E'$ in D_{3h}). The two small ^{13}C couplings are presumed to arise from the axial carbonyls, the two large couplings arise from the carbonyls near the d_{xy} lobes, while the equatorial carbonyl lying on the C_2 axis, and thus in the d_{xy} nodal plane, has zero coupling. A signal attributed to $V(CO)_3$ was observed by Van Zee et al. [60] when vanadium vapor was co-condensed with Ne and CO on a sapphire rod at 4 K. The EPR spectrum is axial and the structure of $V(CO)_3$ is believed to be trigonal planar with a d_{z^2} SOMO ($^2A_1'$ in D_{3h} symmetry). The other three vanadium carbonyls have high-spin ground states: $V(CO)_4$, $^6A_1$ in T_d symmetry [59]; $V(CO)_2$, $^4B_2$ in C_{2v} symmetry [60]; and V(CO), $^6\Sigma$ in $C_{\infty v}$ symmetry [60].

4.2.2 Tris-bipyridyl complexes (see Table 4)

An isotropic spectrum has been reported for $V(bpy)_3$ by several workers [12,61,62], but no anisotropic parameters have been determined. The spectrum of $Nb(bpy)_3$ apparently has been obtained, but only the g value was reported [63]. It has been suggested [62] that the vanadium complex might be formulated more appropriately as $[V^{3+}(bpy^-)_3]$. The size of the isotropic ^{51}V coupling suggests substantial metal character in the SOMO, but there may be significant ligand character in the nominal e orbitals; in the absence of anisotropic spectra, further discussion of this hypothesis seems futile.

4.2.3 Nitrosyl complexes (see Table 7)

γ-Irradiation of $K_3[V(NO)(CN)_5] \cdot 2H_2O$ gave a spectrum believed to be that of $[V(NO)(CN)_5]^{4-}$ [64]; the results fit nicely into the general scheme developed for the Cr(I) analog (see further discussion in Sects. 2.1.2 and 4.3.3).

TABLE 7

Anisotropic EPR parameters for nitrosyl complexes[a]

Species	Medium	$g_{\parallel}$	$g_{\perp}$	$A_{\parallel}^{M}$	$A_{\perp}^{M}$	$A_{\parallel}^{L}$	$A_{\perp}^{L}$	Ref.
$[V(NO)(CN)_5]^{4-}$	$K_3[V(NO)(CN)_5]\cdot 2H_2O$	1.974	2.007	116.0	43.8	1.8 (N)	6.4 (N)	64
$[Cr(NO)(CN)_5]^{3-}$	$K_3Mn(CN)_5NO\cdot 2H_2O$	1.9745	2.0052	30.0	10.8	1.9 (N)	6.5 (N)	49
						13.8 (C_{eq})	8.2 (C_{eq})	
						7.0 (C_{ax})	9.4 (C_{ax})	
$[Cr(NO)(H_2O)_5]^{2+}$	Dioxane/D_2O	1.9130	1.9952	38.2	(18.0)	(2.24) (N)	6.91 (N)	110
$[Cr(NO)(NH_3)_5]^{2+}$	DMF/D_2O	1.946	1.992	35.9	(17.1)			110
$[Mo(NO)(CN)_5]^{3-}$	$K_3Co(CN)_6$	1.9736	2.0168	54.4	25.5	1.28 (N)	3.77 (N)	102
$[Mn(NO)(CN)_5]^{2-}$	$K_3Co(CN)_6$	1.9892	2.0265	152.3	32.2	<1 (N)	4.2 (N)	49
$[Mn(NO)(TPP)CN]^{2+}$	Toluene	1.983	2.019	149.5	48.3			204
$[Tc(NO)Cl_5]^{2-}$	H_2O	1.89	2.10	248	107			208
$[Tc(NO)(NH_3)_4H_2O]^{3+}$	H_2O	1.86	2.11	251	107			208
$[Tc(NO)(NCS)_5]^{2-}$	$CHCl_3$/DMF	1.928	2.045	236	95			209
$[Re(NO)Cl_5]^{2-}$	NEt_4^+ salt	1.842	2.025	626	328			211
$[Re(NO)Br_5]^{2-}$	NEt_4^+ salt	1.980	2.086	600	295			211
$[Fe(NO)(CN)_5]^{-}$	$Na_2Fe(NO)(CN)_5$	2.0142	2.0716					26

[a] Hyperfine couplings in units of 10^{-4} cm^{-1}.

4.2.4 Bis-arene complexes (see Table 5)

The isotropic spectrum of $V(Bz)_2$, first measured by Hausser [65] in 1961, shows hyperfine coupling to ^{51}V and to 12 equivalent protons. Anisotropic spectra of $V(Bz)_2$ were obtained by Schweiger et al. [66], Elschenbroich et al. [67], and Andrews et al. [68]. The interpretation of the anisotropic spectrum of $V(Bz)_2$ has been somewhat controversial. Experimental spectra show only perpendicular features, and most workers have assumed that the parallel features are hidden under one of the perpendicular multiplets and have computed $A_{\parallel}^{V}$ from $\langle A^{V} \rangle$ and $A_{\perp}^{V}$. On the basis of simulation studies, Andrews et al. concluded that there is systematic cancellation of the parallel features and arrived at a somewhat different value of $g_{\parallel}$ from other workers (this reviewer is unconvinced by their arguments).

Henrici-Olivé and Olivé [69] obtained isotropic spectra of $V(Bz)_2$, $V(toluene)_2$ and $V(mesitylene)_2$ and found that the arene had no effect on $\langle g \rangle$, $\langle A^{H} \rangle$ or $\langle A^{V} \rangle$. Isotropic spectra of $V(naphthalene)_2$ and $V(anthracene)_2$ were also obtained by Henrici-Olivé and Olivé [70]; EPR parameters were similar to those of $V(Bz)_2$, but hyperfine coupling to eight (nearly) equivalent protons was observed for both the naphthalene and anthracene sandwiches, showing that coordination is to the terminal ring of anthracene.

Several other vanadium(0) sandwich complexes have been studied: (Cp)V(Ch) by Rettig et al. [71] and $V(Cot)_2$ ($Cot = C_8H_8$) by Thomas and Hayes [72]. Elschenbroich et al. [73] studied $V(\eta^6\text{-}C_5H_5P)_2$ in a [2.2]paracyclophane glass over the temperature range 38–300 K. At very low temperatures, both the g and hyperfine matrices are rhombic, but the x and y components coalesce in the temperature range 170–220 K as rapid ring rotation averages the departure from axial symmetry. Three other complexes ($V(\eta^6,\eta^6\text{-}Ph_2SiPh_2)$, $V(\eta^6\text{-}PhSiPh_3)_2$ [67] and (Bz)V(Biphenyl)V(Bz) [74]) are discussed below in the context of more extensive work on Cr(I) analogs. $V(Bz)_2$ and (Cp)V(Ch) have been used by Hulliger and Baltzer [75] as probes of ferromagnetic coupling in $Ni(Cp)_2$.

In a related development, Ozin et al. [76,77] have prepared the "half-sandwiches", V(Bz) and $V(C_6F_6)$ by matrix isolation techniques. The EPR spectra of these give spin Hamiltonian parameters remarkably similar to those for $V(Bz)_2$, but show coupling to only six protons or fluorine nuclei.

Cloke et al. [78] have reported isotropic and frozen solution spectra of $V(Ar)_2$, Ar = Bz, toluene, $Nb(Ar)_2$, Ar = Bz, toluene, mesitylene, and $Ta(Bz)_2$. The g matrices of the Nb and Ta complexes are more anisotropic than that of $V(Bz)_2$, as expected, but the hyperfine parameters suggest very similar electronic structures.

4.3 Chromium(I), molybdenum(I) and tungsten(I)

4.3.1 Carbonyl complexes (see Table 8)

The only careful EPR study of a Cr(I) carbonyl is the work of Fairhurst et al. [79] on $[Cr(CO)_4]^+$, a tetrahedral, high-spin species produced by γ-irradiation of

TABLE 8
Isotropic EPR parameters for Cr(I) carbonyl complexes in CH_2Cl_2 solution

Complex	T/K	$\langle g \rangle$	$\langle A^P \rangle$[a]	Ref.
trans-$[Cr(CO)_4(PPh_3)_2]^+$	273	2.03	17 (2P)	82
mer-$[Cr(CO)_3(PMe_2Ph)_3]^+$	240	2.016	18.7 (2P) 26.0 (1P)	84
mer-$[Cr(CO)_3\{P(OMe)_3\}_3]^+$	298	2.00	37 (3P)	83
$[Cr(CO)_4(dppm)]^+$	298	2.009	6.5 (2P)	85
trans-$[Cr(CO)_2(dppm)_2]^+$	298	2.00	25.6 (4P)	87
$[Cr(CO)_4(L^{Et})_2]^+$	223	2.018		91
$[Cr(CO)_3(L^{Et})_2(PPh_3)]^+$	233	2.012	14.6 (1P)	91
$[Cr(CO)_3(L^{Et})(dmpe)]^+$	293	2.0199	21.0 (2P) 12.6 (Cr)	91

[a] In units of 10^{-4} cm^{-1}.

$Cr(CO)_6$ in krypton at 77 K. Surprisingly, there has been no detailed study of $[Cr(CO)_6]^+$. A very broad single line, $\langle g \rangle = 1.842$, was observed on electrochemical oxidation of $Cr(CO)_6$ in acetonitrile solution and assigned to $[Cr(CO)_6]^+$ by Pickett and Pletcher [80]. Bond and co-workers [81] obtained a much sharper line, $\langle g \rangle = 1.982$, with ^{53}Cr satellites, $\langle A^{Cr} \rangle = 20$, when $Cr(CO)_6$ or $[Cr(CO)_5F]^-$ was oxidized in CH_2Cl_2 solution at $-80°C$. Addition of acetonitrile resulted in a signal resembling that reported by Pickett and Pletcher. A single line with $\langle g \rangle = 1.969$ was attributed to $Cr(CO)_5F$. In the light of $V(CO)_6$ (see Sect. 4.2.1), these results must be viewed with considerable doubt.

Bond and co-workers have reported isotropic EPR spectra for several phosphine and phosphite derivatives of $[Cr(CO)_6]^+$. Thus *trans*-$[Cr(CO)_4(PPh_3)_2]^+$ [82], *mer*-$[Cr(CO)_3L_3]^+$ (L = PMe_2Ph, $P(OMe)_2Ph$, $P(OMe)_3$, $P(OPh)_3$) [83,84], $[Cr(CO)_4(dppm)]^+$ [85], *trans*-$[Cr(CO)_2(L_2)_2]^+$ and *mer*-$[Cr(CO)_3(\eta^2\text{-}L_2)(\eta^1\text{-}L_2)]^+$ (L_2 = dppm, dppe, $Ph_2PCH_2CH_2AsPh_2$, $Ph_2AsCH_2CH_2AsPh_2$) [86–89], all exhibit spectra in CH_2Cl_2, acetone or methanol solutions; resolution was best in the temperature range 200–240 K, but room-temperature spectra were detectable. In contrast, spectra of *fac*-$[Cr(CO)_3L_3]^+$ were apparently undetectably broad, even at 200 K. The stereochemistry of the observed cations was assumed the same as that of the Cr(0) precursors since the oxidations were electrochemically reversible. In the case of *mer*-$[Cr(CO)_3(PMe_2Ph)_3]^+$, EPR line broadening was observed when *mer*-$Cr(CO)_3(PMe_2Ph)_3$ was present, but not when the *facial* isomer was added [84]. These results seem to be exactly opposite to those in the $V(CO)_6$ series, where *trans*-$V(CO)_4(PMe_3)_2$ was detectable only at very low temperature and *fac*-$V(CO)_3(PMe_3)_3$ gave a liquid solution spectrum (see Sect. 4.2.1).

Conner and Walton [90] obtained spectra of *trans*-$[Mo(CO)_2(CNCy)_4]^+$ and $[Mo(CO)_2(CNR)_2L_2]^+$ (R = ^{i}Pr, ^{t}Bu, *p*-tolyl, xylyl, mesityl, $C_6H_2{}^tBu_3$; L = PPh_3, PEt_3, $PMePh_2$, PEt_2Ph, PPr_3) in frozen CH_2Cl_2 solutions. For the tetraisocyanide, they obtained $g_\parallel = 1.984$, $g_\perp = 2.121$, $A_\parallel^{Mo} = 46$, consistent with the expected $^2B_{2g}$

ground state. The diisocyanide complexes showed approximately axial spectra, $g_{\parallel} \approx 1.98$, $g_{\perp} \approx 2.08$ with ^{31}P hyperfine coupling resolved on the parallel feature, $A_{\parallel}^{P} = 23$. The carbonyl groups were cis in the Mo(0) precursors, but on oxidation, isomerized to the trans conformation. In *cis*-dicarbonyls, one of the π-bonding d_{xz} and d_{xy} orbitals is half-filled, whereas, for a *trans*-dicarbonyl, the π-bonding d_{xz} and d_{yz} orbitals are both doubly occupied; thus the trans isomer should be more stable. These results are thus in good agreement with qualitative electronic structure expectations in sharp contrast to the observations on the analogous Cr(I) systems.

Lappert et al. [91] reported isotropic EPR spectra of a series of Cr(I) carbene complexes obtained by oxidation of Cr(0) complexes: *cis*-$Cr(CO)_4(L^{Et})_2$, *fac*-$Cr(CO)_3[C(OEt)CH(SiMe_2)_2](L_2)$ (L_2=dmpe, dppe), and *fac*-$Cr(CO)_3(L^{Et})(L_2)$ (L_2=dmpe, dppe, $[P(OPh)_3]_2$). They also report spectra assigned to

L^{Et}

$[Cr(CO)_3(L^{Et})_2(PPh_3)]^+$, $[Cr(CO)_2(L^{Et})(PPh_3)(dmpe)]^+$, and $[Cr(CO)(L^{Et})(dmpe)_2]^+$, which were formed by substitution or disproportionation reactions of the other Cr(I) species. Although the stereochemistry of the starting materials was known, the cation conformations were not determined. The *g* values and ^{31}P coupling constants for these complexes are similar to those for the Cr(I) carbonyl phosphine complexes of Bond and co-workers and thus there may have been isomerization, e.g. fac→mer, on oxidation.

Both Bond et al. [86] and Connor and Riley [89] have reported the spectrum of *trans*-$[Mo(CO)_2(dppe)_2]^+$; the isotropic *g* value is somewhat larger than the chromium analog, but otherwise the spectra seem similar. Although molybdenum hyperfine structure was apparent in the published spectra, neither group recognized its presence.

4.3.2 Tris-bipyridyl complexes (see Table 4)

Isotropic spectra have been reported for $[Cr(bpy)_3]^+$ [12,61] and $[Mo(bpy)_3]^+$ [92], but, like the Ti and V analogs, no anisotropic parameters have been determined. Saji and Aoyagui [93] have used EPR line broadening to measure the rate of electron exchange between $Cr(bpy)_3$ and $[Cr(bpy)_3]^+$, $k = 2 \times 10^9$ M^{-1} s^{-1} at 298 K; nearly the same rate was measured for Heisenberg spin exchange in solutions of the cation.

4.3.3 Nitrosyl complexes (see Tables 7 and 9)

There has been considerable interest in the EPR spectra of low-spin d^5 nitrosyl complexes since 1961 when Bernal and Harrison [94] discovered that $[Cr(NO)(CN)_5]^{3-}$ gives a well-resolved isotropic spectrum. Hyperfine coupling to ^{53}Cr and ^{14}N was observed and ^{13}C couplings have been measured using an enriched sample [95]. When hyperfine energies are small compared with the electron Zeeman energy, line positions are independent of the signs of the hyperfine coupling constants, but the relative signs become important when the Zeeman energy is decreased. Thus radiofrequency spectra, obtained by Heuer et al. [96], provided the relative signs of the coupling constants: A^N/A^{Cr}, $A^C/A^{Cr} < 0$.

Anisotropic spectra of $[Cr(NO)(CN)_5]^{2-}$ have been measured in a variety of dilute single crystals and frozen solutions [49,97–101]. The spectrum of $[Mo(NO)(CN)_5]^{3-}$ [102,103] is closely analogous to that of the chromium complex.

Simple LF theory considerations or more detailed MO calculations [104] suggest that, for a C_{4v} complex with a strongly π-acidic NO ligand, the SOMO should be d_{xy} ($2b_2$), as shown in Fig. 5. For $[Cr(NO)(CN)_5]^{2-}$, we expect $g_\parallel < g_e < g_\perp$, in good agreement with experiment.

If the SOMO is primarily of d_{xy} character, the ^{53}Cr hyperfine components are given by eqns. (9a–c). Spin densities calculated from hyperfine data were given for

TABLE 9

Isotropic EPR parameters for nitrosyl complexes

Complex	Solvent	$\langle g \rangle$	$\langle A^M \rangle$[a]	$\langle A^N \rangle$[a]	$\langle A^P \rangle$[a]	Ref.
$[Cr(NO)(CN)_5]^{3-}$	H_2O	1.9949	17.2	4.9		111
$[Cr(NO)(CN)_3(H_2O)_2]^-$	H_2O	1.9880	18.6	5.4		111
$[Cr(NO)(CN)_2(H_2O)_3]$	H_2O	1.9832	20.0	5.4		111
$[Cr(NO)(CN)(H_2O_4]^+$	H_2O	1.9748	21.4	5.3		111
$[Cr(NO)(H_2O)_5]^{2+}$	H_2O	1.9671	24.7	5.4		111
$[Cr(NO)(NCMe)_5]^{2+}$	MeCN	1.98				123
$[Cr(NO)(NCMe)(dppe)_2]^{2+}$	CH_2Cl_2	2.00		4.8	29.0	123
$[Cr(NO)(dppe)_2Cl]^+$	CH_2Cl_2	2.00		4.8	30.5	123
$[Cr(NO)(NCS)_5]^{3-}$	Me_2CO	1.976	19.7	5.4		112
$[Cr(NO)(py)_5]^{2+}$	C_5H_5N	1.976	19.6	5.7		112
$[Cr(NO)(CNPh)_5]^{2+}$	CH_2Cl_2	1.994	15.9	4.1		125
$[Cr(NO)(CNCMe_3)_3dppe]^{2+}$	CH_2Cl_2	1.995	15.9	4.2	28.6	125
$[Cr(NO)(dppe)_2F]^+$	CH_2Cl_2	1.993	16.1	5.0	31.9	125
$CpCr(NO)(PPh_3)Cl$	Toluene	1.994		4.6	20.4	113
$[Mo(NO)(NCMe)_5]^{2+}$	MeCN	1.98	45.3			123
$[Mo(NO)(NCMe)(dppe)_2]^{2+}$	CH_2Cl_2	2.02	23.8	2.3	23.2	123
$[Mo(NO)(dppe)_2Cl]^+$	CH_2Cl_2	2.02	23.4	2.7	23.4	123
$[Mo(NO)(H_2O)Cl_4]^{2-}$	H_2O	1.95	21			124
$CpMn(NO)Me_2$	Toluene	2.020	71			207

[a] In units of 10^{-4} cm^{-1}.

$[Cr(NO)(CN)_5]^{3-}$ in Table 2. Similar calculations for a variety of other V(0), Cr(I), Mo(I), Mn(II), Tc(II), and Re(II) nitrosyl complexes are given in Table 10. Except for the rhenium complexes, where the spin–orbit coupling contributions are large enough to cause serious errors in perturbation theory, the d-orbital spin densities are remarkably constant, $a^2 \approx 0.58 \pm 0.04$, suggesting that the SOMO is indeed nearly identical in all low-spin d^5 nitrosyl complexes with ca. 10% contribution from NO orbitals and 30% from the remaining ligands.

There is a problem, however, which was recognized early on: if the complex has C_{4v} symmetry, inclusion of the NO σ orbitals (a_1 symmetry) or π or π^* orbitals (e symmetry) in the b_2 SOMO is forbidden. The ^{14}N coupling should then arise through polarization and should be isotropic; in fact it is highly anisotropic. As it happened, none of the early studies using dilute single crystals constructed the interaction matrices by a complete rotation study. When McGarvey and Pearlman [99] did such measurements for $[Cr(CN)_5NO]^{3-}$, they found that, although the principal axes of the g and ^{53}Cr hyperfine matrices are co-linear within experimental error, the principal axes of the ^{14}N hyperfine matrix deviate by about 9°, implying that the Cr–N–O bond angle is non-linear. Thus the true symmetry of the complex is at most C_s and admixture of nitrogen 2p character is symmetry-allowed.

Several other d^5 nitrosyl complexes have been the subjects of extensive EPR investigation. Thus Wilkinson and co-workers [105,106] reported the isotropic spectra of $[Cr(NO)(H_2O)_5]^{2+}$ and $[Cr(NO)(NH_3)_5]^{2+}$. Further work refined the isotropic parameters [107–109], and Goodman et al. [110] obtained frozen solution spectra of both complexes. The aquo complex is formed by acid hydrolysis of $[Cr(NO)(CN)_5]^{3-}$, and Burgess et al. [111] found that three of the four intermediates, $[Cr(NO)(CN)_{5-x}(H_2O)_x]^{x-3}$, give distinguishable spectra ($x = 0, 2, 3, 4, 5$). They were

TABLE 10

Computed spin densities in nitrosyl complexes

Complex	ρ_d^M	ρ_p^N	ρ_p^C
$[V(NO)(CN)_5]^{4-}$	0.54		
$[Cr(NO)(CN)_5]^{3-}$	0.62	0.08	0.02 (ax) 0.05 (eq)
$[Mn(NO)(CN)_5]^{2-}$	0.65	0.06	
$[Mo(NO)(CN)_5]^{3-}$	0.62	0.04	
$[Cr(NO)(H_2O)_5]^{2+}$	0.58	0.08	
$[Cr(NO)(NH_3)_5]^{2+}$	0.58		
$[Mn(NO)(TPP)CN]^{2+}$	0.54		
$[Tc(NO)Cl_5]^{2-}$	0.55		
$[Tc(NO)(NH_3)_4(H_2O)]^{3+}$	0.52		
$[Tc(NO)(NCS)_5]^{2-}$	0.61		
$[Re(NO)Cl_5]^{2-}$	0.71		
$[Re(NO)Br_5]^{2-}$	0.86		

able to measure the rates of the steps of the hydrolysis reaction by following the EPR signals of the intermediates as functions of time.

Garif'yanov and Luchkina [112] have reported isotropic spectra for $[Cr(NO)(py)_5]^{2+}$ and $[Cr(NO)(NCS)_5]^{3-}$. Connor et al. [88] have reported the isotropic spectra of *fac*-$[Cr(NO)(NCMe)_3L_2]^{2+}$ and $[Cr(NO)(OCMe_2)_3L_2]^{2+}$ ($\langle g \rangle$ = 1.984–1.993, $\langle A^P \rangle$ = 30–32, (L_2 = dmpe, bis(dicyclohexylphosphino)ethane).

Legzdins and Nurse [113] have reported room-temperature isotropic spectra for $CpCr(NO)(PPh_3)X$ (X = Cl, Br, $CpCr(NO)LI$; L = PPh_3, $P(OPh)_3$, $P(OEt)_3$). The *g* values, ^{31}P and ^{14}N hyperfine couplings are typical of chromium nitrosyl complexes and quite different from piano-stool complexes with ligands less strongly interacting than NO (see Sect. 4.3.5).

Atherton et al. [114,115] studied the isotropic spectrum of $[(Tp)Mo(NO)(NCMe)_2]^+$ and found that, under some circumstances, the ^{93}Mo, ^{95}Mo hyperfine satellites were much broader than the central line (due to non-magnetic Mo isotopes). They present a theory to explain this effect and experimental evidence in support of the theory. Chandramouli et al. [116] have used EPR linewidths to probe the outer-sphere binding of $[Cr(NO)(CN)_5]^{3-}$ to a polyethyleneimine chain.

EPR spectra have been widely used to characterize nitrosyl complexes of Cr(I) and Mo(I). Spin Hamiltonian parameters are usually very similar to those of the species discussed above. Data are available for $[Cr(NO)(CNR)_5]^{2+}$ (R = Me, *p*-ClC_6H_4) [117], $Cr(NO)L_2(H_2O)(CN)_2$ (L = a substituted pyrazoline [118] or imidazoline [119]), $Cr(NO)(en)(H_2O)(CN)_2$ [120], $Cr(NO)(H_2O)L_2$ (L = salicylaldoxime, 1-nitroso-2-naphthol, 1-nitroso-2-naphthol-3,6-disulfonic acid, 8-hydroxyquinoline, the phenylhydrazone of pyruvic acid, acetylacetone, and pyrocatechol) [121,122], $[M(NO)(NCMe)_5]^{2+}$, $[M(NO)(NCMe)(dppe)_2]^{2+}$, $[M(NO)(dppe)_2Cl]^+$ (M = Cr, Mo), and $[Cr(NO)(dppe)_2F]^+$ [123], $[Mo(NO)(H_2O)Cl_4]^{2-}$ [124], $[Cr(NO)(CNPh)_5]^{2+}$, $[Cr(NO)(CNR)_4L]^{2+}$ (R = Me, ^{i}Pr, ^{t}Bu; L = PEt_3, PPr_3, PBu_3, PMe_2Ph, PEt_2Ph), $[Cr(NO)(CNCMe_3)_3dppe]^{2+}$, and $[Cr(NO)(dppe)_2F]^+$ [125]. Cr(I) nitrosyl complexes with sulfur donor ligands have been studied extensively by two Russian groups; data are available for $[Cr(NO)L_2L'_3]$ (L_2 = $[S_2P(OEt)_2]^{2-}$ [126–130], $[S_2P(OEt)Me]^{2-}$ [129], $[S_2PEt_2]^{2-}$ [129], $[S_2COEt]^{2-}$ [126–128,131,132] and $[S_2CNEt_2]^{2-}$ [126,127,132–134], L' = H_2O, PR_3, $P(OR)_3$, $PR_2(OR')$, and AsR_3).

Al Obaidi et al. [135] have reported isotropic and frozen solution spectra of $[Tp^*Mo(NO)L_2]^+$ (L = pyridine, imidazole, pyrazole, *N*-methylimidazole, and 3,5-dimethylpyrazole). Remarkably enough, for these complexes, as well as all those mentioned above for which frozen solution spectra were obtained, the spectra were axial with parameters very similar to those of the parent pentacyanonitrosyl complexes. This observation further strengthens the conclusion that the SOMO in d^5 nitrosyl complexes is confined largely to the metal and the NO group.

4.3.4 Bis-arene complexes (see Table 5)

EPR investigations of this very fruitful class of d^5 sandwich complexes were begun in 1957 by Feltham et al. [136] who obtained the isotropic spectrum of $[Cr(Bz)_2]^+$ in aqueous solution. The isotropic parameters were refined [137–140] and anisotropic spectra measured [141–143] by several groups. Hausser [65] also obtained isotropic spectra of the molybdenum and tungsten analogs, $[Mo(Bz)_2]^+$ and $[W(Bz)_2]^+$.

Expressions for the g and hyperfine matrix components are given in Table 1 for the case of a SOMO largely metal d_{z^2} in character. Since the e_{1g} orbital containing most of the d_{xz}, d_{yz} character lies well above the SOMO, $\delta_{xz,yz}$ is expected to be negative so that $\Delta g_\perp < 0$; in almost all cases, this expectation is fulfilled.

The dipolar contribution to the hyperfine couplings is expected to be positive for $A_\parallel$ and negative for $A_\perp$ for the V, Nb and Ta complexes (the signs are reversed for Cr). Since $A_\parallel$ is small for the V and Cr complexes, it is reasonable to assume that $\langle A^V \rangle < 0$ and $\langle A^{Cr} \rangle > 0$, suggesting that the isotropic coupling arises primarily through polarization of inner-shell s orbitals by spin density in the $3d_{z^2}$ orbital. For the Nb and Ta complexes, on the other hand, $|A_\parallel| > |A_\perp|$, and apparently $\langle A^{Nb} \rangle$, $\langle A^{Ta} \rangle > 0$, suggesting a much greater contribution of the 5s and 6s orbitals in the SOMO.

Using the dipolar parameters P given in Table 3, the EPR parameters of Table 5 lead to the 3d spin densities shown in Table 11. These numbers must be taken with some caution, both because of uncertainties in P and because of limited precision in the coupling constants for the chromium complexes. Nonetheless, there are trends which appear to be real. The computed 3d spin density for $V(Bz)_2$ is in excellent agreement with the metal sphere contribution, 0.67, obtained from an SCF-Xα-SW MO calculation by Andrews et al. [68]. For both the vanadium and chromium complexes, changing the ligation from $(Bz)_2$ to (Cp)(Ch) increases delocalization,

TABLE 11
Computed spin densities for bis-arene complexes

Complex	ρ_d
$V(Bz)_2$	0.66
(Cp)V(Ch)	0.63
$V(Cot)_2$	0.77
V(Bz)	0.86
$Nb(Bz)_2$	0.85
$Ta(Bz)_2$	1.02
$[Cr(Bz)_2]^+$	0.85
(Cp)Cr(Bz)	0.74
$[(Cp)Cr(Ch)]^+$	0.59

whereas changing from $(Bz)_2$ to $(Cot)_2$ (for vanadium) decreases delocalization, trends which are consistent with the observed ring proton hyperfine couplings.

The interpretation of the ring proton hyperfine couplings has been a matter of some concern for these systems. Early on, it was recognized that the coupling constants are much larger than would be expected if the mechanism were polarization of the C–H bonds by spin density in a carbon-based π-orbital. ^{1}H NMR contact shifts, measured for $V(Bz)_2$, $[Cr(Bz)_2]^+$ and methyl-substituted complexes by Anderson and Drago [144] and by Krivospitskii and Chirkin [145] show that the ring proton and methyl proton couplings are positive and negative, respectively, opposite to the well-known results for aromatic radical ions. The contact shift measurements were confirmed by ENDOR studies [66,146] on $V(Bz)_2$, from which we have the complete proton hyperfine matrices as well as a measurement of the rate of benzene ring rotation. The signs of the coupling constants suggested that the ring proton couplings arise from spin density delocalized into the σ-orbitals of the arene. Anderson and Drago [147] performed extended Hückel MO calculations which showed that the largely metal d_{z^2} SOMO does indeed have small contributions from benzene ring in-plane orbitals, leading to a "direct" contribution to A^H comparable with that observed experimentally; the "indirect" contribution arising through polarization of C–H bonds by spin density in the carbon $2p_z$ orbital is about 50 times smaller and of opposite sign.

The temperature dependence of the EPR linewidths in spectra of $[Cr(Bz)_2]^+$, $[Cr(biphenyl)_2]^+$, and $[Cr(terphenyl)_2]^+$ in acetone and pyridine have been studied by Karthe and Kleinwächter [148], who found contributions from rotational averaging of anisotropies (proportional to η/T) and from spin-rotational interaction (proportional to T/η). A linewidth study by Gribov et al. [149] for $[Cr(Bz)_2]^+$, $[Cr(toluene)_2]^+$, $[Cr(m\text{-xylene})_2]^+$, $[Cr(cumene)_2]^+$, and $[Cr(biphenyl)_2]^+$ in ethanol and acetone gave similar results.

There have been several studies motivated (at least initially) by a search for substituent effects. Henrici-Olivé and Olivé [69,70] measured the spectrum of $[Cr(toluene)_2]^+$ and $[Cr(naphthalene)_2]^+$ and found the same $\langle g \rangle$ and $\langle A^H \rangle$ as $[Cr(Bz)_2]^+$. Elschenbroich et al. [150,151] extended this study to $[Cr(phenanthrene)_2]^+$, $[Cr(anthracene)_2]^+$, $[Cr(9,10\text{-dihydro-anthracene})_2]^+$, $[Cr(9,10\text{-dimethylanthracene})_2]^+$, and $[Cr(9,10\text{-dihydro-9,10-dimethylanthracene})_2]^+$. The 9,10-dihydroanthracene complexes show g values about 0.002 smaller than $[Cr(anthracene)_2]^+$, suggesting slightly less delocalization of the unpaired electron. Karthe and Kleinwächter [152] reported isotropic and frozen solution spectra of $[Cr(Ar)_2]^+$ in pyridine where Ar = benzene, toluene, mesitylene, hexamethylbenzene, biphenyl, terphenyl and 4-methylbiphenyl. Virtually the only difference among the spectra was the number of ring proton hyperfine couplings. Interestingly, the spectra of the terphenyl and 4-methylbiphenyl derivatives showed coupling to 8 and 9 protons, respectively, indicating bonding to the middle ring in

$[Cr(terphenyl)_2]^+$ and the unsymmetrical isomer of $[Cr(4\text{-methylbiphenyl})_2]^+$. Elschenbroich et al. [153] carried out a similar survey for $[Cr(Ar)_2]^+$, where Ar = Bz and all 12 possible methyl substitution products ranging from toluene to hexamethylbenzene. Methyl substitution had no effect on $\langle g \rangle$ or $\langle A^{Cr} \rangle$ (measured in methanol at 220 K), $\langle g \rangle = 1.9867$, $\langle A^{Cr} \rangle = 16.6 \pm 0.2$, but the ring proton couplings were found to increase slightly with methylation. Ito et al. [154] have obtained similar results for $[Cr(Ar)_2]^+$ (Ar = benzene, fluorene, naphthalene, phenanthrene, chrysene, pyrene, anthracene, fluoranthrene, and bis-(diphenylene)ethene). They also found that the electrochemical oxidation potentials of the parent Cr(0) complexes are constant within ± 5 mV over the series, in sharp contrast to the range of more than 2 V spanned by the ligand hydrocarbons. Brubaker and co-workers [155] have carried out a similar survey of $[Cr(Ar)_2]^+$ introducing other functional groups: Ar = benzene, toluene, mesitylene, 1,3,5-tri-isopropylbenzene, hexamethylbenzene, biphenyl, anisole, chlorobenzene, benzaldehyde, and ethyl benzoate, as well as [(Bz)Cr(benzaldehyde)]$^+$. The isotropic spectra (in DMSO at 298 K) gave essentially constant g values and chromium hyperfine couplings, $\langle g \rangle = 1.986 \pm 0.001$, $\langle A^{Cr} \rangle = 16.7 \pm 0.3$. The ring proton couplings were found to increase with electron-donating groups and decrease with electron-withdrawing groups. These workers also measured frozen solution spectra in $DMF/CHCl_3$ at 130 K. Again, the parameters showed no dependence on the functional group: $(g_\parallel)_{avg} = 2.0034 \pm 0.0013$, $(g_\perp)_{avg} = 1.9788 \pm 0.0011$, $(A_\perp{}^{Cr})_{avg} = 23.5 \pm 0.3$, $(A_\parallel{}^{H})_{avg} = 2.9 \pm 0.2$, $(A_\perp{}^{H})_{avg} = 3.3 \pm 0.2$. Elschenbroich and Koch [156] have extended this study to $[Cr(Ar)_2]^+$ (Ar = $PhSiMe_3$, 1,4-$(SiMe_3)_2C_6H_4$, and 1,3,5-$(SiMe_3)_3C_6H_3$). Increasing substitution this time had the effect of lowering $\langle g \rangle$, increasing $\langle A^{Cr} \rangle$, and decreasing $\langle A^{H} \rangle$.

Elschenbroich et al. have reported the isotropic and frozen solution spectra of several complexes with heterocyclic ligands: $[Cr(\eta^6\text{-}C_5H_5N)_2]^+$, $[(Bz)Cr(C_5H_5N)]^+$ [157] and $[Cr(\eta^6\text{-}C_5H_5As)_2]^+$ [158]. In contrast to the bis-arene complexes, $g_\parallel$ for $[Cr(\eta^6\text{-}C_5H_5N)_2]^+$ and $[Cr(\eta^6\text{-}C_5H_5As)_2]^+$ is significantly less than g_e, suggesting a change in ground state, possibly with more delocalization of the unpaired electron onto the ligands. In contrast to $V(\eta^6\text{-}C_5H_5P)_2$ [73], see Sect. 4.2.4, the g matrices were still axial down to about 130 K. Freezing out of the ring rotation is easier to observe for vanadium complexes because of the much larger vanadium hyperfine couplings, but the chromium complexes would presumably show rhombic interaction matrices at sufficiently low temperatures.

In addition to several sandwich complexes with 5- and 7-membered rings mentioned above, data are available for [(Bz)Cr(biphenyl)]$^+$ [139], [(Cp)Cr(Ch)]$^+$, (Cp)Cr(Bz) [143], [(Cp)Cr(MeCh)]$^+$, $(Cp)Cr(\eta^6\text{-}C_7H_8)$ [159] and [(Bz)Cr(biphenylene)]$^+$ [160].

The Elschenbroich group has studied several bridged arenes. Isotropic parameters were measured for [Cr([2.2]paracyclophane)]$^+$ and compared with those of $[Cr(p\text{-xylene})_2]^+$ and $[Cr(cyclobutabenzene)_2]^+$ in an attempt to further understand the mechanism of proton coupling [161,162]. Chromium complex cations with singly

and doubly bridged silicon analogs of [2.2]paracyclophane, $[Cr(PhSiMe_2)_2]^+$ and $[Cr(Me_2SiC_6H_4SiMe_2)_2]^+$ have also been studied [163]. Two other systems with tilted ring systems were studied in order to see how much distortion is required to destroy the axial symmetry of the g and hyperfine matrices. A spectrum was obtained for $[Cr(bridge)]^+$, where the rigid bridging ligand tilts the benzene rings at $\pm 9°$ [164]. Spectra of $V(\eta^{12}\text{-}Ph_2SiPh_2)$ were measured and compared with those of $V(\eta^6\text{-}PhSiPh_3)_2$ and $[Cr(\eta^6\text{-}PhSiPh_3)_2]^+$ [67]. The bridging $SiPh_2$ group imparts a substantial ring tilt. In neither case, however, was there any detectable departure from axial symmetry although there was a significant decrease in metal hyperfine coupling.

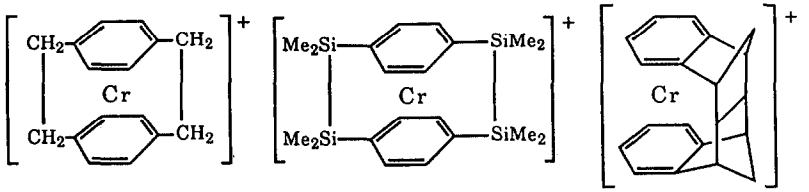

$[Cr([2.2]paracyclophane)]^+$ $[Cr(Me_2SiC_6H_4SiMe_2)_2]^+$ $[Cr(bridge)]^+$

By attaching Lewis base groups to the benzene ring, Elschenbroich et al. have converted $Cr(Bz)_2$ into a chelating ligand: $Cr[PhPPh_3)_2]M(CO)_4$ (M = Cr, Mo, W) [165], $[Cr(PhSCH_3)_2]Mo(CO)_4$ [166], and $[Cr(PhPMe_2)_2]_2Ni$ [167]. On oxidation, an electron is removed from chromium, producing d^5 radical cations.

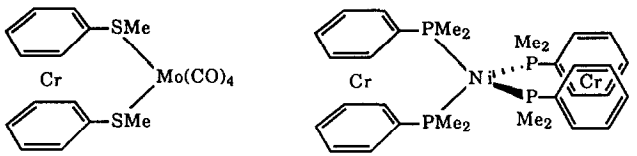

$[Cr(PhSCH_3)_2]Mo(CO)_4$ $[Cr(PhPMe_2)_2]_2Ni$

Finally, Elschenbroich's group have studied several binuclear complexes: $[(Bz)Cr(biphenyl)Cr(Bz)]^z$ and $[Cr_2(biphenyl)_2]^z$ ($z = 1, 2$) [168], (Bz)V(biphenyl)-V(Bz) [74], and $[Cr(PhPMe_2)_2]_2Ni$ [167]. For the dichromium monocations, the EPR parameters are very similar to those of the corresponding mononuclear complex, suggesting that the odd electron is localized on one metal. The divanadium complex and the dichromium dications show spectra with zero-field splittings consistent with electron–electron dipolar interaction over the expected M–M distances. This behavior is in marked contrast with that for the analogous biferrocene dication, which is diamagnetic [169]. The difference in behavior is consistent with the expected difference in side-by-side overlap of d_{z^2} orbitals and d_{xy} or $d_{x^2-y^2}$ orbitals.

4.3.5 "Piano-stool" complexes (see Tables 12 and 13)

In 1968, Keller [170] reported that sublimation of $[CpCr(CO)_3]_2$ onto a cold finger at 77 K gave an anisotropic spectrum ($g=2.117$, 2.030, 1.966, $g_{av}=2.038$) which he assigned to $CpCr(CO)_3$. Subsequently, Madach and Vahrenkamp [171] reported an isotropic signal, $\langle g\rangle=2.025$, in benzonitrile solutions of the dimer which they assigned to $CpCr(CO)_3$; this spectrum is now thought to be due to a benzonitrile substitution product [172].

More recently, Morton and co-workers [173,174] have obtained the spectrum of $CpCr(CO)_3$ in a single crystal of $CpMn(CO)_3$. The spectrum was only observable below 25 K, but gave a g matrix very similar to that found by Keller. The principal axis corresponding to the largest g component was found to lie close to the molecular three-fold axis; the other components are in the normal plane with the smallest component in the direction of one of the carbonyl ligands. The rhombic g matrix implies symmetry lower than C_{3v} and all data are in good agreement with a $^2A'$ ground-state in C_s symmetry. Both ^{53}Cr and ^{13}C hyperfine structure was resolved. The ^{53}Cr hyperfine matrix was somewhat misinterpreted in the original work. The SOMO was written as in the equation

$$|\mathrm{SOMO}\rangle = a\left(\sqrt{\frac{2}{3}}|x^2-y^2\rangle - \sqrt{\frac{1}{3}}|yz\rangle\right) + \ldots \tag{25}$$

but the off-diagonal element in the dipolar hyperfine matrix, eqn. (8e), was ignored. Inclusion of this term leads to rotation of the principal axes in the yz plane to give predicted hyperfine components as shown in eqns. (26a–c). With $P=-34.4\times10^{-4}\,\mathrm{cm}^{-1}$, the

$$A_{xx} = A_s + P\Delta g_{xx} \tag{26a}$$

$$A_{yy} \approx A_s + P(2\sqrt{2}a^2/7 + \Delta g_{yy}) \tag{26b}$$

$$A_{zz} \approx A_s + P(-2\sqrt{2}a^2/7 + \Delta g_{zz}) \tag{26c}$$

TABLE 12

Isotropic EPR parameters for piano-stool complexes of Cr, Mo and W

Species	$\langle g\rangle$	$\langle A^M\rangle^a$	$\langle A^L\rangle^a$	Ref.
$[(C_6Me_6)Cr(CO)_2\{C_2(COOEt)_2\}]^+$	1.9936	16.8	8.4 (2C)	181
$[(C_6Me_6)Cr(CO)_2(HCCPh)]^+$	1.9964	16.1	4.2 (1H)	181
$[(Ch)Mo(dppe)(C{\equiv}CPh)]^+$	1.996	30	21 (2P) 4 (7H)	187
$[(Ch)Mo\{P(OMe)_3\}_2Cl]^+$	1.990	33	30 (2P) 4 (7H)	188
$[(Ch)Mo(dppe)(NCPh)]^{2+}$	1.990	21	21 (2P)	188
$[(Ch)W(dppe)(NCPh)]^{2+}$	1.964			188

[a] In units of $10^{-4}\,\mathrm{cm}^{-1}$.

TABLE 13

EPR parameters for "piano-stool" complexes of Cr, Mo and W[a]

Complex	Medium	T/K	g_x	g_y	g_z	A^{P}_{avg}	Ref.
$CpCr(CO)_3$	$CpMn(CO)_3$	20	2.0353	1.9969	2.1339		173
$Cp^*Cr(CO)_3$	$Cp^*Mn(CO)_3$	20	1.9973	2.0192	2.1215		16
$(C_5Ph_5)Cr(CO)_3$	Toluene	90	1.9952	2.0225	2.1387		176
$CpCr(CO)_2PPh_3$	$CpMn(CO)_2PPh_3$	77	1.9933	2.0170	2.1060	32	175
$Cp^*Cr(CO)_2PMe_3$	$Cp^*Mn(CO)_2PMe_3$	90	1.9980	2.0182	2.0967	36	16
$(C_5Ph_5)Cr(CO)_2PMe_3$	Toluene	120	1.995	2.015	2.12	35	178
$(C_5Ph_5)Cr(CO)_2P(OMe)_3$	Toluene	120	1.994	2.013	2.10	42	178
$[(C_6Me_6)Cr(CO)_2PEt_3]^+$	CH_2Cl_2/THF	90	1.9942	2.0248	2.1086	31.2	178
$[(C_6Me_6)Cr(CO)_2P(OEt)_3]^+$	CH_2Cl_2/THF	90	1.9934	2.0246	2.1100	42.0	178
$[(\eta^6\text{-biphenyl})Cr(CO)_2(PPh_3)]^+$	$CH_2Cl_2/C_2H_4Cl_2$	77	1.992	2.034	2.103	29.2	179
$[(C_6Me_6)Cr(CO)_2\{C_2(COOEt)_2\}]^+$	CH_2Cl_2/THF	90	1.979	1.995	2.007		181
$[(Tbtac)Cr(CO)_3]^+$	Powder	10	1.992	2.040	2.158		182
$[(Tbtac)Mo(CO)_3]^+$	DMF	77	1.906	2.045	2.188		182
$[(Tbtac)W(CO)_3]^+$	DMF	77	1.68	1.76	1.80		182
$Tp'Cr(CO)_3$	CH_2Cl_2	120	1.988	2.036	2.114		185
$TpMo(CO)_3$	CH_2Cl_2	5	1.94	2.08	2.40		185

experimental hyperfine matrix leads to the 3d spin density ($a^2 = 0.66$), smaller by a factor of $\sqrt{2}$ than the original estimate.

Morton et al. [174,175] have reported the spectrum of $CpCr(CO)_2PPh_3$ in a single crystal of the manganese analog; the ^{31}P coupling is nearly isotropic. The analysis was complicated by the presence of four distinct sites in the crystal, each with a slightly different g matrix. Although the g matrices for $CpCr(CO)_3$ and $CpCr(CO)_2PPh_3$ are very similar, the orientation of the axes corresponding to the minimum and intermediate g components are reversed, suggesting that, in the PPh_3 derivative, the ground state is $^2A''$ with 2:1 d_{xy}, d_{xz} metal contributions to the SOMO. Fortier et al. [16] have recently reported the spectra of $Cp^*Cr(CO)_3$ and $Cp^*Cr(CO)_2PMe_3$ in single crystals of the manganese analogs. Again, the g matrices are very similar to that of $CpCr(CO)_3$ and the ^{31}P coupling is nearly isotropic, but the orientations of the principal axes indicate a $^2A''$ ground state for both $Cp^*Cr(CO)_3$ and $Cp^*Cr(CO)_2PPh_3$. Theoretical calculations (see Fig. 2) showed that the $^2A'$ and $^2A''$ states are very close together; small crystal packing forces could tip the balance either way.

Castellani and co-workers [176] have recently reported the spectrum of $(C_5Ph_5)Cr(CO)_3$ in a toluene glass. As in the case of $CpCr(CO)_3$, the spectrum disappears at temperatures above 130 K, suggesting a low-lying excited state and efficient spin-lattice relaxation. The g matrix is again similar to that observed for $CpCr(CO)_3$, but because the measurements were in a glass, assignment of the ground state symmetry was not possible. The largest component of the g matrix was found to be significantly temperature-dependent, possibly because of a temperature-dependent equilibrium between the two ground state configurations.

Connelly and Demidowicz [177] obtained the spectrum of $[C_6Me_6)Cr(CO)_2PPh_3]^+$ in CH_2Cl_2 at 77 K (no room-temperature spectrum could be detected) with parameters very similar to those for the Cp and Cp* derivatives. Recent work by Rieger and co-workers [178] has extended these series to $[(C_6Me_6)Cr(CO)_2L]^+$ (L = PEt_3, $P(OEt)_3$, $P(OPh)_3$), and $(C_5Ph_5)Cr(CO)_2L$ (L = PMe_3, $P(OMe)_3$). The g matrix components are similar to those for the corresponding tricarbonyls, but the ^{31}P hyperfine coupling is significantly anisotropic, particularly for the phosphites. Assuming that the ground state is $^2A''$, the anisotropic phosphorus coupling provides a direct measure of π-back-bonding to phosphorus. As expected, the phosphite ligands prove to be better π-acceptors with ca. 1% 3p spin density; for the phosphines, the 3p spin densities are on the order of 0.3%.

Geiger and co-workers [179] have reported the spectrum of $[(biphenyl)Cr(CO)_2PPh_3]^+$, which is very similar to those of the C_6Me_6 complexes. They also obtained spectra of the binuclear cations $[(biphenyl)\{Cr(CO)_2PPh_3\}_2]^+$ and $[(biphenyl)\{Cr(CO)_2\}_2(\mu\text{-}L_2)]^+$ (L_2 = dppm, dmpe and $(AsPh_2)_2CH_2$). The spectrum of the first of these species is nearly identical to that of the mononuclear complex, suggesting that the unpaired electron is localized on one chromium center. The doubly bridged cations, on the other hand, show coupling to two ^{31}P nuclei

(with half the coupling constant) and smaller g matrix anisotropy, indicating delocalization of the odd electron over both chromium centers. This result contrasts with $[Cr_2(biphenyl)_2]^+$ (see Sect. 4.3.4) where the unpaired electron remains localized. This difference can be understood in terms of overlap of the relevant orbitals: if the z axes are parallel, d_{xy}–d_{xy} overlap in $[(biphenyl)\{Cr(CO)_2\}_2(\mu\text{-}L_2)]^+$ should be much greater than d_{z^2}–d_{z^2} overlap in $[Cr_2(biphenyl)_2]^+$.

Connelly and Johnson [180] obtained an isotropic spectrum for the acetylene complex, $[(C_6Me_6)Cr(CO)_2(RCCR)]^+$ (R = Ph), and more recent studies [181] have extended this series to R = COOEt, 4-$MeOC_6H_4$, $SiMe_3$ and $[(C_6Me_6)Cr(CO)_2(PhCCH)]^+$. The spectra are well-resolved at room temperature and show ^{13}C and ^1H couplings (for R = COOEt and the PhCCH derivative, respectively), suggesting significant delocalization of spin onto the acetylene ligand. The magnitude of the g matrix components also suggest that these complexes are distinctly different from complexes such as $[(C_6Me_6)Cr(CO)_2PPh_3]^+$. On reduction, the R = $SiMe_3$ cation undergoes an interesting rearrangement to the vinylidene complex, $(C_6Me_6)Cr(CO)_2[=C=C(SiMe_3)_2]$.

The related complexes $[(Tbtac)M(CO)_3]^+$ (Tbtac = 1,4,7-tribenzyl-1,4,7-triazacyclononane; M = Cr, Mo, W) have been reported by Beissel et al. [182]. The Cr complex gives a g matrix very similar to that for $CpCr(CO)_3$; that for the Mo complex is somewhat more anisotropic, as expected from the larger spin–orbit coupling in Mo. The g matrix for the W complex, on the other hand, is quite different with all three components less than g_e. No explanation for this anomaly is currently available.

An isotropic spectrum attributed to $TpMo(CO)_3$ was observed by Curtis and co-workers [183], but subsequent work [184] suggested that the signal was an artifact. Very recent work by Baird and co-workers [185] has shown that $TpM(CO)_3$ and $Tp^*M(CO)_3$ (M = Cr, Mo) are also similar to $CpCr(CO)_3$ both in relaxation behavior and in the general shape of the g matrices (the Mo analogs show somewhat greater anisotropy). These workers also obtained room-temperature spectra of $TpCr(CO)_2PMe_3$, $\langle g \rangle = 2.0235$, $\langle A^P \rangle = 31.6$, and $Tp'Cr(CO)_3$ (Tp′ = tetrakis(pyrazolyl)borate) observable up to 120 K.

Green and Pardy [186] have obtained isotropic spectra of $[(Ch)Mo(dppe)X]^+$ (X = Cl, Br, I). The spectra show coupling to ^{31}P, $^{95,97}Mo$, the halogen and probably the cycloheptatrienyl ring protons but were not fully interpreted. Better resolved isotropic spectra have been obtained by Whitely and co-workers for $[ChMo(dppe)(C{\equiv}CR)]^+$ (R = Ph, ^{t}Bu) [187], $[ChMo\{P(OMe)_3\}_2Cl]^+$, $[ChMo\{(dppe)NCMe]^{2+}$, $[ChW(dppe)Cl]^+$, and $[ChW(dppe)NCMe]^{2+}$ [188]. These are clearly quite different from the Cr(I) Cp and Bz piano-stool complexes in that they give well-resolved isotropic spectra at room temperature with coupling to the C_7H_7 protons. They are thus similar to $[Cr(Bz)_2]^+$ and it is tempting to suppose that the order of splitting of the t_{2g} set is inverted, leaving d_{z^2} as the SOMO. Further work is needed before this hypothesis can be verified.

Symons et al. [189] have reported the formation of anion radicals formulated as $[CpM(CO)_3I]^-$ (M = Mo, W). While these are formally d^5, they are also formal 19-electron complexes. Large iodine hyperfine couplings are observed, suggesting that the odd electron is significantly delocalized. Tyler and co-workers [190] have studied the reaction of $(C_5Ph_5)_2Mo_2(CO)_6$ with L_2 = 2,3-bis(diphenylphosphino)-maleic anhydride to generate 19-electron radicals, $(C_5Ph_5)Mo(CO)_2L_2$ where the unpaired electron is probably mostly ligand based. In addition, isotropic EPR spectra were obtained which were assigned to the apparent 17-electron complexes, $(C_5Ph_5)Mo(CO)L_2$ (L_2 bidentate) and $(C_5Ph_5)Mo(CO)_2L_2$ (L_2 monodentate). However, the ^{93,95}Mo coupling (ca. 0.5 G) and g values (2.003) suggest that the SOMO is again largely ligand-based.

4.4 Manganese(II), technetium(II) and rhenium(II)

4.4.1 Manganese(II) complexes (see Table 14)

EPR spectra of low-spin Mn(II) complexes have been elusive, in part because of the alluring distraction of high-spin Mn(II) decomposition products which have easily observed spectra. The literature is full of high-spin spectra attributed to low-spin Mn(II) and Mn(0) complexes. Thus the hexakisisocyanide complexes, $[Mn(CNR)_6]^{2+}$, are low-spin judging from magnetic susceptibilities, but the spectrum reported by Fantucci et al. [191] was an artifact, and Nielson and Wherland [192] were unable to detect a resonance down to 77 K; liquid helium temperature will probably be required. Bond et al. [193] prepared *mer*-$[Mn(CO)_3(dppm)Cl]^+$, low-spin according to the susceptibility, but the reported EPR spectrum appears to be that of a high-spin decomposition product.

Because the ^{55}Mn hyperfine interaction is large and very anisotropic in low-spin Mn(II) complexes, isotropic spectra tend to be poorly resolved and undiluted powders give very broad lines. Thus the spectrum of *trans*-$[Mn(CO)_2(dppe)_2]^{2+}$ in a powdered sample of the PF_6 salt gave a single broad line [194].

In their study of Mn(tspc) (tspc = 4,4′,4″4‴-tetrasulfophthalocyanine), Smith and co-workers [195] found that the axial diaquo adduct was high-spin but that coordinating solvents such as pyridine gave low-spin adducts. However, in most cases mixtures were obtained, and the complex spectra could not be entirely interpreted. More basic ligands such as imidazole led to autoxidation to the Mn(III) complex.

For a long time, the only well-resolved low-spin Mn(II) spectrum known was that of $[Mn(CN)_6]^{2-}$, obtained by Baker et al. [39] in a dilute single crystal of $K_4Fe(CN)_6$ at 12 K. The EPR parameters are closely analogous to those for $[Fe(CN)_6]^{3-}$ (see Sects. 3.2.2 and 4.5.3). Spectra of two low-spin organo-manganese(II) complexes were reported in the 1980s by Wilkinson and co-workers: Mn(dmpe)$_2$(*o*-xylylene) [196] and *trans*-Mn(dmpe)$_2$Me$_2$ [197], both showing hyperfine coupling to ^{55}Mn and four equivalent ^{31}P nuclei. The original interpretation of the spectrum of Mn(dmpe)$_2$(*o*-xylylene) failed to take into account the non-

TABLE 14

EPR parameters for some Mn(II) complexes[a]

Complex	g_1	g_2	g_3	A_1^{Mn}	A_2^{Mn}	A_3^{Mn}	β/deg[b]	A_{avg}^{P}	Ref.
$[Mn(CN)_6]^{4-}$	2.624	2.182	0.63	84.5	46.5	104	–	–	39
$Mn(dmpe)_2$(*o*-xylylene)	2.110	2.035	2.000	27	27	125	41	24.5	6, 196
trans-$Mn(dmpe)_2Me_2$			2.038			136	–	28	197
trans-$[Mn(dppm)_2(CO)(CNBu)]^{2+}$	2.107	2.051	1.998	30.2	20.6	146.9	–	26	199
trans-$[Mn(dppm)_2(CO)(CNallyl)]^{2+}$	2.042	2.102	1.989	21.0	7.3	147.4	8	26	199
trans-$[Mn(dppm)_2(CO)CN]^{+}$	2.046	2.121	1.984	30.0	2.4	146.1	20	26	199
cis-$[Mn(dppe)(CO)_2(PEt_3)Br]^{+}$	2.032	2.044	1.979	0	27.2	163.4	–	23 (2P) 26 (1P)	199
cis-$[Mn(dppe)(CO)_2(PEt_3)CN]^{+}$	2.086	2.048	2.004	11.0	19.8	144.0	5	24	199

[a] Hyperfine couplings in units of 10^{-4} cm^{-1}.

[b] Angle between the z principal axes of the g and A matrices assuming common y axes.

coincidence of the principal axes of the g and ^{55}Mn hyperfine matrices; the spectrum was reinterpreted [6] to give the parameters listed in Table 14. The spectrum of $Mn(dmpe)_2Me_2$ was interpreted as axial, but the matrices are almost certainly rhombic. Parameters corresponding to g_{min} are given in Table 14; many other features are resolved, but a complete interpretation has not been done. If the SOMO is $d_{x^2-y^2}$, as expected from the coupling to four equivalent ^{31}P nuclei, the value of g_{min} is anomalously high, suggesting a possible problem in calibration.

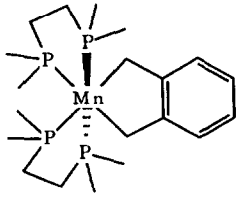

$Mn(dmpe)_2$(o-xylylene)

Carriedo et al. [198] reported the isotropic and frozen solution spectra of *trans*-$[Mn(CO)(CN^tBu)(dppm)_2]^{2+}$ in CH_2Cl_2/THF. The frozen solution spectrum was very well resolved, with hyperfine coupling to ^{55}Mn and four ^{31}P nuclei. A preliminary interpretation [6] of the EPR parameters suggested that the SOMO is primarily d_{xy} in character. Further work [199] on *trans*-$[Mn(CO)(dppm)_2L]^{2+}$ ($L=CN^tBu$, CNallyl), *trans*-$[Mn(dppm)_2(CO)CN]^+$, and *cis*-$[Mn(dppe)(CO)_2(PEt_3)X]^+$ ($X=$ Br, CN) has shown that the matrix principal axes are variably non-coincident with orientation differences ranging from near zero for the dppe complexes up to about 20° for the dppm complexes. The ^{55}Mn hyperfine coupling leads to an estimate of the 3d spin density of about 0.7 for all complexes. The principal axis non-coincidence appears to arise through d_{xy}/d_{xz} hybridization to avoid anti-bonding overlap of the SOMO with the methylene groups of the dppm ligands.

Abakumov et al. [200] reported that $Mn_2(CO)_{10}$ and $Re_2(CO)_{10}$ react with *o*-quinones to form complexes of the type $Mn(CO)_4L$. If we regard L as a catecholate dianion, then the formal oxidation state of manganese is +2. However, these complexes give EPR spectra with $\langle g \rangle$ close to g_e and very small ^{55}Mn couplings; thus they are better regarded as semiquinones complexed to Mn(I). Analogous dioxygen complexes, $Mn(CO)_4L(O_2)$ ($L=CO$, PPh_3, PBu_3, $P(OEt)_3$) have been prepared by Lindsell and Preston [201] by photolysis of $Mn_2(CO)_8L_2$ in the presence of O_2. Again, the EPR parameters suggest that these complexes are best regarded as superoxide complexes of Mn(I).

4.4.2 Nitrosyl complexes (see Tables 7 and 9)

EPR spectra of $[Mn(NO)(CN)_5]^{2-}$ [49,202,203] were reported by several groups; the parameters are consistent with the theory developed for the Cr(I) analog (see Sect. 4.3.3). Wayland and Olson [204] found that the high-spin complex

[Mn(TPP)CN] (H_2TPP = tetraphenylporphyrin) reversibly adds NO to form a low-spin nitrosyl complex with EPR parameters very similar to those of $[Mn(NO)(CN)_5]^{2-}$.

Mn(II) nitrosyl complexes, $[Mn(NO)(L_2)Cl]^{2-}$ ($L_2 = S_2COR$, S_2CSR and S_2CNR_2; (R = Et, Ph), have been studied by Garif'yanov and Luchkina [205] and by Jezierski [206]. Becalska and Hill [207] have reported isotropic spectra for $CpMn(NO)Me_2$ and $MeCpMn(NO)R_2$ (R = Me, Et, Pr).

Isotropic and frozen solution spectra of several technecium nitrosyl complexes have been reported: $[Tc(NO)(NH_3)_4(H_2O)]^{3+}$ and $[Tc(NO)Cl_5]^{2-}$ [208], $[Tc(NO)(NCS)_5]^{2-}$ [209], and $Tc(NO)(PMe_2Ph)_2Cl_3$ [210]. Mercati et al. [211] have reported EPR spectra of polycrystalline samples of $[NEt_4]_2[Re(NO)X_5]$ (X = Cl, Br).

4.4.3 "Sandwich" complexes (see Table 15)

Manganocene, $Mn(Cp)_2$, had long been known to have a high-spin ground state [212–214] and to exhibit a nearly isotropic signal near $g = 2$ when, in 1974, three groups independently found evidence for a high-spin/low-spin equilibrium, the position of which is highly medium-dependent. Orchard and co-workers [215] used photoelectron spectroscopy to probe the system, and Ammeter et al. [18,216] obtained EPR spectra in which the high-spin signal broadened and became much more complex at very low temperatures. Ammeter found that $Mn(Cp)_2$ was mainly high spin when doped into single crystals of $Mg(Cp)_2$, but in $Fe(Cp)_2$, $Ru(Cp)_2$ or $Os(Cp)_2$, the spectra were mainly low-spin below 30 K. Rettig and co-workers [217] investigated $Mn(MeCp)_2$ and found that it has a low-spin configuration in low-temperature frozen solutions. Subsequently, Robbins and co-workers [218,219] prepared $Mn(Cp^*)_2$ and found that this complex is entirely low-spin in frozen toluene and

TABLE 15

EPR parameters for manganocenes and rhenocenes[a]

Species	Medium	T/K	$g_\parallel$	$g_\perp$	$A_\parallel^M$	$A_\perp^M$	Ref.
$Mn(Cp)_2$	$FeCp_2$	4	3.519	1.223	52.3	$\leqslant 26$	216
	$RuCp_2$	4	3.548	1.069	58.7	$\leqslant 70$	18, 216
	$OsCp_2$	4	3.534	1.126			18
$Mn(MeCp)_2$	$Mg(MeCp)_2$	4	2.998	1.887	13.7	24.6	18, 216
	$Fe(MeCp)_2I$	4	3.063	1.847	11.4	24.5	18, 216
	$Fe(MeCp)_2II$	4	3.060	1.891			18
	MeCyclohexane	4	2.909	1.893			18
	Toluene	4	2.887	1.900			217
$Mn(Cp^*)_2$	$Fe(Cp^*)_2$	12	3.508	1.17	61.9		219
	Toluene	12	3.26	1.68			219
$Re(Cp^*)_2$	Toluene	10	5.081	<0.34	529	<67	224

[a] Hyperfine couplings in units of 10^{-4} cm^{-1}.

methylcyclohexane solutions and in dilute crystals of $Fe(Cp^*)_2$. An X-ray structure of $Mn(Cp^*)_2$ [220] showed that the static Jahn–Teller distortion corresponds to a ring displacement to a Z-like structure. Two groups [221–223] have studied the high-spin/low-spin equilibrium for $Mn(Cp)_2$ and a variety of derivatives using ^1H and ^2H NMR spectroscopy.

Bandy et al. [224] have recently synthesized and characterized $Re(Cp^*)_2$ and reported EPR spectra of a frozen toluene solution at 10 K. Only the parallel features were observed; the perpendicular features apparently were outside the available magnetic field range.

4.4.4 "Piano-stool" complexes (see Tables 16 and 17)

Although no spectra have been reported for the parent complex, $[CpMn(CO)_3]^+$, a large number of derivatives have been studied.

Connelly et al. obtained poorly resolved isotropic spectra of the Mn(II) piano-stool complexes $[(MeCp)Mn(CO)L_2]^+$ (L = PPh_3, $PMePh_2$, dppe/2) [225], and $[(\eta^5\text{-}C_6H_6Ph)Mn(CO)dppe]^+$ [226]. This work was followed up in a more complete study by Pike et al. [227] of $[CpMn(CO)L_2]^+$ (L = PMe_3, PPh_3, dppe/2, dmpe/2, dppm/2), $[CpMn(CO)_2PPh_3]^+$, $[(MeCp)Mn(CO)dppe]^+$, $[(\eta^5\text{-}C_6H_6Ph)Mn(CO)L_2]^+$ (L = PMe_3, dppe/2, dmpe/2), $[(\eta^5\text{-}C_6H_6Ph)Mn(CO)_2L]^+$ (L = PMe_3, PBu_3), $[(\eta^5\text{-}C_6HMe_5Ph)Mn(CO)dppe]^+$, and $[(\eta^5\text{-}C_7H_8Ph)Mn(CO)dppe]^+$, all in frozen $CH_2Cl_2/C_2H_4Cl_2$. Isotropic spectra were resolved in only a few cases. The g matrices of the monocarbonyl complexes were similar to that for $CpCr(CO)_3$, and the ^{55}Mn hyperfine interaction was consistent with a $^2A'$ ground state. In all cases, the principal axes of the g and ^{55}Mn hyperfine matrices had significantly different orientations. Spectra of the dicarbonyl complexes were different, particularly in

TABLE 16

Isotropic EPR parameters for Mn piano-stool complexes

Species	$\langle g \rangle$	$\langle A^M \rangle^a$	$\langle A^L \rangle^a$	Ref.
$Cp^*Mn(CO)_2S^tBu$	2.03	48.7		228
$Cp^*Mn(CO)_2SePh$	2.07	44.5		228
$CpMn(CO)_2(3\text{-}MeC_6H_4NH)$	2.0114	47		230
$Cp^*Mn(CO)_2(4\text{-}MeC_6H_4NH)$	2.0140	47.8		232
$MeCpMn(CO)_2(C_6H_5NH)$	2.0136	47.5		232
$Cp^*Mn(CO)_2(4\text{-}NH_2C_6H_4NH)$	2.0114	42.4	7 (NH), 6 (N)	232
$MeCpMn(CO)_2(4\text{-}NMe_2C_6H_4NH)$	2.0086	39.8	7.2 (NH), 6.1 (N)	232
$MeCpMn(CO)_2$(imidazolate)	2.035	58		232
$MeCpMn(CO)_2(NCCHCN)$	2.038	56		232
$MeCpMn(CO)_2$(indolate)	2.025	53		232
$MeCpMn(CO)_2(Ph_2NNH)$	2.015	49.4	5.6 (N)	232

[a] In units of 10^{-4} cm^{-1}.

TABLE 17

Anisotropic EPR parameters for Mn piano-stool complexes[a]

Complex	g_1	g_2	g_3	A_1^{Mn}	A_2^{Mn}	A_3^{Mn}	β/deg[b]	A_{avg}^{P}
$[CpMn(CO)(dppe)]^+$	2.188	2.021	2.001	37.6	0	114.2	43	28.5
$[(\eta^5\text{-}PhC_6H_6)Mn(CO)(dppe)]^+$	2.080	2.057	1.994	39.9	0	141.8	27	27.3
$[(\eta^5\text{-}PhC_6HMe_5)Mn(CO)(dppe)]^+$	2.080	2.058	1.991	44.2	0	142.0	22	25.9
$[(\eta^5\text{-}PhC_7H_8)Mn(CO)(dppe)]^+$	2.050	2.033	1.996	44.7	0	146.9	21	24.0
$[CpMn(CO)(dppm)]^+$	2.164	2.015	1.992	43.2	0	124.0	29	30.0
$[CpMn(CO)(PMe_3)_2]^+$	2.141	2.032	1.997	16.0	16.5	119.0	55	31.7
$[CpMn(CO)_2(PPh_3)]^+$	2.188	2.034	2.002	10	32.9	98.4	74	29.8

[a] In $CH_2Cl_2/C_2H_4Cl_2$ at 120 K; data from ref. 227; hyperfine couplings in units of 10^{-4} cm^{-1}.

[b] Angle between the z principal axes of the g and A matrices assuming common y axes.

the orientations of the matrix principal axes, and are believed to have $^2A''$ ground states.

Along similar lines, Winter et al. [228] obtained isotropic spectra of $Cp^*Mn(CO)_2L$ (L = S^{t}Bu, SePh), and Sellmann et al. [229,230] found that the Mn(I) *m*-toluidine complex $CpMn(CO)_2(RNH_2)$ (R = 3-$CH_3C_6H_4$) is readily oxidized to $CpMn(CO)_2(RNH)$, $\langle g \rangle = 2.011$, $\langle A^{Mn} \rangle = 47$, which Sellmann characterized as a Mn-stabilized aminyl radical. Gross and Kaim [231] extended this series to $CpMn(CO)_2L$ (L = 4-$Me_2NC_6H_4NH^-$, 4-$CH_3C_6H_4NH^-$, 4-NH-$C_5H_4N^-$ and $C_3H_3N_2^-$) and pointed out that the departure of $\langle g \rangle$ from g_e and the relatively large ^{55}Mn coupling suggest that these species are better regarded as low-spin Mn(II) complexes. Spectra were also obtained of $CpMn(CO)_2$(4-cyanopyridine) and $[\{CpMn(CO)_2\}_2L]^-$ (L = 4,4'-bipyridyl, pyrazine or 1,4-dicyanobenzene). In these spectra, $\langle g \rangle = 2.000$–$2.001$ and $\langle A^{Mn} \rangle = 4$–$7$, so that these complexes are indeed radical anions stabilized by coordination to the $CpMn(CO)_2$ group. Gross and Kaim [232] have further extended this study to a variety of complexes $(C_5H_{5-n}Me_n)Mn(CO)_2L$ ($n = 0$, 1 and 5), where L is an anionic unsaturated nitrogen ligand, including the conjugate bases of imidazole, benzimidazole, benztriazole, purine, adenine, indole and methanedinitrile. A reasonably good correlation was found between $\langle g \rangle$ and $\langle A^{Mn} \rangle$, reflecting the effect on these parameters of spin delocalization onto the ligands.

4.5 Iron(III), ruthenium(III) and osmium(III)

EPR parameters have been reported for hundreds of Fe(III), Ru(III) and Os(III) complexes. In nearly all cases, the spectra are devoid of hyperfine (or superhyperfine) structure so that discussion necessarily has focussed on the *g* matrix components. Most interpretations have used the Bleaney–O'Brien theory to compute the ligand-field parameters Δ/λ and V/λ (see Sect. 3.2.2). König [233] discussed the theory as applied to Fe(III) complexes and reviewed representative examples of Fe(III) EPR spectra.

4.5.1 High-spin and low-spin configurations

Virtually all Ru(III) and Os(III) complexes have the low-spin configuration, but Fe(III) complexes are much more varied. With classical weak-field ligands (π-donors) such as halide ions, Fe(III) complexes have the high-spin configuration, but strong-field ligands (π-acceptors) such as CN^- give low-spin ground states. With ligands of intermediate π-donor/acceptor ability, the case becomes much less clear. It has long been known that many complexes of iron(III) are near the crossover point between ^6A and ^2T ground states, and, in some systems, the two spin states are present simultaneously. The early work on spin equilibria was reviewed by Martin and White [234] and the theory was discussed by Harris [235]. Spin state transitions were first observed for iron(III) dithiocarbamates, and these have been extensively investigated; this work was reviewed by Coucouvanis [236].

Intermolecular interactions (ferromagnetic or antiferromagnetic coupling), which are often important in spin state transitions, have been investigated by Hendrickson et al. [237]. A recent review by Bacci [238] discusses the role of vibronic coupling in the interconversion of spin states.

In general, when both configurations are observable, the doublet state is lower in energy and predominates at low temperatures while the higher entropy sextet state becomes important at high temperatures. (If the sextet state is lower in energy, its favorable entropy will ensure its dominance at all temperatures.) When both configurations are simultaneously present in significant concentrations, the rate of interconversion is often sufficiently rapid to broaden the resonances, leading to a featureless low-spin signal near $g=2$ which is difficult to distinguish from one of the high-spin features. When the energy difference is sufficiently large or the rate of spin conversion is sufficiently slow, however, well-resolved spectra typical of low-spin d^5 systems (one g component less than g_e, the other two larger than g_e) are observed at 4 K and sometimes even at 77 K.

The nature of the high spin/low spin equilibrium is usually highly medium-dependent. Changes in solvent or counterion have often been found to turn the effect on or off or substantially change the temperature range over which the two configurations are simultaneously present. Indeed, in a few cases, magnetic moment vs. temperature curves show a sharp transition, suggesting a cooperative transition and thus strong interactions between paramagnetic centers.

4.5.2 Halide complexes (see Table 18)

A spectrum attributed to *mer*-$Fe(PMe_3)_3Cl_3$ was reported by Walker and Poli [239]; although the anisotropic g matrix (2.647, 2.012, 1.695) is consistent with a Fe(III) complex with a near-degenerate ground state, the assignment needs supporting evidence.

In a seminal paper, Hudson and Kennedy [38] reported EPR parameters for a number of chloride and bromide complexes of Ru and Os: *mer*-RuL_3Cl_3 ($L=PMe_2Ph$, PEt_2Ph, PBu_2Ph, $AsPr_3$, SEt_2, S^iPrPh, py), *mer*-$Ru(SMePh)_3Br_3$, *trans*-$[Ru(depe)_2Cl_2]^+$, *cis*- and *trans*-$[Ru(dmpe)_2Cl_2]^+$, *trans*-$[Ru(PEt_3)_2Cl_4]^-$, *mer*-OsL_3Cl_3 ($L=PMe_2Ph$, PBu_2Ph, $AsMe_2Ph$, py), *mer*-$Os(PBu_3Ph)_3Br_3$, *fac*-$Os(PBu_2Ph)_3Cl_3$, and *trans-trans-trans*-$[Os(PEt_3)_2(C_2H_4)_2Cl_2]^+$. Hill [240] studied *mer*-$Os(PEt_2Ph)_3Cl_3$ diluted in a single crystal of the rhodium analog. Kremer [241] reported spectra of $[Os(CO)(py)X_4]^-$ ($X=Cl$, Br), and $[Os(CO)_2Br_4]^-$. Sarma et al. [242] have reported strangely similar EPR parameters for the mer and fac isomers of $Ru(DMSO)_3Cl_3$.

DeSimone [37] has reported spectra of $[M(diars)_2Cl_2]^+$ ($M=Fe$, Ru, Os; diars = 1,2-$C_6H_4(Me_2As)_2$). Manoharan et al. [243] reported EPR spectra of $Ru(AsPh_3)_2(CH_3OH)Cl_3$, *trans*-$[Ru(AsPh_3)_2Cl_4]^-$, and the trigonal bipyramidal complex $Ru(AsPh_3)_2Cl_3$. This work was followed by studies by Morrazzoni and co-workers [244–246] of *mer*-$M(AsPh_3)_3Cl_3$, $ML(p\text{-tolyl-NC})_2X_3$ ($M=Ru$, Os),

TABLE 18
EPR parameters for halide complexes of Ru(III) and Os(III)

Species	Medium	T/K	g_x	g_y	g_z	Ref.
mer-$Ru(PMe_2Ph)_3Cl_3$	Et_2O	100	2.99	2.03	1.66	38
cis-$[Ru(dmpe)_2Cl_2]^+$	MeOH	100	2.59	2.13	1.88	38
trans-$[Ru(dmpe)_2Cl_2]^+$	MeOH	100	3.18	1.88	1.57	38
trans-$[Ru(PEt_3)_2Cl_4]^-$	$Me_2CO/MeOH$	100	2.51	2.51	1.64	38
trans-$[Ru(AsPh_3)_2Cl_4]^-$	Powder	77	2.49	2.49	1.73	243
mer-$Ru(SMePh)_3Cl_3$	$CHCl_3$	100	2.70	2.29	1.68	38
mer-$Ru(py)_3Cl_3$	$Me_2CO/CHCl_3$	100	3.97	–	–	38
trans-$Ru(AsPh_3)_2Cl_3$	C_6H_6	77	2.469	2.469	1.946	244
mer-$Os(PBu_2Ph)_3Cl_3$	Single crystal	100	3.30	1.65	0.36	38
fac-$Os(PBu_2Ph)_3Cl_3$	EPA	100	1.83	1.83	1.28	38
trans-$[Os(depe)_2Cl_2]^+$	$CHCl_3$	100	3.19	1.73	–	38
mer-$Os(py)_3Cl_3$	$Me_2CO/CHCl_3$	100	3.75	1.37	–	38
trans-$[Os(CO)(py)Cl_4]^-$	NEt_4^+ salt	4	2.55	2.55	1.72	240
trans-$[Os(CO)_2Br_4]^-$	NBu_4^+ salt	4	2.46	2.46	1.81	240

[a] In units of 10^{-4} cm^{-1}.

$RuL_2(CH_3OH)X_3$, and the trigonal pyramidal complexes RuL_2X_3 ($L = PPh_3$, $AsPh_3$; $X^- = Cl^-$, Br^-). Mehdi and Agarwala reported spectra of several of these compounds, together with a series of diketonate complexes $RuL'_2(L_2)X_2$ ($L' = PPh_3$, $AsPh_3$; L_2 = acac, $(PhCO)_2CH$, PhCOCHCOMe; $X^- = Cl^-$, Br^-) [247], and Ru(3-bromotropolonate)L_2X_2 ($L = PPh_3$, $AsPh_3$; $X^- = Cl^-$, Br^-) [248].

Catalá et al. [249] obtained an axial spectrum for $Ru(PMe_2Ph)_2(SC_6F_5)_3$ (an X-ray structure showed that the complex is approximately octahedral with an *ortho*-fluorine atom occupying the sixth coordination site).

4.5.3 Cyanide complexes (see Table 19)

The spectrum of $[Fe(CN)_6]^{3-}$ in a single crystal of $K_3Co(CN)_6$ was obtained by Bleaney and co-workers [39] during the formative years of EPR spectroscopy. The interpretation of the spectrum prompted a theoretical approach which was discussed above (see Sect. 3.2.2). Subsequent to this work, X-ray studies by Kohn and Townes [250(a)] and by Reynhardt and Boeyens [250(b)] showed that $K_3Co(CN)_6$ exhibits polytypism with at least five different crystal modifications: one-layer (1M), three-layer (3M) and seven-layer (7M*) monoclinic and two-layer (2Or) and four-layer (4Or) orthorhombic. De Boer and co-workers [250(c)] have very recently reported spectra of $[Fe(CN)_6]^{3-}$ in the 1M, 3M and 2Or modifications of $K_3Co(CN)_6$. The 1M results are consistent with the results reported by Bleaney [39] with two ions per unit cell giving distinguishable EPR signals. The 3M and 2Or structures show six and four distinguishable ions per unit cell, respectively. Resonances corresponding to the different sites have differently oriented g matrix

TABLE 19
EPR parameters for Fe(III) cyanide complexes

Species	Medium	T/K	g_x	g_y	g_z	Ref.
$[Fe(CN)_6]^{3-}$	$K_3Co(CN)_6$	20	2.35	2.10	0.915	39
$[Fe(CN)_6]^{3-}$	I-NaCl	4	2.262	2.918	0.635	251(b)
	II		1.189	2.843	1.208	
	III		2.488	0.215	2.383	
$[Fe(CN)_6]^{3-}$	I-KCl	4	2.079	3.056	0.400	251(b)
	II		1.048	2.941	1.314	
$[Fe(CN)_5NH_3]^{2-}$	$Na_2[Fe(NO)(CN)_5]\cdot 2H_2O$	4	0.845	2.177	2.995	252
$[Fe(en)(CN)_4]^-$	$K[Co(en)(CN)_4]\cdot H_2O$	4	3.15	1.99	0.82	253
$[Fe(bpy)(CN)_4]^-$	$H[Fe(bpy)(CN)_4]\cdot 2H_2O$	77	2.50	2.30	1.65	254
$[Fe(phen)(CN)_4]^-$	$H[Fe(phen)(CN)_4]\cdot 2H_2O$	77	2.7	2.7	1.6	254
cis-$[Fe(bpy)_2(CN)_2]^+$	DMA/water	73	2.74	2.47	1.54	255
cis-$[Fe(phen)_2(CN)_2]^+$	DMA/water	73	2.63	2.63	1.42	255

principal axes, and the different hosts give slightly different g matrix principal values. These results point to the importance of understanding the detailed structures of host crystals in EPR studies. On the other hand, the EPR spectra gave a clear distinction amongst the different crystal modifications and sites within a crystal, details which are obtained only from weak reflections in an X-ray study. In any case, this work clearly indicates that the large g matrix anisotropies for $[Fe(CN)_6]^{3-}$ reflect the low symmetry of the crystal sites rather than Jahn–Teller distortions of a hypothetical isolated $[Fe(CN)_6]^{3-}$ ion.

Box et al. [251(a)] obtained spectra of $[Fe(CN)_6]^{3-}$ in an X-irradiated single crystal of $Na_4Fe(CN)_6\cdot 10H_2O$. Three different sites were observed with slightly different g matrix components, but similarly oriented principal axes, one of which was in a C–Fe–C direction. The three sites may correspond to different arrangements of other radiation-induced defects near the $[Fe(CN)_6]^{3-}$ center, but no attempt was made at further interpretation. De Boer and co-workers [251(b)] have recently reported a study of a more easily understood system. The spectra of $[Fe(CN)_6]^{3-}$ in dilute single crystals of NaCl and KCl show resonances from several distinguishable sites. Since the complex replaces an MCl_6^{5-} unit, there must be two cation vacancies which may be arranged in a variety of ways relative to the $[Fe(CN)_6]^{3-}$ center. Using the orientations of the g matrix principal axes, three of the sites were identified with specific arrangements of cation vacancies as shown in Fig. 10.

Ezzeh and McGarvey [252] obtained the spectrum of $[Fe(NH_3)(CN)_5]^{2-}$ in a single crystal of $Na_2[Fe(NO)(CN)_5]\cdot 2H_2O$. The principal axes of the g matrix are along the Fe–N bond and bisect the equatorial C–Fe–C bond angles, suggesting that the SOMO is d_{xz} or d_{yz}. ^{14}N hyperfine structure was resolved when the field was oriented along the Fe–N bond ($A_z^N = 8.1$) but not for the other two axes ($A_{x,y}^N < 3$). Since NH_3 is not capable of π-back-bonding, the d_{xz} and d_{yz} orbitals lie

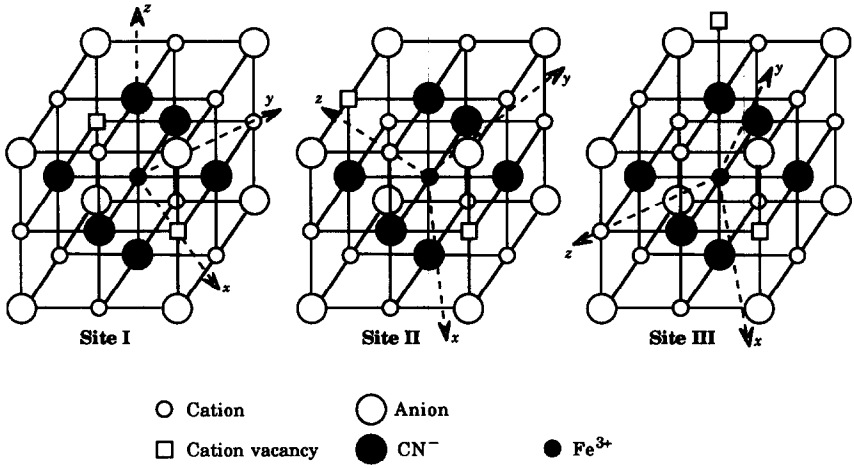

Fig. 10. Models for Sites I, II and III of $Fe(CN)_6^{3-}$ in NaCl and KCl. The broken lines show the orientations of the principal axes of the g matrix. After Wang et al. [251(b)].

above d_{xy}, and the complex has a ^2E ground state; Jahn–Teller distortion via the equatorial scissors bending mode removes the degeneracy, leaving one of these orbitals as the SOMO. Thus the electronic structure is analogous to that of *trans*-$V(PMe_3)_2(CO)_4$ (see Sects. 2.1.2 and 4.2.1).

The spectrum of $[Fe(en)(CN)_4]^-$ in $K[Co(en)(CN)_4]\cdot H_2O$ [253] exhibits a surprisingly large g matrix anisotropy, comparable with that of $[Fe(CN)_6]^{3-}$. In contrast, polycrystalline samples of $H[FeL_2(CN)_4]\cdot 2H_2O$ and *cis*-$[Fe(L_2)_2(CN)_2]ClO_4$ (L_2 = bpy, phen) show smaller anisotropies [254]. The latter complexes in frozen DMA/H_2O solutions [255] give similar anisotropies, although the parameters are somewhat different than those from the polycrystalline samples. Reiff and DeSimone [255] concluded that the electronic structures of the bpy and phen complexes are similar to those of the tris-chelate complexes with d_z^2 as the SOMO (see Sect. 4.5.4).

A species believed to be $[Fe(NO)(CN)_5]^-$ was produced by γ-irradiation of $Na_2[Fe(NO)(CN)_5]$ [26] (see Sects. 3.1.1 and 4.3.3).

4.5.4 Tris-bipyridyl and related N_6 complexes (see Table 20)

Fe, Ru and Os bipyridyl and related complexes have been studied very intensively, largely because of interest in their use in artificial photosynthesis schemes [256,257]. DeSimone and Drago [13] studied the EPR spectra of $[M(L_2)_3]^{3+}$ (M = Fe, Ru, Os; L_2 = bpy, phen) as well as the 4,4′-dimethyl- and 5,5′-dimethylbipyridyl complexes of Fe(III). The complexes were diluted into the corresponding $Co(III)PF_6$ salts and spectra were obtained of polycrystalline samples. Parts of this work were repeated by Merrithew et al. [254] and Quayle and Lunsford [258] have reported the spectrum of $[Ru(bpy)_3]^{3+}$ in a zeolite.

TABLE 20
EPR parameters for bpy and phen complexes of Fe, Ru and Os[a]

Complex	$g_\perp$	$g_\parallel$	η	k	$g_\parallel$ (calcd.)
$[Fe(bpy)_3]^{3+}$	2.61	1.61	0.331	1.063	+1.61
			3.009	1.230	−1.61
$[Fe(phen)_3]^{3+}$	2.69	1.19	0.499	0.990	+1.19
			1.994	1.193	−1.19
$[Ru(bpy)_3]^{3+}$	2.64	1.14	0.524	0.931	+1.14
			1.973	1.155	−1.14
$[Ru(phen)_3]^{3+}$	2.63	1.00	0.578	0.911	+1.00
			1.797	1.124	−1.00
$[Os(bpy)_3]^{3+}$	2.49	<0.4	3.937[b]	1.191[b]	−1.74
$[Os(phen)_3]^{3+}$	2.43	<0.4			

[a] In $[Co(bpy)_3](PF_6)_3$ or $[Co(phen)_3](PF_6)_3$ at 77 K; data from ref. 13.
[b] From Kober and Meyer [260].

In their original work, DeSimone and Drago [13] interpreted the EPR parameters as suggesting a $a_1^2e^3$ ground state configuration in opposition to theoretical expectations (see Sect. 2.1.3). However, a study of $[Fe(phen)_3]^{3+}$ in a single crystal of $[Fe(phen)_3](ClO_4)_3 \cdot H_2O$ [259] showed that the principal axis corresponding to $g_\parallel$ is parallel to a C_3 axis of the complex, suggesting a $^2A_1$ ground state. Kober and Meyer [260] re-interpreted the data for $[Fe(bpy)_3]^{3+}$ using a re-worked theoretical treatment of spin–orbit coupling for a low-spin d^5 system in D_3 symmetry. Although the basic theory appears to be correct, their equations for the g components do not reduce to the perturbation theory results in the limit of small λ/Δ. Equations for the g components given by McGarvey [31] can be modified to apply to a d^5 system in a trigonal ligand field

$$g_\parallel = g_e \cos 2\gamma - 2k \sin^2\gamma \tag{27a}$$

$$g_\perp = g_e \cos^2\gamma + \sqrt{2}k \sin 2\gamma \tag{27b}$$

where γ is given by eqn. (28), $\eta = \lambda/\Delta$, and k is the orbital reduction factor.

$$\tan 2\gamma = \frac{\sqrt{2}\eta}{1-\eta/2} \tag{28}$$

Applying these expressions to the data of DeSimone and Drago [13] for $[Fe(bpy)_3]^{3+}$ and $[Ru(bpy)_3]^{3+}$, assuming that $g_\perp$ is positive but allowing $g_\parallel$ to be either positive or negative, we obtain the values of η and k given in Table 20. Since configuration interaction can lead to values of k greater than unity, there is no obvious way to choose between positive and negative $g_\parallel$. If Δ were constant, η would be proportional to λ and should increase in the series Fe, Ru, Os. However, Kober and Meyer [260] argue that Δ should increase in this series, paralleling the octahedral

splitting Δ_{oct}; if this is so, $g_{\parallel}$ is probably negative for all three complexes. No parallel feature was detected in the spectrum of $[Os(bpy)_3]^{3+}$, but Kober and Meyer [260] found two features in the near-IR spectrum which they assigned to transitions among the "t_{2g}" levels. From these band maxima, they were able to obtain estimates of η and k which, when substituted into eqns. (27a,b) give $g_{\perp}$ in perfect agreement with experiment and predict $g_{\parallel} = -1.74$. If this value is correct, the parallel feature should have been observable; it is unclear why it was not.

EPR spectra for several related complexes have been reported: $[Fe(tpy)_2]^{3+}$ in frozen H_2SO_4 (tpy = 2,6-(2'-pyridyl)pyridine) [261], *cis*-$[Fe(bpy)_2R_2]^{+}$ (R = Me, Et, ^{n}Pr) [262], $[Ru(bpy)(DPA)_2]^{+}$ and $[Ru(bpy)_2(DPA)]^{2+}$ (DPA = di-(2-pyridyl)-amide) [263].

4.5.5 Ammine complexes (see Table 21)

The spectrum of $[Ru(NH_3)_6]^{3+}$, obtained many years ago by Griffiths et al. [264], was re-interpreted by Daul and Goursot [265].

There have been several other reports of EPR spectra of ammine complexes. Kaplan and Navon [266] and Sakaki et al. [267] have reported spectra of $[M(NH_3)_5X]^{2+}$ (M = Ru, Os; X = Cl, Br, I). The latter group [268] has also reported spectra of *trans*-$[Ru(NH_3)_4X_2]^{+}$ (X = Cl, Br), *trans*-$[Ru(en)_2Cl_2]^{+}$, and $[Ru(CO)Cl_5]^{2-}$. A recent report by de Rezende et al. [269] added *trans*-$[Ru(NH_3)_4\{P(OEt)_3\}(H_2O)]^{3+}$ to the list. Raynor and co-workers have measured spectra of $[Fe(cyclam)X_2]^{+}$ ($X^- = Cl^-, Br^-, NCS^-$) [270], *cis*-$[Ru(en)_2Cl_2]^{+}$, *trans*-$[Ru(en)_2X_2]^{+}$ (X = Cl, Br, I, SCN), $[Ru(cyclam)Cl_2]^{+}$, and *trans*-$[Ru(dadn)X_2]^{+}$ (X = Cl, Br), in water, DMF, DMSO, and HMPA, together with a host of solvolysis products [271].

DeSimone [37] has briefly reported EPR parameters for $[Fe(en)_3]^{3+}$, and

TABLE 21

EPR parameters for ammine complexes of Fe, Ru and Os

Complex	Medium	T/K	g_x	g_y	g_z	Ref.
$[Fe(en)_3]^{3+}$			2.68	2.68	<0.6	37
$[Fe(diammac)]^{3+}$	DMF/H_2O	77	2.841	2.463	1.631	273
$[Fe(cyclam)Cl_2]^{+}$	DMSO	77	3.26	2.23	1.15	270
$[Ru(NH_3)_6]^{3+}$	$[Ru(NH_3)_6]Cl_3 \cdot 3HgCl_2$	20	2.21	2.05	1.5	264
$[Ru(en)_3]^{3+}$	$[Rh(en)_3]Cl_3 \cdot NaCl \cdot 6H_2O$	4	2.640	2.640	0.330	272
$[Ru(NH_3)_5Cl]^{2+}$	$[Co(NH_3)_5Cl]Cl_2$	77	2.98	1.51	0.99	267
trans-$[Ru(NH_3)_4Cl_2]^{+}$	*trans*-$[Co(NH_3)_4Cl_2]Cl$	77	3.33	1.54	1.18	268
trans-$[Ru(en)_2Cl_2]^{+}$	$THF/DMF/CHCl_3$	77	3.14	2.25	1.11	268
trans-$[Ru(en)_2Br_2]^{+}$	DMF	77	3.02	2.36	0.99	271
cis-$[Ru(en)_2Cl_2]^{+}$	DMF	77	2.82	2.41	1.02	271
$[Ru(cyclam)Cl_2]^{+}$	DMF	77	3.18	1.95	1.16	271
$[Os(NH_3)_5Cl]^{2+}$	$[Co(NH_3)_5Cl]Cl_2$	77	2.41	1.69	1.47	267

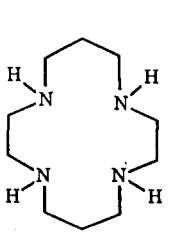

cyclam

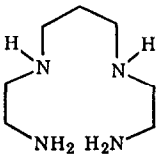

dadn

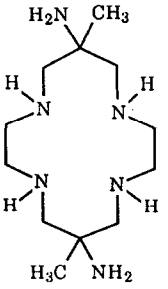

diammac

Stanko et al. [272] have reported the spectrum of $[Ru(en)_3]^{3+}$ diluted in a single crystal of $[Rh(en)_3]Cl_3 \cdot NaCl \cdot 6H_2O$. The ethylenediamine complexes give axial g matrices, suggesting electronic structures qualitatively similar to those of the corresponding bpy complexes. Bernhardt et al. [273,274] recently reported EPR parameters for $[Fe(diammac)]^{3+}$. With six similar ligands, the coordination sphere is nearly octahedral and consequently the g matrix is quite anisotropic.

4.5.6 Porphyrin and other N_4X_2 complexes (see Table 22)

One of the major applications of EPR spectroscopy to iron(III) chemistry has been in the study of porphyrin complexes in biological macromolecules, both directly

TABLE 22

EPR parameters for Fe(III) porphyrin and other N_4X_2 complexes

Complex	Medium	T/K	g_x	g_y	g_z	Ref.
$[Fe(TPP)(4\text{-}NH_2py)_2]^+$	CH_2Cl_2	100	2.830	2.289	1.603	284
$[Fe(TPP)(pyrazole)_2]^+$	CH_2Cl_2	100	2.615	2.378	1.714	284
$[Fe(TPP)(s\text{-}triazine)_2]^+$	CH_2Cl_2	100	2.747	2.284	1.646	284
$[Fe(TPP)(Im)_2]^+$	CH_2Cl_2	100	2.869	2.287	1.563	284
$[Fe(TPP)(N\text{-}MeIm)_2]^+$	CH_2Cl_2	100	2.886	2.294	1.549	284
$[Fe(TPP)(2\text{-}MeIm)_2]^+$	CH_2Cl_2	4	3.399	(1.74)	1.188	284
$[Fe(PPIX)(2\text{-}MeIm)_2]^+$	CH_2Cl_2	2	3.48	2.36	1.05	285
$[Fe(TPP)(py)_2]^+$	CH_2Cl_2	4	3.4	(1.7)	1.2	284
$[Fe(PPIX)(py)_2]^+$	CH_2Cl_2	2	3.43	2.25	0.98	285
$[Fe(TPP)(py)_2]^+$	Crystal, ClO_4 salt	6	3.70	1.12	0.46	286
$[Fe(TPP)(CN)_2]^-$	Crystal, K salt	6	3.70	1.05	0.52	286
$[Fe(TPP)(SPh)_2]^-$	Crystal, K salt	160	2.336	2.215	1.962	280
Fe(OEP)(tht)(SPh)	Toluene	95	2.38	2.27	1.93	281
$[Fe(TPP)(tht)_2]^+$	CH_2Cl_2	10	2.89	2.37	1.46	302
Fe(TPP)Me	Toluene	115	2.60	2.27	1.89	301
$[Fe(PC)(OH)_2]^-$	Powder	110	2.31	2.11	1.96	305
$[Fe(dmg)_2(Im)_2]^+$	Powder	295	2.28	2.28	1.96	303
$[Fe(dmgb)Cl_2]^-$	CH_3CN	110	2.341	2.191	1.962	304

and in model systems. Reviews of this work by Blumberg et al. [275,276], Weissbluth [277,278], and Smith and Pilbrow [10] have concentrated on biological systems. In the following, we will confine our attention to model systems, primarily axial adducts of Fe(III) complexes of tetraphenylporphyrin (TPP), octaethylporphyrin (OEP) and protoporphyrin IX (PPIX) and derivatives thereof.

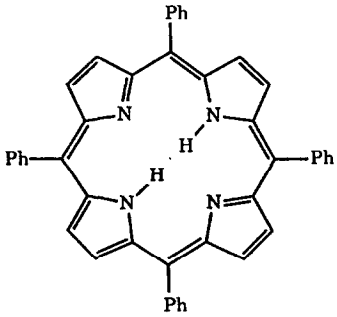

H_2TPP

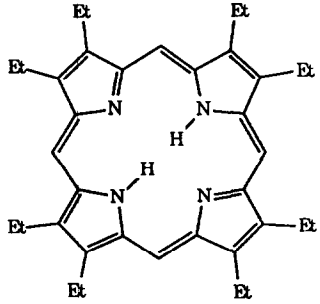

H_2OEP

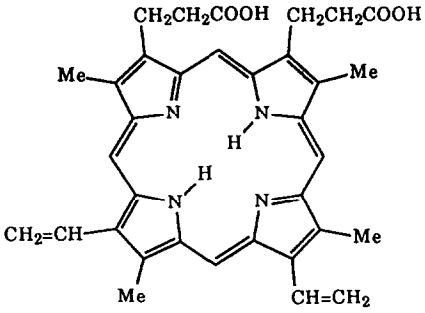

H_2PPIX

The porphyrin ring is weakly π-donating so that d_{xy} lies lower than d_{xz} and d_{yz}. If the axial ligands were purely σ-donating, the d_{xz}/d_{yz} degeneracy would remain and a Jahn–Teller distortion would be expected. However, in general, π-interactions of the axial ligands lift the degeneracy, and, with an appropriate definition of axes, the energy level diagram of Fig. 8 results. Consider a π-donor ligand. If the ligand p-π orbital is normal to the xz plane (taking z as the normal to the porphyrin ring and x as one of the Fe–N bond vectors), a simple perturbation theory treatment suggests that $g_x < g_y < g_z$, i.e. the g_{inter} axis corresponds to the direction of the p-π orbital.

Strouse and co-workers have reported single-crystal EPR measurements on several Fe(III) TPP complexes: [K(18-crown-6)][Fe(TPP)$(SPh)_2$] [279], Fe(TPP)(SR)(HSR) (R = Ph, *m*-tolyl, benzyl, i-amyl), and Fe(NH_2TPP)(SPh)(HSPh) (H_2NH_2TPP = tetra-(*o*-aminophenyl)porphyrin) [280]. In every case, the principal

axis of g_{max} was close (usually within 10°) to z as expected, but the g_{min} axis, though often close to x, was more variable. Strouse and co-workers show that d_{xz}/d_{yz} hybridization occurs when the ligand twists such that p-π is no longer normal to the xz plane. As shown in Fig. 11, the g axes twist in the opposite sense so that neither axis is in the p-π direction (see Sect. 3.1.3 for a detailed discussion of a similar effect for d_{xy}/d_{xz} hybridization). When the ligand has twisted 45°, one of the g axes is again in the p-π direction, but now it corresponds to g_{min}.

In their work on Fe(III) hemes and related proteins, Blumberg et al. [275,276] found that a plot of V/Δ vs. Δ/λ ("rhombicity" vs. tetragonal splitting) provides a means of classifying axial ligands and thus of characterizing the heme site in proteins. Several groups have collected spectra of numerous model systems to extend and refine this classification scheme [281–284]. Although the original classification was largely empirical, Strouse and co-workers [280] have put the correlation on a firmer basis. Consider the π-interaction of the t_{2g} metal orbitals with ligand orbitals. Let the energy of interaction be π when the d-orbital is antisymmetric with respect to the symmetry plane of the ligand and π' when the d-orbital is symmetric with respect to the symmetry plane. Thus, the π interaction energies with the four pyrrole groups are $2\pi_p$ for d_{xz} and d_{yz}, $4\pi_p'$ for d_{xy}. For two axial ligands with xz symmetry planes (see Fig. 11), the d_{xz} and d_{yz} interaction energies are $2\pi_a'$ and $2\pi_a$, respectively. Thus, if we ignore differences in σ-interaction energies, the ligand-field parameters are given by the equations

$$V = E(d_{yz}) - E(d_{xz}) = 2(\pi_a - \pi_a') \tag{29a}$$

$$\Delta = [E(d_{xz}) + E(d_{yz})]/2 - E(d_{xy}) = (\pi_a + \pi_a') + (2\pi_p - 4\pi_p') \tag{29b}$$

For axial ligands which are similar to pyrrole (e.g. imidazole), we expect $\pi_a \approx \pi_p$, $\pi_a' = \pi_p'$, so that $V/\Delta \approx 2/3$. Strouse presents a correlation which suggests that $(2\pi_p$—

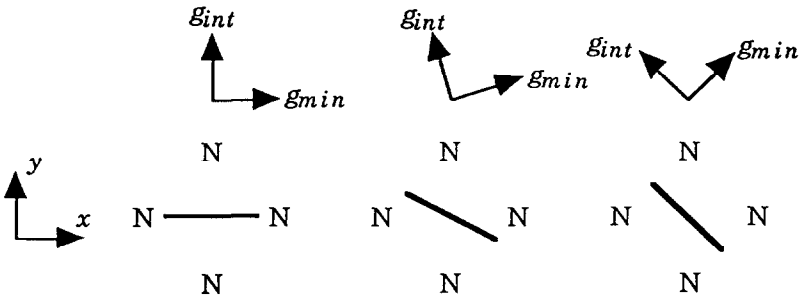

Fig. 11. The effect of rotation of the plane of axial ligands in an Fe(III) porphyrin complex is to rotate the in-plane g matrix principal axes in the opposite sense.

$4\pi_p'$) is near zero so that, more generally, the rhombicity parameter is expected to be a measure of the asymmetry of the axial ligand interaction (eqn. (30)).

$$\frac{V}{\Delta} \approx 2\frac{\pi_a - \pi_a'}{\pi_a + \pi_a'} \tag{30}$$

For TPP, OEP and PPIX bis-L_2 complexes, where L is an unhindered imidazole or a basic pyridine (e.g. 4-aminopyridine), spectra are well resolved at 77 K, $g_{max} \approx 2.7$–2.8 and $V/\Delta \approx 0.61$–0.67 [284], as expected from the analysis given above. For hindered imidazoles or unactivated pyridines, on the other hand, spectra are only observable at lower temperatures. Powder or frozen-solution spectra typically show a well-resolved feature at low field ($g \approx 3.4$), a feature near $g = 2.4$, and a very broad feature near $g = 1$, usually together with a high-spin feature near $g = 6$. These spectra, which have been termed "highly anisotropic low-spin (HALS)" or "strong g_{max}", have led to some confusion. The $g = 2.4$ features were treated as real by Migita and Iwaizumi [285], obtaining $V/\Delta \approx 0.5$, $\Delta/\lambda \approx 2.5$. Walker et al. [284] regarded the $g = 2.4$ features as artifacts and computed the missing g component assuming $g_x^2 + g_y^2 + g_z^2 = 16$, obtaining $V/\Delta \approx 0.15$, $\Delta/\lambda \approx 6$–8. Strouse and co-workers [286] obtained single-crystal EPR spectra of $[Fe(TPP)(py)_2]ClO_4 \cdot 2THF$ and found $g_{min} = 0.46$; analysis of the data suggested that this component is negative, leading to $V/\Delta = 0.08$, $\Delta/\lambda = 0.17$. The apparent near-degeneracy of the d_{xz} and d_{yz} orbitals is consistent with the crystal structure, which showed that the two pyridine ligands lie in perpendicular planes. Very similar results were obtained for $K[Fe(TPP)(CN)_2] \cdot 2$acetone, and $[Fe(TPP)(CN)(py)] \cdot H_2O$ [286]. EPR and X-ray crystallographic studies of $[Fe(TPP)(2\text{-MeIm})_2]^+$ [287,288] led to similar conclusions. The bulkier 2-MeIm ligand leads to ruffling of the porphyrin ring, which in turn forces the imidazole rings into a perpendicular conformation. Further studies of $[Fe(TPP)L_2]^+$ (L = *cis*-(two forms) and *trans*-methylurocanate) [289], $[Fe(TPP)(Im)_2]^+$ [290], $[Fe(TPP)(N\text{-MeIm})_2]^+$ [291], and pyridine and imidazole adducts of hindered Fe(III) porphyrin complexes [292–294] have confirmed and refined this analysis.

Mashiko et al. [295] have reported spectra of an Fe(III) TPP derivative in which an imidazole ligand is attached via a carbon chain to one of the phenyl groups of TPP. Gunter et al. [296] reported EPR data for complexes of $[Fe(por)]^+$ (por = tetra-(*o*-nicotinamido)phenylporphyrin). Schaeffer et al. [297] have reported EPR spectra for a series of "basket-handle" Fe(III) porphyrin complexes in which a variety of axial ligating groups are attached to the porphyrin.

There have been several reports of alkoxyl, hydroxyl and peroxyl $[Fe(TPP)]^+$ adducts [298–300]. Guilard and co-workers [301] have reported EPR data for a series of alkyl and aryl derivatives, Fe(por)R (por = TPP, OEP, tetra-*m*-tolylporphyrin, tetra-*p*-tolylporphyrin; R = Me, Bu, Ph, p-tolyl); these five-coordinate complexes exhibited either high-spin or mixed-spin states. McKnight et al. [302] have recently reported spectra of $[Fe(por)(tht)_2]^+$ (por = TPP, OEP; tht = tetrahydrothiophene).

A number of N_4X_2 complexes related to the porphyrins have been studied.

Nishida et al. [303] reported a room-temperature powder spectrum of $[Fe(dmg)_2(Im)_2]^+$. Stynes et al. [304] have recently reported spectra of $[Fe(dmgb)X_2]^-$ (X = Cl, Br, NCS), and $[Fe(dmgb)(NCMe)_2]^+$. Kennedy et al. [305] have reported spectra of a variety of Fe(III) phthalocyanine bis-adducts, $[(Ph_2P)_2N][Fe(PC)X_2]$ (X = OH, OPh, NCO, NCS, N_3, CN), which proved to be low-spin. A series of mono-adducts, Fe(PC)X (X = Cl, Br, I, RCO_2, RSO_3) showed mixed-spin states. Taqui Khan et al. [306] have reported spectra of picen, picoph and picdien complexes of Ru(III) with Cl^-, Im, and 2-MeIm as axial ligands.

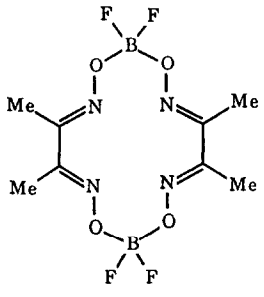

dmgb

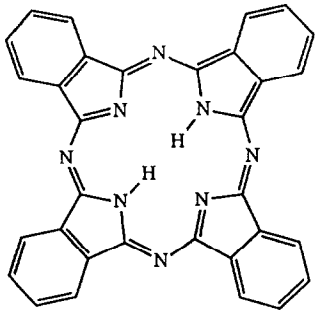

H_2PC

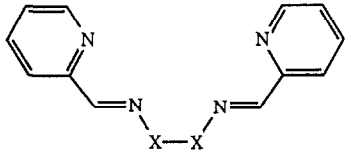

picen: X–X = CH_2CH_2
picoph: X–X = C_6H_4
picdien: X–X = $CH_2CH_2NHCH_2CH_2$

4.5.7 O_6 and S_6 complexes (see Table 23)

An early study by Jarrett [307] of $Fe(acac)_3$ and $Ru(acac)_3$, diluted in a single crystal of $Al(acac)_3$, showed that the iron complex has a high-spin ground state. The *g* matrix for $Ru(acac)_3$ is rhombic, consistent with Jahn–Teller distortion of the expected ^2E ground state (see Sect. 2.1.3). DeSimone [37] has also reported $Ru(acac)_3$ and $[Ru(ox)_3]^{3-}$ in various glasses. The *g* matrix for $Ru(acac)_3$ is somewhat different in the glasses, probably reflecting constraints imposed by the $Al(acac)_3$ crystal. EPR parameters obtained for $[Ru(H_2O)_6]^{3+}$ by Bernhard et al. [308] were re-interpreted by Daul and Goursot [265].

Chakravorty and co-workers have reported spectra of Ru(III) complexes of a number of salicylaldehyde derivatives, Ru(RsalR′)$_3$ (R = H, Me; R′ = H, Me, Et) [309].

Lever and co-workers [310,311] have studied a number of formal Ru(III) complexes with the 3,5-di-*tert*-butylcatecholate ligand (DTBC), potentially able to

TABLE 23
EPR parameters for O_6 and S_6 complexes of Fe, Ru and Os

Complex	Medium	T/K	g_x	g_y	g_z	Ref.
$Ru(acac)_3$	$Al(acac)_3$	80	2.82	1.28	1.74	307
$Fe(sacsac)_3$	Polycrystalline sample	140	2.14	2.09	2.01	327
$Ru(sacsac)_3$	$CHCl_3$/toluene	77	2.109	2.031	1.992	37
$Os(sacsac)_3$	$CHCl_3$/toluene	77	2.138	1.89	1.76	37
$[Fe(mnt)_3]^{3-}$	$(Ph_4P)_4[Fe(mnt)_3]$	90	2.225	2.114	1.986	327
$[Ru(mnt)_3]^{3-}$	Acetone	77	2.120	2.026	1.968	37
$[Os(mnt)_3]^{3-}$	Acetone	77	2.19	2.01	1.82	37
$Ru(Et_2dtc)_3$[a]	Polycrystalline sample	77	2.156	2.109	1.979	37

[a] $A_{\parallel}^{Ru} = 35 \times 10^{-4}\ cm^{-1}$, $A_{\perp}^{Ru} = 21 \times 10^{-4}\ cm^{-1}$.

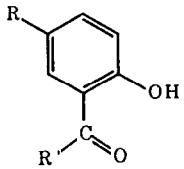

HRsalR'

transfer more electrons, becoming a semiquinone or diketone. In practice, *trans*-$[RuL_2(DTBC)_2]^-$ (L = pyridine or a substituted pyridine) gives a highly anisotropic rhombic g matrix, suggesting that the SOMO is largely metal based. In contrast, $[Ru(bpy)(DTBC)_2]^-$ gives an axial spectrum with substantially smaller g matrix anisotropy, suggesting more delocalization of spin density onto the ligands.

Because of the early recognition of spin equilibria in Fe(III) dithiocarbamate complexes, these systems have attracted a good deal of interest. The first EPR studies were frustrated by the failure to observe the low-spin resonance [312] or confused by an apparent Cu(II) artifact [313]. Hall and Hendrickson [314] conducted a careful study of $Fe(Me_2dtc)_3$ diluted in a polycrystalline sample of the Co(III) analog and found that the high-spin resonances were still observable at 85 K and that the low-spin signal was well resolved and unambiguous only at 12 K. The same complex in a $CHCl_3$ glass gave extremely broad lines from which little information could be extracted. Polycrystalline samples of $Fe[HOCH_2CH_2)_2dtc]_3 \cdot 3H_2O$ apparently have a small energy gap so that the EPR resonances were extremely broad, even at 4 K [315]. Perry et al. [316] found that the high-spin/low-spin energy difference is also small in monothiocarbamate complexes so that there is a significant high-spin population at 12 K; the low-spin features appear as a broad structureless signal near $g = 2$.

A series of papers by Gelerinter and co-workers has focussed on a relatively sharp resonance near $g = 2$ in spectra of Fe(III) dithiocarbamates [317–321] and

thioseleno- and diselenocarbamates [322–325]. Although Hall and Hendrickson [314] suggested that this feature might be artifactual, Gelerinter has shown that it is highly structured with three g components and ^{14}N hyperfine structure. The small g anisotropy and relatively large nitrogen coupling suggest that the feature arises from a conformation best described as an Fe(II) complex with radical cation ligand. Thus, for example, in the complexes $Fe(Se_2CNR_2)_3$ ($NR_2 = NBz_2$, NC_4H_8 (pyrrolidyl), NC_5H_{10} (piperidyl), the g components are approximately 2.02, 2.06 and 2.07, each feature a ca. 14 G triplet.

There has been considerable work on Fe(III) complexes with bidentate sulfur-donor ligands. Powder spectra of $Fe(sacsac)_3$ were reported by two groups [326,327]. This work was repeated by Cotton and Gibson [328], together with spectra of a variety of other Fe(III) complexes with bidentate sulfur-donor and sulfur/oxygen donor ligands: $[Fe(L_2)_3]^{3-}$ ($L_2 = S_2C{=}C(CN)_2$, $S_2C_2O_2$), and $[Fe(L_2)]$ ($L_2 =$ S_2COEt, S_2CSEt, S_2CPh, and $RC(S)CHC(O)R'$; R, R' = Me, Ph). Complexes with the sulfur/oxygen donors showed a high-spin/low-spin equilibrium with the low-spin configuration dominating at low temperatures. Rickards et al. [329] reported an axial spectrum for $Fe(ttd)_2(dtt)$ and a rhombic spectrum for $Fe(ttd)(dtt)_2$, but were unable to detect a spectrum for $Fe(dtt)_3$ (dtt = 4-methyldithiobenzoate; ttd = 4-methyltrithioperbenzoate).

Recently, Mukherjee et al. have reported spectra of a series of dithiophosphinate complexes, $M(S_2PR_2)_3$ (M = Ru, Os; R = 4-methylphenyl, 2,4-dimethylphenyl, 3,4-dimethylphenyl, 2-methyl-5-chlorophenyl, and 3,4-dichlorophenyl [330], and M = Fe, Ru, Os; R = 2,4,5-trimethylphenyl [331]); the Fe complex proved to be high-spin, but the Ru and Os complexes gave very nearly identical g matrices with relatively small anisotropies.

DeSimone [37] measured the spectra of a variety of tris-complexes of Ru and Os with bidentate sulfur-donor ligands: $[Ru(L_2)_3]^{3-}$ ($L_2 = S_2C_2O_2$, mnt), $Ru(L_2)_3$ ($L_2 = Me_2dtc$, Et_2dtc, sacsac, S_2PPh_2), $[Os(mnt)_3]^{3-}$, and $Os(sacsac)_3$. Kirmse et al. [332] found that the spectrum of $[Ru(mnt)_3]^{3-}$ in acetone solution is observable from 4 K to room temperature. For these sulfur-donor tris-chelates, the g matrices are rhombic, but with relatively small anisotropies. Despite the presumed trigonal symmetry, they appear to be comparable with low-symmetry d^5 complexes having a d_{xy} SOMO, and Kirmse's result suggests a long relaxation time and thus a far from degenerate ground state. DeSimone [37] analyzed the g matrices in some detail and, with the ^{101}Ru hyperfine matrix obtained from the spectrum of a ^{101}Ru-enriched sample of $Ru(Et_2dtc)_3$, concluded that the SOMO in the sulfur-donor tris-chelates is indeed d_{xy} and is largely metal-based. The implication of this conclusion is that these complexes are subject to a rather significant distortion from D_3 symmetry, the reasons for which apparently have not been elucidated.

4.5.8 Bidentate and tridentate (N, O, S) complexes

Chakravorty and co-workers [333] have obtained spectra of the fac and mer isomers of $Fe(L)_3$ (HL = 2-nitroso-4-R-phenol; R = Me, ^{t}Bu, Cl, Br). The fac isomers

gave axial spectra whereas spectra of the mer isomers were rhombic. These workers have also reported spectra of Ru(III) and Os(III) complexes of: oximes, *trans*-Ru{RC(O)C(R′)=NOH}{RC(O)C(R′)=NO}X_2 (R = Ph, Me; R′ = H, Me, Ph; X = Cl, Br) [334], thiohydroxamates, *fac*-Ru{RC(S)N(O)R′}$_3$ (R = Ph, benzyl, *p*-anisyl; R′ = Me, H) [335], azopyridines, [Ru(phenyl-2-pyridyldiazene)$_2Cl_2$]$^+$ (three isomers) [336], salicylaldimines, Ru(Rsalal)$_3$ (R = H, Me, OMe, CO_2Et, Cl) [337], 8-quinolinol, Ru(Q)$_3$, Os(Q)$_3$, [Os(Q)$_2X_2$]$^-$ (HQ = 8-quinolinol or 2-methyl-8-quinolinol; X = Cl, Br) [337]; and thiocarbonates, *trans*-[Ru(S_2CSR)$_2$(PPh_3)$_2$]$^+$ (R = Et, i-Pr, CH_2Ph) [338]. The *g* components are rather similar for all complexes. Gupta and Dikshit [339] have reported spectra of Ru(mpq)$_2$LCl (L = DMF, pyridine, and Ru(mpq)(phen)Cl_2).

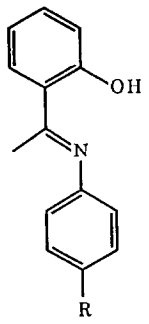

HRsalal

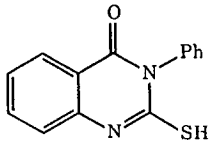

Hmpq

Spectra of several thiosemicarbazone complexes have been reported, including [Fe(salthsa)$_2$]$^-$ (X = X′ = Cl, Br; X = H, X′ = NO_2), which showed high-spin/low-spin equilibria [340–342], [Fe(DMT)$_2$]$^+$ [343], Fe(AT)$_2$]$^+$ (NRR′ = NH_2 [344], NHPh, NMe_2, piperidinyl, 4-methylpiperidinyl [345], NH_2, NMe_2 [346], NEt_2, NPr_2 [347]), and [Fe(pythsa)$_2$]Cl (R = Me, Et, Ph) [348]. In the latter system, abrupt low-spin/high-spin transitions are observed near room temperature.

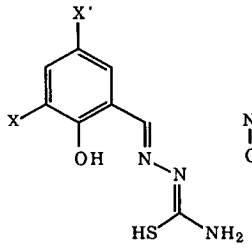

Hsalthsa

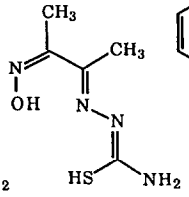

HDMT

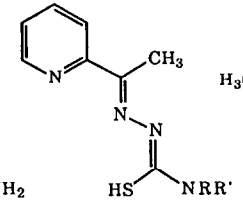

HAT

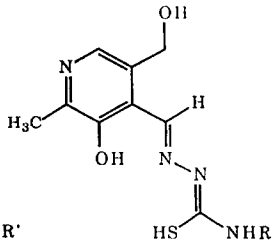

Hpythsa

Mohan et al. have reported spectra of [Fe(3-MeOSPH)$_2$]X ($X^- = Cl^-$, NO_3^-, PF_6^- and BPh_4^-) [349]. Costes et al. [350] have reported spectra of the low-spin/high-spin complex [Fe(AE)$_2$](BPh_4).

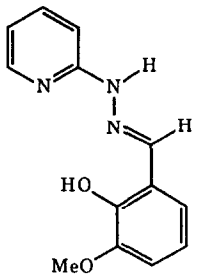

H-3-MeOSPH

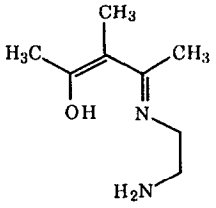

HAE

Hendrickson and co-workers have employed EPR spectra in their studies of low-spin/high-spin equilibria in Fe(III) complexes of several tridentate Schiff base ligands: $[Fe(SalAPA)_2]^+$ [351–353] and $[Fe(R\text{-}SalR'en)_2]^+$ (R = OMe, OEt, allyl; R' = Et, CH_2Ph) [354–357].

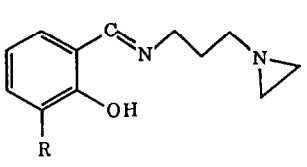

HSalAPA

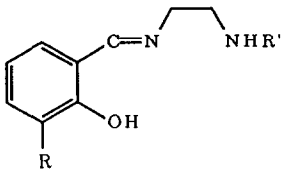

HRSalR'en

Maeda et al. [358,359] have reported spectra of the spin crossover systems $[Fe(acpa)_2]X \cdot H_2O$ and $[Fe(bzpa)_2]X \cdot 2H_2O$ (X = PF_6, NO_3, BPh_4) both as powders and adsorbed on SiO_2 to investigate the effects of dilution on the spin transition.

Chakravorty and co-workers have reported two series of Ru(III) complexes in which a ring carbon is coordinated to the metal: $[Ru(NNS)_2]^+$ and $[Ru(HNNS)(NNS)Cl]^+$ [360]; *trans*-$Ru(NNO)(PPh_3)_2X$ (R = H, Me; R' = H, Me, OMe, Cl, NO_2; X = Cl, Br) [361].

The spectra of a number of salen, vanen, salphen, acen and bzacen Fe(III) complexes have been reported with axial CN and Im ligands [362,363], as well as $[Fe(acen)L_2]^+$ (L = 4-methylpyridine, 2,4-dimethylpyridine and L_2 = 1,3-di(4-pyridyl)propane) [364]. The powder spectra of $[Fe(vanen)(5\text{-}PhIm)_2](BPh_4)$, $[Fe(acen)(N\text{-}MeIm)_2](BPh_4)$ and $[Fe(bzacen)(N\text{-}MeIm)_2](ClO_4)$ show the effects of low-spin/high-spin equilibria which are strongly influenced by the nature of the axial ligands [365,366]. The series has been extended to Fe(salen)(tge)L (tge = ethyl thioglycolate; L = Im, H_2O) [367].

Taqui Khan et al. [306] have reported spectra of a series of salen, salphen and saldien Ru(III) complexes with Cl, CO, Im and 2-MeIm as axial ligands.

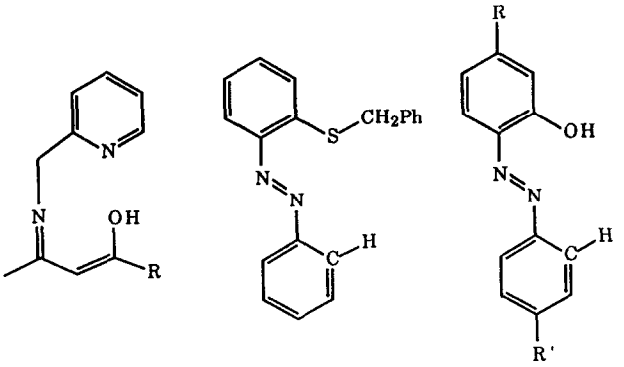

Hacpa, R = Me
Hbzpa, R = Ph

HNNS

H_2NNO

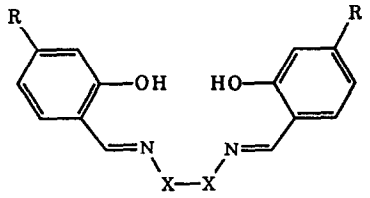

H_2salen, R = H, X–X = CH_2CH_2
H_2vanen, R = OMe, X–X = CH_2CH_2
H_2salphen, R = H, X–X = C_6H_4
H_2saldien, R = H, X–X = $CH_2CH_2NHCH_2CH_2$

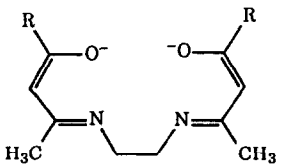

H_2acen, R = H
H_2bzacen, R = Ph

4.5.9 Dithiolene complexes

McCleverty et al. [368] reported isotropic spectra of a series of 5-coordinate Fe(III) 1,2-dithiolene complexes, $[FeL(S_2C_2R_2)_2]^-$ (L = PEt_3, PBu_3, PEt_2Ph, $PEtPh_2$, PPh_3, $P(CH_2CH_2CN)_3$, $P(OPh)_3$, $AsPr_3$, CN^-, N_3^-, NCO^-; R = CN (mnt), CF_3). The spectra of the phosphine and phosphite adducts, which were best resolved, had $\langle g \rangle = 2.044–2.048$, $\langle A^P \rangle = 23–27$. The spectrum of the PEt_3 adduct in CH_2Cl_2/DMF at 100 K gave nearly axial g and ^{31}P hyperfine matrices (2.031, 2.032, 2.060) and (27.8, 23.4, 24.4), but with $g_\parallel$ and $A_\parallel$ corresponding to different orientations. The g matrix is not typical of a low-spin d^5 complex; the anisotropy is relatively small and there is no component less than g_e. There may be significant delocalization of spin onto the dithiolene ligands in these complexes (see further discussion of the Co(IV) analogs in Sect. 4.4.3).

4.5.10 Sandwich complexes (see Table 24)

Early attempts to obtain spectra of ferrocenium ion, $[Fe(Cp)_2]^+$, were unsuccessful, owing to the short relaxation times of this Jahn–Teller species. The first report of the EPR spectrum of an Fe(III) sandwich complex was that of Maki and

TABLE 24
EPR parameters for Fe, Ru and Os sandwich complexes

Complex	Medium	T/K	$g_\perp$	$g_\parallel$	Ref.
$[Fe(B_9C_2H_{11})_2]^-$	$CHCl_3$/DMF	85	1.486	3.944	18, 369
$[Fe(B_9C_2H_9Me_2)_2]^-$	$CHCl_3$/DMF	85	1.654	3.786	18, 369
$CpFe(B_9C_2H_{11})$	$CHCl_3$/DMF	85	1.716	3.579	18, 369
$[(C_6Me_6)Fe(B_4C_2H_4Et_2)]^+$	CH_2Cl_2	77	2.002	2.486	370
$[Fe(Cp)_2]^+$	Acetone	20	1.30	4.36	371
	H_2SO_4	20	1.10	4.35	383
	$[Co(Cp)_2]PF_6$	4	0.917	4.57	383
$[Fe(MeCp)_2]^+$	DMF	20	1.67	3.83	372
$[Fe(Cp^*)_2]^+$	$[Fe(Cp^*)_2]PF_6$ powder	12	1.92	4.002	381
$[Ru(Cp^*)_2]^+$	CH_2Cl_2	4	2.00	2.06	387
$[Os(Cp^*)_2]^+$	CH_2Cl_2	5	1.99	5.27	388
$[Fe(\eta^5\text{-}C_9Me_7)_2]^+$	CH_2Cl_2	4	2.15	2.93	389

Berry [369] for the carborane complexes, $[Fe(\eta^5\text{-}B_9C_2H_9RR')_2]^-$ (R = R' = H, Me; and R = H, R' = Ph), and $CpFe(\eta^5\text{-}B_9C_2H_{11})$. The spectrum of the related complex, $[(\eta^6\text{-}C_6Me_6)Fe(\eta^5\text{-}Et_2C_2B_4H_4)]^+$ has been reported recently by Geiger and co-workers [370].

The first reports of the spectra of $[Fe(Cp)(RCp)]^+$ (R = H, Me, Ph, CH_2OH, CH_2OMe, CH_2NMe_2, HCO, MeCO, PhCO, and $[Fe(RCp)_2]^+$; R = Me, Bu, Ph) by Prins et al. [371–375] were complicated by conflicting reports of spectra [376–378], apparently of impurities, which were assigned to ferrocenium. Several other workers confirmed Prins' results [379–381], but it became apparent that the detailed EPR parameters for ferrocenium derivatives are strongly medium-dependent.

At about this time, Ammeter and Swalen [382] conducted a careful study of the EPR spectrum of cobaltacene, a Jahn–Teller active d^7 complex, and this work led to important insights on the Jahn–Teller distortions of orbitally degenerate metallocenes which were applied by Ammeter [18,383,384] to Fe(III) complexes. Ammeter's 1978 paper remains by far the best survey of the theory and EPR results for orbitally degenerate sandwich complexes.

Other work on ferrocenium ion and derivatives thereof include spectra of a number of methyl-substituted complexes [385] and a study of $[Fe(Cp)_2]^+$ in zeolites [386]. Spectra of $[Ru(Cp^*)_2]^+$ and $[Os(Cp^*)_2]^+$ have been reported by Koelle and Salzer [387] and O'Hare et al. [388], respectively.

It will be recalled (see Sect. 2.1.4) that one of the differences between $\eta^5\text{-}C_5H_5$ and $\eta^6\text{-}C_6H_6$ ligands is the relative energy of the π^* orbitals; the higher energies of those orbitals in Cp complexes is thought to result in less π-back-bonding and the orbital ordering, $d_{z^2} < d_{xy}, d_{x^2-y^2}$. If this is true, one might expect a reversed ordering in η^6-indenyl complexes where the π^* orbitals lie lower in energy. O'Hare et al. [389] have very recently reported the spectrum, observable up to 100 K, of

$[Fe(permethylindenyl)_2]^+$, which appears to have a non-degenerate $^2A_1$ ground state, consistent with photoelectron spectra of the Fe(II) precursor, which suggest an a_1 HOMO.

4.5.11 "Piano-stool" complexes (see Table 25)

Isotropic EPR signals have been assigned to $[CpFe(CO)(COCH_3)L]^+$ (L = PPh_3, CH_3CN) [390], and $[CpFe(CO)L_2]^+$ ($L_2 = C(O)CH_2CH(CH_3)NHBz$) [391], but no details were given. Klingler and Kochi [392] obtained single-line spectra, $\langle g \rangle = 2.059$, for CpFe(CO)(CN)(COR) (R = Me, Ph). Therien and Trogler [393] reported $\langle g \rangle = 2.009$, $A^P = 113$ for $[CpFe(CO)(PPh_3)CH_3]^+$; both parameters seem out of line with those for similar complexes.

Lapinte and co-workers have reported spectra of $[Cp^*Fe(dppe)(CH_2OH)]^+$ [394] and $[Cp^*Fe(dppe)(CH_2OMe)]^+$ [395]; addition of potassium *tert*-butoxide to a THF solution of the latter followed by immediate quenching to 77 K resulted in new EPR features which were assigned to the methoxycarbene complex, Cp*Fe(dppe)CHOMe. In all three cases, the *g* matrices were rhombic although there were only hints of resolution for two smaller components in the spectra of $[Cp^*Fe(dppe)(CH_2OMe)]^+$ ($g_\parallel = 2.48$, $g_\perp \approx 2.03$) and Cp*Fe(dppe)CHOMe ($g_\parallel = 2.40$, $g_\perp \approx 2.08$); the expected ^{31}P hyperfine couplings were not resolved. Astruc and co-workers have reported spectra of the related complexes $[Cp^*Fe(dppe)Me]^+$, $[Cp^*Fe\{P(OMe)_3\}_2Me]^+$ [396] and $[Cp^*Fe(Me_2dtc)L]^+$ (L = CO, MeCN, Me_2CO, CH_2Cl_2) [397]. Connelly et al. [398] have recently obtained frozen solution spectra of $[CpFe(dppm)(C{\equiv}CR)]^+$ (R = COOEt, COOMe, ^{t}Bu, Ph), and $[Cp^*Fe(dppe)(C{\equiv}CR)]^+$ (R = ^{t}Bu, Ph). These spectra were only observable at reduced temperatures and resemble those of $CpCr(CO)_2PR_3$ (see Sect. 4.3.5) with the now-familiar pattern: $g_1 < g_e < g_2 < g_3$. Astruc and co-workers [399] obtained a spectrum which they assigned to the Fe(I) complex $CpFe(PPh_3)_2$, formed in the reaction of CpFe(toluene) with PPh_3 in THF at 253 K. The EPR parameters are so similar ($g_1 = 1.99$, $g_2 = 2.08$, $g_3 = 2.30$, $A_1^P = 20.1$, A_2^P, A_3^P unresolved) to those obtained by Connelly et al. [398] that it is probable that the electronic structures are similar.

Spectra of the related cation radical $[CpFe(2,4\text{-dimethylpentadienyl})]^+$ were reported by Elschenbroich et al. [400]. An isotropic spectrum was seen at 203 K in DME, $\langle g \rangle = 2.1163$, and a rhombic frozen solution spectra at 113 K. The *g* matrix is similar to those for the piano-stool complexes described above. These workers also described spectra for the "open ring" complex $[Fe(2,4\text{-dimethylpentadienyl})_2]^+$, which also showed a single line at 203 K, $\langle g \rangle = 2.0860$, and a rhombic frozen solution spectra at 113 K. Although the two spectra were described as similar and very different from that of $[Cp_2Fe]^+$, the open-ring complex has all three *g* components greater than g_e, suggesting a significantly different ground-state electronic configuration.

The only Ru(III) piano-stool complexes studied to date are $[(C_5Ph_5)Ru(CO)(PEt_3)X]^+$ (X = Br, Me, Et, COMe, CMe=CMe_2), the spectra of

TABLE 25

EPR parameters for "piano-stool" complexes of Fe and Ru

Complex	Medium	T/K	g_x	g_y	g_z	A^{La}	Ref.
$[CpFe(dppm)C{\equiv}CCOOEt]^+$	$CH_2Cl_2/C_2H_4Cl_2$	90	1.990	2.046	2.3621	16(2P)	398
$[CpFe(dppm)C{\equiv}C^tBu]^+$	$CH_2Cl_2/C_2H_4Cl_2$	90	1.994	2.049	2.318	15(2P)	398
$[Cp^*Fe(dppe)C{\equiv}C^tBu]^+$	$CH_2Cl_2/C_2H_4Cl_2$	90	1.980	2.036	2.442	13(2P)	398
$[Cp^*Fe(dppe)CH_3]^+$	PF_6 salt	10	1.99	2.04	2.45		396
$[Cp^*Fe(CO)(Me_2dtc)]^+$	PF_6 salt	10	2.049	2.107	2.239		397
$[CpFe(\eta^5\text{-}C_7H_{11})]^+$	DME	113	2.0020	2.1033	2.2255		400
$[Fe(\eta^5\text{-}C_7H_{11})_2]^+$	DME	113	2.0155	2.0689	2.1822		400
$[(C_5Ph_5)Ru(CO)(PEt_3)Br]^+$	CH_2Cl_2	77	1.992	2.140	2.292	112(Br)	401
$[(C_5Ph_5)Ru(CO)(PEt_3)COMe]^+$	CH_2Cl_2	77	1.992	2.036	2.063		401

[a] In units of 10^{-4} cm^{-1}.

which were reported recently by Connelly and Manners [401]. For X=Br and COMe, the g components are similar to those of the Fe(III) analogs; although no ^{31}P coupling was observed, there was apparent $^{79,81}Br$ splitting of the g_{min} feature. The spectra of the X=Me, Et and CMe=CMe_2 derivatives were inexplicably isotropic.

4.6 *Cobalt(IV), rhodium(IV) and iridium(IV)*

4.6.1 *Halide complexes* (see Table 26)

The EPR spectrum of $IrCl_6^{2-}$ in Na_2PtCl_6 and K_2PtCl_6 was obtained by the Oxford group [264,402,403] in the early days of EPR spectroscopy and has the distinction of being the first spectrum to show ligand hyperfine coupling. These workers also studied $IrCl_6^{2-}$ in crystals of $(NH_4)_2PtCl_6$ [404] and $IrBr_6^{2-}$ in Na_2PtBr_6 [402]. This early work was summarized and the theory discussed by Thornley [40,405]. More recently, spectra have been reported for $IrCl_6^{2-}$ in Cs_2ZrCl_6 and Cs_2HfCl_6 [406] and for $RhCl_6^{2-}$ in Cs_2PtCl_6 [407].

In connection with their study of Ru(III) and Os(III) complexes, Hudson and Kennedy [38] obtained spectra of *cis*-$Ir(PPr_3)_2Cl_4$ and *trans*-$Ir(AsPr_3)_2Cl_4$.

4.6.2 *Aquo and hydroxo complexes*

Sidorov et al. [408] obtained isotropic and frozen solution spectra of $Ba[Rh(OH)_6]$ or RhO_2 in 4 M H_2SO_4 and in concentrated HCl solutions. In further work, the same group [409] obtained a broad-line spectrum in 3.3 M NaOH solution ($g_\parallel = 2.056$, $g_\perp = 2.256$), which was assigned to $[Rh(OH)_6]^{2-}$ and a well-resolved spectrum in 15 M H_2SO_4 ($g_1 = 2.083$, $g_2 = 2.034$, $g_3 = 1.987$) which was attributed to *cis*-$[Rh(H_2O)_4(OH)_2]^{2+}$; spectra at intermediate pH values were assigned to other hydroxo complexes. These authors surveyed the literature on formal Rh(IV) EPR spectra [410] and found that most other examples were better characterized as Rh(III) with radical cation ligands.

TABLE 26

EPR parameters for some Ir(IV) halide complexes[a]

Complex	Medium	T/K	g_1	g_2	g_3	A_1^M	A_2^M	A_3^M	Ref.
$IrCl_6^{2-}$	Na_2PtCl_6	20	2.20	2.07	1.05	25.5	25.5	24	403
$IrBr_6^{2-}$	Na_2PtBr_6	20	2.25	2.21	0.75			25.5	403
cis-$Ir(PPr_3)_2Cl_4$	EPA	100	2.65	2.56	–				38
trans-$Ir(AsPr_3)_2Cl_4$	Crystal	100	2.43	2.43	0.80				38

[a] Hyperfine couplings in units of 10^{-4} cm^{-1}.

4.6.3 Dithiolene complexes

Three groups independently reported spectra of the five-coordinate complexes $CoL(S_2C_2R_2)_2$ ($L=P(OPh)_3$, PPh_3, $AsPh_3$, $SbPh_3$, $R=CF_3$ [411]; $L=P(OPh)_3$, $R=$ Ph [412]; and $L=P(OPh)_3$, PPh_3, PBu_3, $AsPh_3$, $R=Ph$, CF_3 [368,413]). The isotropic parameters ($\langle g\rangle \approx 2.015$, $\langle A^{Co}\rangle \approx 23$, $\langle A^{P}\rangle \approx 7$) suggest a small, but significant cobalt spin density. Only the parallel features were resolved in the anisotropic spectra measured by Balch [411] and Genser [412], but, assuming that the spectra are axial, $A_{\parallel} - \langle A^{Co}\rangle$ leads to estimates of the cobalt spin densities ranging from 0.17 to 0.29, again suggesting substantial delocalization and consistent with the abnormal g matrix found for the Fe(III) analogs [368] (see Sect. 4.5.1). These spectra were assigned to square pyramidal complexes with nominal C_{2v} symmetry. If this were true, the principal axes of the g and A matrices would have to be coincident. However, the spectrum published by Genser shows *nine* apparent parallel features, an anomaly similar to that seen in several Mn(II) spectra (see Sect. 4.4.1). This observation suggests that the g and A^{Co} principal axes are significantly non-coincident and calls the assigned structures into question; there is probably more information to be gained from EPR spectra of these systems. A broad line with no resolved hyperfine structure was reported for the related complex $Co[C_6H_4(NH)_2]_2$ [414].

4.6.4 Organometallic complexes (see Table 27)

Halpern et al. [415] report that oxidation of the Co(III) complexes $Co(dmg)_2(H_2O)R$ ($R=$ Me, Et, ^{n}Pr, ^{i}Pr, Bz, *p*-NO_2Bz, *p*-ClBz, *p*-FBz, *p*-MeBz) gave radical cations which exhibited EPR spectra in frozen aqueous methanol. In subsequent work [416,417], isotropic spectra with resolved ^{59}Co and ^{14}N hyperfine structure were obtained, e.g. for $R=Ph$, $\langle A^{Co}\rangle = 12$, $\langle A^{N}\rangle = 2.3$ (four equivalent nitrogens). Frozen-solution spectra have well-resolved parallel features, but only hints of the perpendicular features. However, computer simulations using perpendicular features computed from $\langle g\rangle$ and $g_{\parallel}$, $\langle A^{Co}\rangle$ and $A_{\parallel}$, gave a good account of the experimental spectra (published spectra showed the expected eight parallel features). Cobalt 3d spin densities, estimated in the usual way, are 0.10 ± 0.01 (except the $R=$ Ph derivative which gave a 3d spin density of 0.08). Spectra of $R=^{13}CH_3$ and CD_3 complexes showed only slight line broadening, thus ruling out significant axial delocalization (possibly excepting the $R=Ph$ complex). The authors argued that the small ^{14}N couplings rule out significant delocalization onto the glyoximate ligands (this argument is open to question) and postulated a SOMO predominantly cobalt $3d_{x^2-y^2}$ in character, but with a significant $4p_z$ contribution. Such a contribution would lead to partial cancellation of terms in the dipolar hyperfine coupling and account for the small observed couplings. A similar conclusion has been reached for cobalt in quite another context [418] and may be reasonable. Marov et al. [419] have reported similar spectra when inorganic Co(III) complexes were oxidized at low temperatures in the presence of dimethylglyoxime and related oximes. Although the axial ligation is unclear in these cases, the similarity of the EPR parameters

TABLE 27

EPR parameters for some organocobalt(IV) complexes[a]

Species	Medium	T/K	g_1	g_2	g_3	A_1^{Co}	A_2^{Co}	A_3^{Co}	Ref.
$[Co(dmg)_2(H_2O)Me]^+$	$MeOH/H_2O$	163	2.026	2.026	2.025	4.8	4.8	29.1	417
$[Co(dmg)_2(H_2O)^iPr]^+$	$MeOH/H_2O$	163	2.030	2.030	2.037	4.0	4.0	34.9	417
$[Co(dmg)_2(H_2O)Ph]^+$	$MeOH/H_2O$	163	2.022	2.022	2.016	5.3	5.3	24.8	417
$[Co(salen)Et]^+$	$MeOH/H_2O$	77	1.998	2.09	2.218	25.2	ca 39	74.6	423
$[Co(acen)Et]^+$	$MeOH/H_2O$	77	2.001	2.08	2.180	24.3	ca 27	82.4	423
$[Cp(PPh_3)CoC_4Ph_4]^+$	$CH_2Cl_2/C_2H_4Cl_2$	77	2.075			55			426

[a]Hyperfine couplings in units of 10^{-4} cm^{-1}.

suggest similar electronic structures. Toscano et al. [420] have recently reported isotropic parameters for the closely related complexes $[Co(4\text{-}CNpy)(dmg)_2R]^+$ (R = Me, Et, ^{n}pr, ^{i}Pr, Bz). Vol'pin and co-workers [421] have reported an isotropic spectrum for the rhodium analog $[Rh(dmg)_2(py)Et]^+$, and also obtained spectra for $[Rh(L_4)(py)Et]^+$ (L_4 = salen, acen and a variety of other Schiff base ligands) [422]. The parameters suggest electronic structures similar to those of the cobalt complexes. These authors have also published a useful review of organocobalt(IV) and organorhodium(IV) chemistry [423].

Anson et al. [424] have reported the spectrum of *trans*-Co(CHBA-DCB)(^{t}Bupy)$_2$ in frozen toluene at 10 K. Only the parallel features were resolved with $g_\parallel = 2.011$, $A_\parallel^{Co} = 15$, but these are similar to those for the dimethylglyoxime complexes discussed above and the electronic structure is probably also similar. A similar series of complexes, $[Co(HPSA)_2]^{2-}$ (R = 5-Cl, 5-NO_2, 4-NO_2), was prepared by electrochemical oxidation of Co(III) precursors by Okawa and co-workers [425]. Isotropic spectra in CH_2Cl_2 solutions gave $\langle g \rangle = 2.00$, $\langle A^{Co} \rangle = 20$, again similar to other Co(IV) spectra.

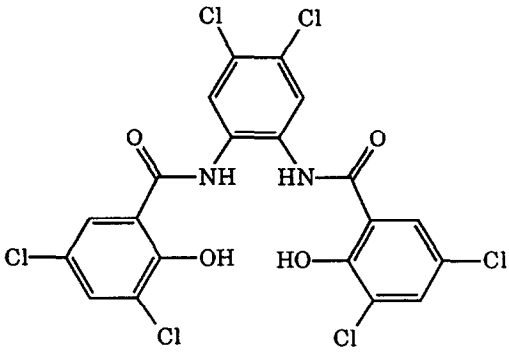

H_4CHBA-DCB

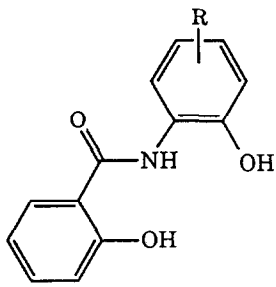

H_3HPSA

Kelly and Geiger [426] have reported a spectrum of the cobaltacyclopentadiene cation $[Cp(PPh_3)CoC_4Ph_4]^+$ in frozen $CH_2Cl_2/C_2H_4Cl_2$. The resolved features at the low-field end of the spectrum correspond to $g = 2.075$, $A^{Co} = 55$, but two more widely spaced features at high field suggest a spectrum complicated by principal axis non-coincidence. The ^{59}Co couplings are rather larger than seen for the other organocobalt(IV) complexes, possibly because of less cancellation of the dipolar contributions of cobalt 4p admixtures in the SOMO.

REFERENCES

1 B.A. Goodman and J.B. Raynor, Adv. Inorg. Chem. Radiochem., 13 (1970) 136.
2 J.E. Wertz and J.R. Bolton, Electron Spin Resonance, McGraw-Hill, New York, 1972.
3 N.M. Atherton, Electron Spin Resonance, Ellis Horwood, Chichester, 1973.

4 A. Bencini and D. Gatteschi, in G.A. Melson and B.A. Figgis (Eds.), Transition Metal Chemistry, Vol. 8, Marcel Dekker, New York, 1982, p. 1.
5 P.H. Rieger, in M. Chanon, M. Julliard and J.C. Poite (Eds.), Paramagnetic Organometallic Species in Activation/Selectivity, Catalysis, NATO ASI series. Series C, Mathematical and Physical Sciences, Vol. 257, Kluwer, Dordrecht, 1989, p. 375.
6 P.H. Rieger, in W.C. Trogler (Ed.), Organometallic Radical Processes, (J. Organomet. Chem. Library, Vol. 22), Elsevier, Amsterdam, 1990, p. 270.
7 Electron Spin Resonance, The Royal Society of Chemistry, London, 1973.
8 M.C. Baird, Chem. Rev., 88 (1988) 1217.
9 N.G. Connelly and W.E. Geiger, Adv. Organomet. Chem., 23 (1984) 1.
10 T.D. Smith and J.R. Pilbrow, Biol. Magn. Reson., 2 (1980) 85.
11 E.C. Constable, Adv. Inorg. Chem., 34 (1989) 1.
12 E. König, Z. Naturforsch. Teil A, 19 (1964) 1139.
13 R.E. DeSimone and R.S. Drago, J. Am. Chem. Soc., 92 (1970) 2343.
14 F.H. Burstall and R.S. Nyholm, J. Chem. Soc., (1952) 3570.
15 I. Hanazaki and S. Nagakura, Bull. Chem. Soc. Jpn., 44 (1971) 2312.
16 S. Fortier, M.C. Baird, K.F. Preston, J.R. Morton, T. Ziegler, T.J. Jaeger, W.C. Watkins, J.H. MacNeil, K.A. Watson, K. Hensel, Y. Le Page, J.-P. Charland and A.J. Williams, J. Am. Chem. Soc., 113 (1991) 542.
17 K.D. Warren, Struct. Bonding (Berlin), 27 (1976) 45.
18 J.H. Ammeter, J. Magn. Res., 30 (1978) 299.
19 M.-M. Coutière, J. Demuynck and A. Veillard, Theor. Chim. Acta, 27 (1972) 281.
20 J. Weber, A. Goursot and E. Penigault, J. Mol. Struct., 60 (1980) 397.
21 J.K. Burdett, Molecular Shapes, Wiley, New York, 1980, p. 64.
22 A. Ceulemans and L.G. Vanquickenborne, Struct. Bonding., 71 (1989) 125.
23 V. Černý, Chem. Phys., 46 (1980) 205.
24 H.H. Tippens, Phys. Rev., 160 (1967) 343.
25 J.E. Wertz and J.R. Bolton, Electron Spin Resonance, McGraw-Hill, New York, 1972, p. 279.
26 M.B.D. Bloom, J.B. Raynor and M.C.R. Symons, J. Chem. Soc. A, (1971) 3209.
27 B.M. Peake, P.H. Rieger, B.H. Robinson and J. Simpson, J. Am. Chem. Soc., 102 (1980) 156.
28 N.M. Atherton, Electron Spin Resonance, Ellis Horwood, Chichester, 1973, pp. 239–244.
29 B.R. McGarvey, J. Phys. Chem., 71 (1967) 51.
30 J.S. Griffith, The Theory of Transition-Metal Ions, Cambridge University Press, Cambridge, 1961, pp. 345–347, 362.
31 B.R. McGarvey, in R.L. Carlin (Ed.), Transition Metal Chemistry, Vol. 3, Marcel Dekker, New York, 1966, p. 90.
32 J.E. Wertz and J.R. Bolton, Electron Spin Resonance, McGraw-Hill, New York, 1972, pp. 314–324.
33 B. Bleaney and M.C.M. O'Brien, Proc. Phys. Soc. London Sect. B, 69 (1956) 1216.
34 J.S. Griffith, The Theory of Transition-Metal Ions, Cambridge University Press, Cambridge, 1961, pp. 363–365.
35 C.P.S. Taylor, Biochim. Biophys. Acta, 491 (1977) 137.
36 T.L. Bohan, J. Magn. Reson., 26 (1977) 109.
37 R.E. DeSimone, J. Am. Chem. Soc., 95 (1973) 6238.
38 A. Hudson and M.J. Kennedy, J. Chem. Soc. A, (1969) 1116.
39 J.M. Baker, B. Bleaney and K.D. Bowers, Proc. Phys. Soc. London Sect. B, 69 (1956) 1205.
40 J.M.H. Thornley, J. Phys., 1 (1968) 1024.

41 J.S. Griffith, Mol. Phys., 21 (1971) 135.
42 S.A. Cotton, Inorg. Nucl. Chem. Lett., 8 (1972) 371.
43 C. Froese, J. Chem. Phys., 45 (1966) 1417.
44 J.R. Morton and K.F. Preston, J. Magn. Reson., 30 (1977) 577.
45 F. Herman and S. Skillman, Atomic Structure Calculations, Prentice-Hall, Englewood Cliffs, NJ, 1963.
46 A.K. Koh and D.J. Miller, At. Data Nucl. Data Tables, 33 (1985) 235.
47 E. Clementi and C. Roetti, At. Data Nucl. Data Tables, 14 (1974) 177.
48 A.D. McLean and R.S. McLean, At. Data Nucl. Data Tables, 26 (1981) 197.
49 J.J. Fortman and R.G. Hayes, J. Chem. Phys., 43 (1965) 15.
50 J.A. Bandy, A. Berry, M.L.H. Green, R.N. Perutz, K. Prout and J.-N. Verpeaux, J. Chem. Soc. Chem. Commun., (1984) 729.
51 D.W. Pratt and R.J. Myers, J. Am. Chem. Soc., 89 (1967) 6470.
52 K.A. Rubinson, J. Am. Chem. Soc., 98 (1976) 5188.
53 M.P. Boyer, Y. LePage, J.R. Morton, K.F. Preston and M.J. Vuolle, Can. J. Spectrosc., 26 (1981) 181.
54 J.H. Ammeter, L. Zoller, J. Bachmann, P. Baltzer, E. Gamp, R. Bucher and E. Deiss, Helv. Chim. Acta, 64 (1981) 1063.
55 S.W. Bratt, A. Kassyk, R.N. Perutz and M.C.R. Symons, J. Am. Chem. Soc., 104 (1982) 490.
56 J.M. McCall, J.R. Morton and K.F. Preston, Organometallics, 4 (1985) 1272.
57 S. Bellard, K.A. Rubinson and G.M. Sheldrick, Acta Crystallogr. Sect. B, 35 (1979) 271.
58 J.M. McCall, J.R. Morton and K.F. Preston, J. Magn. Res., 64 (1985) 414.
59 J.R. Morton and K.F. Preston, Organometallics, 3 (1984) 1386.
60 R.J. Van Zee, S.B.H. Bach and W. Weltner, Jr., J. Phys. Chem., 90 (1986) 583.
61 B. Elschner and S. Herzog, Arch. Sci. (Geneva), 11 (1958) 100.
62 A. Davison, N. Edelstein, R.H. Holm and A.H. Maki, Inorg. Chem., 4 (1965) 55.
63 E. Wulf and S. Herzog, Z. Anorg. Allg. Chem., 387 (1972) 81.
64 P.T. Manoharan, S. Vijaya, J.R. Shock and M.T. Rogers, J. Chem. Phys., 63 (1975) 2507.
65 K.H. Hausser, Naturwissenshaften, 48 (1961) 426; Z. Naturforsch., Teil A, 16 (1961) 1190.
66 A. Schweiger, R. Wolf, H.H. Günthard, J.H. Ammeter and E. Deiss, Chem. Phys. Lett., 71 (1980) 117.
67 C. Elschenbroich, J. Hurley, B. Metz, W. Massa and G. Baum, Organometallics, 9 (1990) 889.
68 M.P. Andrews, S.M. Mattar and G.A. Ozin, J. Phys. Chem., 90 (1986) 1037.
69 G. Henrici-Olivé and S. Olivé, Z. Phys. Chem. (Frankfurt), 56 (1967) 223.
70 G. Henrici-Olivé and S. Olivé, J. Am. Chem. Soc., 92 (1970) 4831.
71 M.F. Rettig, C.D. Stout, A. Klug and P. Farnham, J. Am. Chem. Soc., 92 (1970) 5100.
72 J.L. Thomas and R.G. Hayes, Inorg. Chem., 11 (1972) 348.
73 C. Elschenbroich, M. Nowotny, B. Metz, W. Massa, J. Graulich, K. Biehler and W. Sauer, Angew. Chem. Int. Ed. Engl., 30 (1991) 547.
74 C. Elschenbroich and J. Heck, Angew. Chem. Int. Ed. Engl., 20 (1981) 267.
75 J. Hulliger and P. Baltzer, Solid State Commun., 60 (1968) 71.
76 G.A. Ozin, S. Mattar, M.P. Andrews, H.X. Huber and D.R. McIntosh, J. Am. Chem. Soc., 105 (1983) 6170.
77 M.P. Andrews, S.M. Mattar and G.A. Ozin, J. Phys. Chem., 90 (1986) 744.
78 F.G.N. Cloke, A.N. Dix, J.C. Green, R.N. Perutz and E.A. Seddon, Organometallics, 2 (1983) 1150.
79 S.A. Fairhurst, J.R. Morton and K.F. Preston, Chem. Phys. Lett., 104, (1984) 112.
80 C.J. Pickett and D. Pletcher, J. Chem. Soc. Dalton Trans., (1975) 879.

81 R.N. Bagchi, A.M. Bond, R. Colton, D.L. Luscombe and J.E. Moir, J. Am. Chem. Soc., 108 (1986) 3352.
82 R.N. Bagchi, A.M. Bond, G. Brain, R. Colton, T.L.E. Henderson and J.E. Kevekordes, Organometallics, 3 (1984) 4.
83 A.M. Bond, S.W. Carr and R. Colton, Inorg. Chem., 23 (1984) 2343.
84 R.N. Bagchi, A.M. Bond and R. Colton, J. Electroanal. Chem., 199 (1986) 297.
85 A.M. Bond, R. Colton, J.E. Kevekordes and P. Panagiotidou, Inorg. Chem., 26 (1987) 1430.
86 A.M. Bond, R. Colton and J.J. Jackowski, Inorg. Chem., 14 (1975) 2526.
87 R.N. Bagchi, A.M. Bond, R. Colton, I. Creece, K. McGregor and T. Whyte, Organometallics, 10 (1991) 2611.
88 J.A. Connor, P.I. Riley and C.J. Rix, J. Chem. Soc. Dalton Trans., (1977) 1317.
89 J.A. Connor and P.I. Riley, J. Chem. Soc. Dalton Trans., (1979) 1231.
90 K.A. Conner and R.A. Walton, Inorg. Chem., 25 (1986) 4422.
91 M.F. Lappert, R.W. McCabe, J.J. MacQuitty, P.L. Pye and P.I. Riley, J. Chem. Soc. Dalton Trans., (1980) 90.
92 D.W. DuBois, R.T. Iwamoto and J. Kleinberg, Inorg. Nucl. Chem. Lett., 6 (1970) 53.
93 T. Saji and S. Aoyagui, Bull. Chem. Soc. Jpn., 46 (1973) 2101.
94 I. Bernal and S.E. Harrison, J. Chem. Phys., 34 (1961) 102; 38 (1963) 2581. See also R.G. Hayes, J. Chem. Phys., 38 (1963) 2580.
95 J.B. Spencer and R.J. Myers, J. Am. Chem. Soc., 86 (1964) 522.
96 K. Heuer, R. Neubert and H.D. Sonneck, Exp. Tech. Phys., 13 (1965) 231.
97 H.A. Kuska and M.T. Rogers, J. Chem. Phys., 40 (1964) 910; 42 (1965) 3034.
98 B.A. Goodman, J.B. Raynor and M.C.R. Symons, J. Chem. Soc. A, (1966) 994.
99 B.R. McGarvey and J. Pearlman, J. Chem. Phys., 46 (1967) 4992.
100 V. Kalis, V.V. Orlov and V.I. Ermakov, Zh. Strukt. Khim., 15 (1974) 701.
101 V.V. Orlov, V. Kalis and V.I. Ermakov, Zh. Strukt. Khim., 16 (1975) 132.
102 R.G. Hayes, J. Chem. Phys., 47 (1967) 1692.
103 S. Sarkar and A. Müller, Z. Naturforsch. Teil B, 33 (1978) 1053.
104 P.T. Manoharan and H.B. Gray, Inorg. Chem., 5 (1966) 823.
105 I. Bernal, S.D. Robinson, L.S. Meriwether and G. Wilkinson, J. Chem. Soc. Chem. Commun., (1965) 571.
106 L.S. Meriwether, S.D. Robinson and G. Wilkinson, J. Chem. Soc. A, (1966) 1488.
107 J. Danon, H. Panepucci and A.A. Misetich, J. Chem. Phys., 44 (1966) 4154.
108 P.T. Manoharan, H.A. Kuska and M.T. Rogers, J. Am. Chem. Soc., 89 (1967) 4564.
109 H. Kobeyashi, I. Tsujikawa, M. Mori and Y. Yamamoto, Bull. Chem. Soc. Jpn., 42 (1969) 709.
110 B.A. Goodman, J.B. Raynor and M.C.R. Symons, J. Chem. Soc. A, (1968) 1973.
111 J. Burgess, B.A. Goodman and J.B. Raynor, J. Chem. Soc. A, (1968) 501.
112 N.S. Garif'yanov and S.A. Luchkina, Izv. Akad. Nauk SSSR Ser. Khim., (1970) 455.
113 P. Legzdins and C.R. Nurse, Inorg. Chem., 24 (1985) 327.
114 N.M. Atherton, G. Denti, M. Ghedini and C. Oliva, J. Magn. Reson., 43 (1981) 167.
115 N.M. Atherton and C. Oliva, J. Chem. Soc. Faraday Trans. 2, 79 (1983) 167.
116 G.V.R. Chandramouli, C.W. Schläpfer and A. von Zelewsky, Magn. Reson. Chem., 29 (1991) S16.
117 M.K. Lloyd and J.A. McCleverty, J. Organomet. Chem., 61 (1973) 261.
118 R.C. Maurya and D.D. Mishra, Transition Met. Chem., 12 (1987) 551.
119 R.C. Maurya and D.D. Mishra, Synth. React. Inorg. Met. Org. Chem., 20 (1990) 1013.
120 A. Keller and B. Jezowska-Trzebiatowska, Inorg. Chim. Acta, 51 (1981) 123.
121 S.A. Luchkina and T.P. Tokareva, Zh. Neorg. Khim., 17 (1972) 2456.

122 S.A. Luchkina and A.A. Egorova, J. Mol. Struct., 19 (1973) 607; Zh. Neorg. Khim., 19 (1974) 1288.
123 S. Clamp, N.G. Connelly, G.E. Taylor and T.S. Louttit, J. Chem. Soc. Dalton Trans., (1980) 2162.
124 S. Sarkar and A. Müller, Angew. Chem. Intl. Ed. Engl., 16 (1977) 468.
125 D.E. Wigley and R.A. Walton, Inorg. Chem., 22 (1983) 3138.
126 N.S. Garif'yanov and S.A. Luchkina, Dokl., Akad. Nauk SSSR, 189 (1969) 543; Teor. Eksp. Khim., 5 (1969) 571.
127 N.S. Garif'yanov and O.I. Kondrat'eva, Teor. Eksp. Khim., 7 (1971) 258.
128 N.S. Garif'yanov, A.D. Troitskaya, A.I. Razumov, I.V. Ovchinnikov, P.A. Guvevich and O.I. Kondrat'eva, Zh. Neorg. Khim., 17 (1972) 1346.
129 E.V. Semenov, P.M. Solozhenkin, N.I. Zemlyanskii, O.N. Grishina and Ya.I. Mel'nik, Dokl. Akad. Nauk Tadzh. SSR, 15 (1972) 37.
130 A.I. Chuikova, A.D. Troitskaya, N.S. Akhmetov, A.E. Ivantsov, O.I. Kondrat'eva, I.V. Ovchinnikov, Zh. Obshch. Khim., 51 (1981) 1243.
131 N.S. Garif'yanov, A.D. Troitskaya, A.I. Razumov, P.A. Gurevich and O.I. Kondrat'eva, Zh. Obshch. Khim., 41 (1971) 710.
132 O.I. Kondrat'eva, A.D. Troitskaya, N.A. Chadaeva, G.M. Usacheva, A.I. Chuikova and A.E. Ivantsov, Zh. Obshch. Khim., 43 (1973) 2087.
133 N.S. Garif'yanov, A.D. Troitskaya, A.I. Razumov, I.V. Ovchinnikov, P.A. Gurevich and O.I. Kondrat'eva, Dokl. Akad. Nauk SSSR, 196 (1971) 1346.
134 A.I. Chuikova, K.I. Kuz'min, A.D. Troitskaya, I.V. Ovchinnikov and O.I. Kondrat'eva, Zh. Obshch. Khim., 47 (1977) 1886.
135 N. Al Obaidi, A.J. Edwards, C.J. Jones, J.A. McCleverty, B.D. Neaves, F.E. Mabbs and D. Collison, J. Chem. Soc. Dalton Trans., (1989) 127.
136 R.D. Feltham, P. Sogo and M. Calvin, J. Chem. Phys., 26 (1957) 1354.
137 N.N. Bubnov and V.M. Chibrikin, Zh. Fiz. Khim., 33 (1959) 1891.
138 S.I. Vetchinkin, S.P. Solodovnikov and V.M. Chibrikin, Opt. Spectrosc. (USSR), 8 (1960) 71.
139 R.D. Feltham, J. Inorg. Nucl. Chem., 16 (1961) 197.
140 K.H. Hausser, Z. Naturforsch. Teil A, 14 (1959) 425; Naturwissenshaften, 48 (1961) 666.
141 R. Prins and F.J. Reinders, Chem. Phys. Lett., 3 (1969) 45.
142 B.G. Gribov, B.I. Kozyrkin, A.D. Krivospitskii and G.R. Chirkin, Dokl. Akad. Nauk SSSR, 193 (1970) 91.
143 C. Elschenbroich and F. Gerson, J. Organomet. Chem., 49 (1973) 445.
144 S.E. Anderson, Jr. and R.S. Drago, J. Am. Chem. Soc., 92 (1970) 4344.
145 A.D. Krivospitskii and G.K. Chirkin, Zh. Strukt. Khim., 15 (1974) 25.
146 R. Wolf, A. Schweiger and H.H. Günthard, Mol. Phys., 53 (1984) 567, 585.
147 S.E. Anderson and R.S. Drago, J. Am. Chem. Soc., 91 (1969) 3656; Inorg. Chem., 11 (1972) 1564.
148 W. Karthe and W. Kleinwächter, Ann. Phys. (Leipzig), 21 (1968) 137.
149 B.G. Gribov, B.I. Kozyrkin, A.D. Krivospitskii and G.R. Chirkin, Dokl. Akad. Nauk SSSR, 193 (1970) 91.
150 C. Elschenbroich, E. Bilger and R. Möckel, Z. Naturforsch. Teil B, 38 (1983) 1357.
151 C. Elschenbroich, R. Möckel and E. Bilger, Z. Naturforsch. Teil B, 39 (1984) 375.
152 W. Karthe and W. Kleinwächter, Z. Phys. Chem. (Leipzig), 247 (1971) 241.
153 C. Elschenbroich, R. Möckel, U. Zenneck and D.W. Clark, Ber. Bunsenges. Phys. Chem., 83 (1979) 1008.
154 N. Ito, T. Sagi, K. Suga and S. Aoyauui, J. Organomet. Chem., 229 (1982) 43.

155 T.T.-T. Li, W. Kung, D.L. Ward, B. McCulloch and C.H. Brubaker, Jr., Organometallics, 1 (1982) 1229.
156 C. Elschenbroich and J. Koch, J. Organomet. Chem., 229 (1982) 139.
157 C. Elschenbroich, J. Koch, J. Kroker, M. Wünsch, W. Massa, G. Baum and G. Stork, Chem. Ber., 121 (1988) 1983.
158 C. Elschenbroich, J. Kroker, W. Massa, M. Wünsch and A.J. Ashe, III, Angew. Chem. Intl. Ed. Engl., 25 (1986) 571.
159 C.H. Elschenbroich, F. Gerson and F. Stohler, J. Am. Chem. Soc., 95 (1973) 6956.
160 C. Elschenbroich, J. Schneider, W. Massa, G. Baum and H. Mellinghoff, J. Organomet. Chem., 355 (1988) 163.
161 C. Elschenbroich, R. Möckel and U. Zenneck, Angew Chem. Intl. Ed. Engl., 17 (1978) 531.
162 C. Elschenbroich, J. Koch, J. Schneider, B. Spangenberg and P. Schiess, J. Organomet. Chem., 317 (1986) 41.
163 C. Elschenbroich, J. Hurley, W. Massa and G. Baum, Angew. Chem. Intl. Ed. Engl., 27 (1988) 684.
164 C. Elschenbroich, J. Schneider, H. Prinzbach and W.-D. Fessner, Organometallics, 5 (1986) 2091.
165 C. Elschenbroich and F. Stohler, Angew. Chem. Intl. Ed. Engl., 14 (1975) 174.
166 H. Burdorf and C. Elschenbroich, Z. Naturforsch. Teil B, 36 (1981) 94.
167 C. Elschenbroich, G. Heikenfeld, M. Wünsch, W. Massa and G. Baum, Angew, Chem. Intl. Ed. Engl., 27 (1988) 414.
168 C. Elschenbroich and J. Heck, Angew. Chem. Intl. Ed. Engl., 16 (1977) 479; J. Am. Chem. Soc., 101 (1979) 6773.
169 W.H. Morrison and D.N. Hendrickson, Inorg. Chem., 14 (1975) 2331.
170 H.F. Keller, Z. Naturforsch. Teil B, 23 (1968) 133.
171 T. Madach and H. Vahrenkamp, Z. Naturforsch. Teil B, 33 (1978) 1301; 34 (1979) 573.
172 P.J. Krusic, private communication, 1992.
173 P.J. Krusic, S.J. McLain, J.R. Morton, K.F. Preston and Y. LePage, J. Magn. Reson., 74 (1987) 72.
174 J.R. Morton, K.F. Preston, N.A. Cooley, M.C. Baird, P.J. Krusic and S.J. McLain, J. Chem. Soc. Faraday Trans. 1, 83 (1987) 3535.
175 N.A. Cooley, M.C. Baird, J.R. Morton, K.F. Preston and Y. LePage, J. Magn. Reson., 76 (1988) 325.
176 R.J. Hoobler, M.A. Hutton, M.M. Dillard, M.P. Castellani, A.L. Rheingold, A.L. Rieger, P.H. Rieger, T.C. Richards and W.E. Geiger, Organometallics, 12 (1993) 116.
177 N.G. Connelly and Z. Demidowicz, J. Organomet. Chem., 73 (1974) C31.
178 M.P. Castellani, N.G. Connelly, A.L. Rieger and P.H. Rieger, to be published.
179 N. Van Order, Jr., W.E. Geiger, T.E. Bitterwold and A.L. Rheingold, J. Am. Chem. Soc., 109 (1987) 5680.
180 N.G. Connelly and G.A. Johnson, J. Organomet. Chem., 77 (1974) 341.
181 N.G. Connelly, A.G. Orpen, A.L. Rieger, P.H. Rieger, C.J. Scott and G. Rosair, J. Chem. Soc. Chem. Commun., (1992) 1293.
182 T. Beissel, B.S.P.C. Della Vedova, K. Wieghardt and R. Boese, Inorg. Chem., 29 (1990) 1736.
183 K.-B. Shiu, M.D. Curtis and J.C. Huffman, Organometallics, 2 (1983) 936.
184 M.D. Curtis, K.-B. Shiu, W.M. Butler and J.C. Huffman, J. Am. Chem. Soc., 108 (1986) 3335.
185 J.H. MacNeil, W.C. Watkins, M.C. Baird and K.F. Preston, Organometallics, 11 (1992) 2761.

186 M.L.H. Green and R.B.A. Pardy, Polyhedron, 4 (1985) 1035.
187 J.S. Adams, C. Bitcon, J.R. Brown, D. Collison, M. Cunningham and M.W. Whiteley, J. Chem. Soc. Dalton Trans., (1987) 3049.
188 C. Bitcon, R. Breeze, P.F. Miller and M.W. Whiteley, J. Organomet. Chem., 364 (1989) 181.
189 M.C.R. Symons, S.W. Bratt, and J.L. Wyatt, J. Chem. Soc. Dalton Trans., (1983) 1377.
190 M. Fei, S.K. Sur and D.R. Tyler, Organometallics, 10 (1991) 419.
191 P. Fantucci, R. Naldini, F. Cariati, V. Valenti and C. Bussetto, J. Organomet. Chem., 64 (1974) 109.
192 R.M. Neilson and S. Wherland, Inorg. Chem., 24 (1985) 3458.
193 A.M. Bond, R. Colton and M.J. McCormick, Inorg. Chem., 16 (1977) 155.
194 M.R. Snow and M.H.B. Stiddard, J. Chem. Soc. A, (1966) 777.
195 D.J. Cookson, T.D. Smith, J.F. Boas and J.R. Pilbrow, J. Chem. Soc. Dalton Trans., (1976) 1791.
196 C.G. Howard, G.S. Girolami, G. Wilkinson, M. Thornton-Pett and M.B. Hursthouse, J. Chem. Soc. Dalton Trans., (1983) 2631.
197 G.S. Girolami, G. Wilkinson, A.M.R. Galas, M. Thornton-Pett and M.B. Hursthouse, J. Chem. Soc. Dalton Trans., (1985) 1339.
198 G.A. Carriedo, V. Riera, N.G. Connelly and S.J. Raven, J. Chem. Soc. Dalton Trans., (1987) 1769.
199 G.A. Carriedo, N.G. Connelly, S. Garcia-Granda, A.G. Orpen, A.L. Rieger, P.H. Rieger, V. Riera and G.M. Rosair, J. Chem. Soc. Dalton Trans., in press.
200 G.A. Abakumov, V.K. Cherkasov, K.G. Shalnova, I.A. Teplova and G.A. Razuvaev, J. Organomet. Chem., 236 (1982) 333.
201 W.E. Lindsell and P.N. Preston, J. Chem. Soc. Dalton Trans., (1979) 1105.
202 D.A.C. McNeil, J.B. Raynor and M.C.R. Symons, Proc. Chem. Soc., (1964) 364; J. Chem. Soc., (1965) 410.
203 P.T. Manoharan and H.B. Gray, J. Chem. Soc. Chem. Commun., (1965) 324.
204 B.B. Wayland and L.W. Olson, Inorg. Chim. Acta, 11 (1974) L23.
205 N.S. Garif'yanov and S.A. Luchkina, Izv. Akad. Nauk SSSR Ser. Khim., (1969) 471.
206 A. Jezierski, J. Mol. Struct., 115 (1984) 11.
207 A. Becalska and R.H. Hill, J. Chem. Soc. Chem. Commun., (1989) 1626.
208 G.C. Yang, M.W. Heitzmann, L.A. Ford and W.R. Benson, Inorg. Chem., 21 (1982) 3242.
209 J. Baldas, J.F. Boas, J. Bonnyman and G.A. Williams, J. Chem. Soc. Dalton Trans., (1984) 827.
210 R. Kirmse, B. Lorenz and K. Schmidt, Polyhedron, 2 (1983) 935.
211 G. Mercati, F. Morazzoni, F. Cariati and D. Giusto, Inorg. Chim. Acta, 29 (1978) 165.
212 G. Wilkinson, F.A. Cotton and J.M. Birmingham, J. Inorg. Nucl. Chem., 2 (1956) 95.
213 J. Voitländer and E. Schimitschek, Z. Elektrochem., 61 (1957) 941.
214 R. Krieger and J. Voitländer, Z. Naturforsch. Teil A, 27 (1972) 1082.
215 S. Evans, M.L.H. Green, B. Jewitt, G.H. King and A.F. Orchard, J. Chem. Soc. Faraday Trans. 2, 70 (1974) 356.
216 J.H. Ammeter, R. Bucher and N. Oswald, J. Am. Chem. Soc., 96 (1974) 7833.
217 M.E. Switzer, R. Wang, M.F. Rettig and A.H. Maki, J. Am. Chem. Soc., 96 (1974) 7669.
218 J.C. Smart and J.L. Robbins, J. Am. Chem. Soc., 100 (1978) 3936.
219 J.L. Robbins, N.M. Edelstein, S.R. Cooper and J.C. Smart, J. Am. Chem. Soc., 101 (1979) 3853.
220 D.K. Freyberg, J.L. Robbins, K.N. Raymond and J.C. Smart, J. Am. Chem. Soc., 101 (1979) 892.
221 D. Cozak, J. Demers and G. Gauvin, Can. J. Chem., 64 (1986) 71.

222 N. Hebendanz, G.H. Köhler, G. Müller and J. Riede, J. Am. Chem. Soc., 108 (1986) 3281.
223 F.H. Köhler and B. Schlesinger, Inorg. Chem., 31 (1992) 2853.
224 J.A. Bandy, F.G.N. Cloke, G. Cooper, J.P. Day, R.B. Girling, R.G. Graham, J.C. Green, R. Grinter and R.N. Perutz, J. Am. Chem. Soc., 110 (1988) 5039.
225 N.G. Connelly and M.D. Kitchen, J. Chem. Soc. Dalton Trans., (1977) 931.
226 N.G. Connelly, M.J. Freeman, A.G. Orpen, A.R. Sheehan, J.B. Sheridan and D.A. Sweigart, J. Chem. Soc. Dalton Trans., (1985) 1019.
227 R.D. Pike, A.L. Rieger and P.H. Rieger, J. Chem. Soc. Faraday Trans. 2, 85 (1989) 3913.
228 A. Winter, G. Huttner, L. Zsolnai, P. Kronick and M. Gottlieb, Angew. Chem. Intl. Ed. Engl., 23 (1984) 975.
229 D. Sellmann, J. Müller and P. Hofmann, Angew. Chem. Intl. Ed. Engl., 21 (1982) 691.
230 D. Sellmann and J. Müller, J. Organomet. Chem., 281 (1985) 249.
231 R. Gross and W. Kaim, Angew. Chem. Intl. Ed. Engl., 24 (1985) 856.
232 R. Gross and W. Kaim, Inorg. Chem., 26 (1987) 3596; J. Chem. Soc. Faraday Trans. 1, 83 (1987) 3549.
233 E. König, in E.A. Koerner von Gustorf, F.-W. Grebels and I. Fischler (Eds.), The Organic Chemistry of Iron, Vol. 1, Academic Press, New York, 1978, p. 257.
234 R.L. Martin and A.H. White, in R.L. Carlin (Ed.), Transition Metal Chemistry, Vol. 4, Dekker, New York, 1968, p. 113.
235 G. Harris, Theor. Chim. Acta, 10 (1968) 119, 155.
236 D. Coucouvanis, Prog. Inorg. Chem., 26 (1979) 301.
237 D.N. Hendrickson, M.S. Haddad, W.D. Federer and M.W. Lynch, Coord. Chem., 21 (1980) 75.
238 M. Bacci, Coord. Chem. Rev., 86 (1988) 245.
239 J.D. Walker and R. Poli, Inorg. Chem., 228 (1989) 1793.
240 N.J. Hill, J. Chem. Soc. Faraday Trans. 2, (1972) 427.
241 S. Kremer, Inorg. Chim. Acta, 85 (1984) 57.
242 U.C. Sarma, K.P. Sarma and R.K. Poddar, Polyhedron, 7 (1988) 1727.
243 P.T. Manoharan, P.K. Mehrotra, M.M. Taqui Khan and R.K. Andal, Inorg. Chem., 12 (1973) 2753.
244 A. Araneo, G. Mercati, F. Morazzoni and T. Napoletano, Inorg. Chem., 16 (1977) 1196.
245 G. Mercati and F. Morazzoni, Gazz. Chim. Ital., 109 (1979) 161.
246 D. Gussoni, G. Mercati and F. Morazzoni, Gazz. Chim. Ital., 109 (1979) 545.
247 O.K. Mehdi and U. Agarwala, Inorg. Chem., 19 (1980) 1381.
248 O.K. Mehdi and U. Agarwala, J. Inorg. Nucl. Chem., 42 (1980) 1413.
249 R.M. Catalá, D. Cruz-Garritz, P. Sosa, P. Terreros, H. Torrens, A. Hills, D.L. Hughes and R.L. Richards, J. Organomet. Chem., 359 (1989) 219.
250 (a) J.A. Kohn and W.D. Townes, Acta Crystallogr., 14 (1961) 617.
(b) E.C. Reynhardt and J.C.A. Boeyens, Acta. Crystallogr. Sect. B, 28 (1972) 524.
(c) J.-P. Willems, M.P.J.W. Clephas and E. de Boer, J. Chem. Soc. Faraday Trans., submitted for publication.
251 (a) H.C. Box, K.T. Lilga and E.E. Budzinski, J. Chem. Phys., 66 (1977) 2135.
(b) D.M. Wang, S.M. Meijers and E. de Boer, Mol. Phys., 70 (1990) 1135.
R. Kirmse, R. Böttcher, J.P. Willems, E.J. Reijerse and E. de Boer, J. Chem. Soc. Faraday Trans., 87 (1991) 3105.
252 C. Ezzeh and B.R. McGarvey, J. Magn. Reson., 15 (1974) 183.
253 Y. Kuroda, M. Goto and T. Sakai, Bull. Chem. Soc. Jpn., 62 (1989) 3614.
254 P.B. Merrithew, C.C. Lo and A.J. Modestino, Inorg. Chem., 14 (1975) 242.
255 W. Reiff and R.E. DeSimone, Inorg. Chem., 12 (1973) 1793.

256 A. Juris, V. Balzani, F. Barigelletti, S. Campagna, P. Belser and A. Von Zelewsky, Coord. Chem. Rev., 84 (1988) 85.
257 T.J. Meyer, Acc. Chem. Res., 22 (1989) 163; Pure Appl. Chem., 62 (1990) 1003.
258 W.H. Quayle and J.H. Lunsford, Inorg. Chem., 21 (1982) 97.
259 J. Baker, L.M. Englehardt, B.N. Figgis and A.H. White, J. Chem. Soc. Dalton Trans., (1975) 530.
260 E.M. Kober and T.J. Meyer, Inorg. Chem., 22 (1983) 1614; Inorg. Chem., 23 (1984) 3877.
261 W.M. Reiff, J. Am. Chem. Soc., 96 (1974) 3829.
262 W. Lau, J.C. Huffman and J.K. Kochi, Organometallics, 1 (1982) 155.
263 D.E. Morris, Y. Ohsawa, D.P. Segers, M.K. DeArmond and K.W. Hauck, Inorg. Chem., 23 (1984) 3010.
264 J.H.E. Griffiths, J. Owen and I.M. Ward, Proc. R. Soc. London Ser. A, 219 (1953) 526.
265 C. Daul and A. Goursot, Inorg. Chem., 24 (1985) 3554.
266 D. Kaplan and G. Novon, J. Phys. Chem., 78 (1974) 700.
267 S. Sakaki, N. Hagiwara, Y. Yanase and A. Ohyoshi, J. Phys. Chem., 82 (1978) 1917.
268 S. Sakaki, Y. Yanase, N. Hagiwara, T. Takeshita, H. Naganuma, A. Ohyoshi and K. Ohkubo, J. Phys. Chem., 86 (1982) 1038.
269 N.M.S. de Rezende, S. de C. Martins, L.A. Marinho, J.A. Viana dos Santos, M. Tabak, J.R. Perussi and D.W. Franco, Inorg. Chim. Acta, 182 (1991) 87.
270 A. Desideri, J.B. Raynor and C.-K. Poon, J. Chem. Soc. Dalton Trans., (1977) 2051.
271 J.B. Raynor and B.G. Jeliazkowa, J. Chem. Soc. Dalton Trans., (1982) 1185.
272 J.A. Stanko, H.J. Peresie, R.A. Bernheim, R. Wang and P.S. Wang, Inorg. Chem., 12 (1973) 634.
273 P.V. Bernhardt, P. Comba, T.W. Hambly and G.A. Lawrence, Inorg. Chem., 30 (1991) 942.
274 H. Stratemeier, M.A. Hitchman, P. Comba, P.V. Bernhardt and M.J. Riley, Inorg. Chem., 30 (1991) 4088.
275 W.E. Blumberg and J. Peisach, Adv. Chem. Ser., 100 (1971) 271.
276 J. Peisach, W.E. Blumberg and A. Adler, Ann. N.Y. Acad. Sci., 206 (1973) 310.
277 M. Weissbluth, Struct. Bonding (Berlin), 2 (1967) 1.
278 M. Weissbluth, Hemoglobin, Springer-Verlag, New York, 1974, p. 99.
279 M.P. Bryn and C.E. Strouse, J. Am. Chem. Soc., 103 (1981) 2633.
280 M.P. Byrn, B.A. Katz, N.L. Keder, K.R. Levan, C.J. Magurany, K.M. Miller, J.W. Pritt and C.E. Strouse, J. Am. Chem. Soc., 105 (1983) 4916.
281 S.C. Tang, S. Koch, G.C. Papaefthymiou, S. Foner, R.B. Frankel, J.A. Ibers and R.H. Holm, J. Am. Chem. Soc., 98 (1976) 2414.
282 E.W. Ainscough, A.W. Addison, D. Dolphin and B.R. James, J. Am. Chem. Soc., 100 (1978) 7585.
283 R. Quinn, M. Nappa and J.S. Valentine, J. Am. Chem. Soc., 104 (1982) 2588.
284 F.A. Walker, D. Reis and V.L. Balke, J. Am. Chem. Soc., 106 (1984) 6888.
285 C.T. Migita and M. Iwaizumi, J. Am. Chem. Soc., 103 (1981) 4378.
286 D. Inniss, S.M. Soltis and C.E. Strouse, J. Am. Chem. Soc., 110 (1988) 5644.
287 F.A. Walker, B.H. Huynh, W.R. Scheidt and S.R. Osvath, J. Am. Chem. Soc., 108 (1986) 5288.
288 W.R. Scheidt, J.F. Kirner, J.L. Hoard and C.A. Reed, J. Am. Chem. Soc., 109 (1987) 1963.
289 R. Quinn, J.S. Valentine, M.P. Byrn and C.E. Strouse, J. Am. Chem. Soc., 109 (1987) 3301.
290 S.M. Soltis and C.E. Strouse, J. Am. Chem. Soc., 110 (1988) 2824.
291 T.B. Higgins, M.K. Safo and W.R. Scheidt, Inorg. Chim. Acta, 178 (1990) 261.
292 H. Nasri, Y. Wang, B.H. Huynh, F.A. Walker and W.R. Scheidt, Inorg. Chem., 30 (1991) 1483.

293 K. Hatano, M.K. Safo, F.A. Walker and W.R. Scheidt, Inorg. Chem., 30 (1991) 1643.
294 M.K. Safo, G.P. Gupta, F.A. Walker and W.R. Scheidt, J. Am. Chem. Soc., 113 (1991) 5497.
295 T. Mashiko, C.A. Reed, K.J. Haller, M.E. Kastner and W.R. Scheidt, J. Am. Chem. Soc., 103 (1981) 5758.
296 M.J. Gunter, G.M. McLaughlin, K.J. Berry, K.S. Murray, M. Irving and P.E. Clark, Inorg. Chem., 23 (1984) 283.
297 C. Schaeffer, M. Momenteau, J. Mispelter, B. Loock, C. Huel and J.-M. Lhoste, Inorg. Chem., 25 (1986) 4577.
298 T. Otsuka, T. Ohya and M. Sato, Inorg. Chem., 24 (1985) 776.
299 N. Kobayashi, Inorg. Chem., 24 (1985) 3324.
300 K. Tajima, J. Jinno, K. Ishizu, H. Sakurai and H. Ohya-Nishiguchi, Inorg. Chem., 28 (1989) 709.
301 A. Tabard, P. Cocolios, G. Lagrange, R. Gerardin, J. Hubsch, C. Lecomte, J. Zarembowitch and R. Guilard, Inorg. Chem., 27 (1988) 110.
302 J. McKnight, M.R. Cheesman, C.A. Reed, R.D. Orosz and A.J. Thompson, J. Chem. Soc. Dalton Trans., (1991) 1887.
303 Y. Nishida, S. Oshio and S. Kida, Inorg. Chim. Acta, 23 (1978) 59.
304 D.V. Stynes, H. Noglik and D.W. Thompson, Inorg. Chem., 30 (1991) 4567.
305 D.J. Kennedy, K.S. Murray, P.R. Zwack, H. Homberg and W. Katz, Inorg. Chem., 25 (1986) 2539.
306 M.M. Taqui Khan, D. Srinivas, R.I. Kureshy and N.H. Khan, Inorg. Chem., 29 (1990) 2320.
307 H.S. Jarrett, J. Chem. Phys., 27 (1957) 1298.
308 P. Bernhard, A. Stebler and A. Ludi, Inorg. Chem., 23 (1984) 2151.
309 N. Bag, G.K. Lahiri, S. Bhattacharya, L.R. Falvello and A. Chakravorty, Inorg. Chem., 27 (1988) 4396.
310 A.B.P. Lever, P.R. Auburn, E.S. Dodsworth, M. Haga, W. Liu, M. Melnik and W.A. Nevin, J. Am. Chem. Soc., 110 (1988) 8076.
311 P.R. Auburn, E.S. Dodsworth, M. Haga, W. Lei, W.A. Nevin and A.B.P. Lever, Inorg. Chem., 30 (1991) 3502.
312 N.S. Garif'yanov, S.E. Kamenev, B.M. Kozyrev and I.V. Ovchinnikov, Dokl. Akad. Nauk SSSR, 177 (1967) 880.
313 R. Rickards, C.E. Johnson and H.A.O. Hill, J. Chem. Phys., 53 (1970) 3118.
314 G.R. Hall and D.N. Hendrickson, Inorg. Chem., 15 (1976) 607.
315 K.B. Pandeya and R. Singh, Inorg. Chim. Acta, 147 (1988) 5.
316 D.L. Perry, L.J. Wilson, K.R. Kunze, L. Maleki, P. Deplano and E.F. Trogu, J. Chem. Soc. Dalton Trans., (1981) 1294.
317 C. Flick and E. Gelerinter, Chem. Phys. Lett., 23 (1973) 422.
318 C. Flick, E. Gelerinter, J.B. Zimmerman and N.V. Duffy, Inorg. Chem., 15 (1976) 2945.
319 D.P. Rininger, N.V. Duffy, R.C. Weir, E. Gelerinter, J. Stanford and D.L. Uhrich, Chem. Phys. Lett., 52 (1977) 102.
320 E. Gelerinter, M.E. Stefanov, T.E. Lockhart, D.P. Rininger and N.V. Duffy, J. Inorg. Nucl. Chem., 42 (1980) 1137.
321 N.V. Duffy, T.E. Lockhart, E. Gelerinter, D. Todoroff and D.L. Uhrich, Inorg. Nucl. Chem. Lett., 17 (1981) 1.
322 W. Dietzsch, E. Gelerinter and N.V. Duffy, Inorg. Chim. Acta, 145 (1988) 13.
323 W. Dietzsch, N.V. Duffy, E. Gelerinter and E. Sinn, Inorg. Chem., 28 (1989) 3079.
324 E. Gelerinter, N.V. Duffy, W. Dietzsch, T. Thanyasiri and E. Sinn, Inorg. Chim. Acta, 177 (1990) 185.
325 E. Gelerinter, N.V. Duffy, S.S. Yarish, W. Dietzsch and R. Kirmse, Chem. Phys. Lett., 184 (1991) 375.

326 K. Knauer, P. Hemmerich, J.D.W. van Voorst, Angew. Chem. Intl. Ed. Engl., 6 (1967) 262.
327 R. Beckett, G.A. Heath, B.F. Hoskins, B.P. Kelly, R.L. Martin, I.A.G. Roos and P.L. Weickhardt, Inorg. Nucl. Chem. Lett., 6 (1970) 257.
328 S.A. Cotton and J.F. Gibson, J. Chem. Soc. A, (1971) 803.
329 R. Rickards, C.E. Johnson and H.A.O. Hill, J. Chem. Soc. A, (1971) 1755.
330 R.N. Mukherjee, S. Shankar, V.V. Vijaya and P.K. Gogoi, Polyhedron, 4 (1985) 1717.
331 R.N. Mukherjee and B.B.S. Shastri, Indian J. Chem., 29A (1990) 809.
332 R. Kirmse, W. Dietzsch and E. Hoyer, Inorg. Nucl. Chem. Lett., 10 (1974) 819.
333 P. Basu, S.B. Choudhury, S. Pal and A. Chakravorty, Inorg. Chem., 28 (1989) 2680.
334 A.R. Chakravarty and A. Chakravorty, Inorg. Chem., 20 (1981) 275; J. Chem. Soc. Dalton Trans., (1982) 615.
335 S. Bhattacharya, P. Ghosh and A. Chakravorty, Inorg. Chem., 24 (1985) 3224.
336 G.K. Lahiri, S. Bhattacharya, S. Goswami and A. Chakravorty, J. Chem. Soc. Dalton Trans., (1990) 561.
337 G.K. Lahiri, S. Bhattacharya, B.K. Ghosh and A. Chakravorty, Inorg. Chem., 26 (1987) 4324.
338 A. Pramanik, N. Bag, G.K. Lahiri and A. Chakravorty, J. Chem. Soc. Dalton Trans., (1990) 3823.
339 H.K. Gupta and S.K. Dikshit, Polyhedron, 6 (1987) 1009.
340 V.V. Zelentsov, G.M. Larin, E.V. Ivanov, N.V. Gerbeleu and A.V. Ablov, Teor. Eksp. Khim., 7 (1971) 798.
341 A.V. Ablov, V.V. Zelentsov, V.I. Shipilov, N.V. Gerbeleu and Ch. V. Dyatlova, Dokl. Akad. Nauk SSSR, 222 (1975) 1115.
342 A.V. Ablov, V.V. Zelentsov, V.I. Shipilov, N.V. Gerbeleu and Ch. V. Dyatlova, Koord. Khim., 2 (1976) 170.
343 R. Raina and T.S. Srivastava, Indian J. Chem., 21A (1982) 490.
344 R. Raina and T.S. Srivastava, Indian J. Chem., 22A (1983) 701.
345 B.S. Garg, M.R.P. Kurup, S.K. Jain and Y.K. Bhoon, Transition Met. Chem., 13 (1988) 247.
346 D.X. West, P.M. Ahrweiler, G. Ertein, J.P. Scovill, D.L. Klayman, J.L. Flippen-Anderson, R. Gilardi, C. George and L.K. Pannell, Transition Met. Chem., 10 (1985) 264.
347 D.X. West, C.S. Carlson and A.E. Liberta, Transition Met. Chem., 16 (1991) 53.
348 N.S. Gupta, M. Mohan, N.K. Jha and W.E. Antholine, Inorg. Chim. Acta, 184 (1991) 13.
349 M. Mohan, N.S. Gupta, L. Chandra, N.K. Jha and R.S. Prasad, Inorg. Chim. Acta, 141 (1988) 185.
350 J.P. Costes, F. Dahan and J.-P. Laurent, Inorg. Chem., 29 (1990) 2448.
351 W.D. Federer and D.N. Hendrickson, Inorg. Chem., 23 (1984) 3870.
352 M.D. Timken, A.M. Abdel-Mawgoud and D.N. Hendrickson, Inorg. Chem., 25 (1986) 160.
353 M.D. Timken, C.E. Strouse, S.M. Soltis, S. Daverio, D.N. Hendrickson, A.M. Abdel-Mawgoud and S.R. Wilson, J. Am. Chem. Soc., 108 (1986) 395.
354 M.S. Haddad, W.D. Federer, M.W. Lynch and D.N. Hendrickson, J. Am. Chem. Soc., 102 (1980) 1468.
355 M.S. Haddad, M.W. Lynch, W.D. Federer and D.N. Hendrickson, Inorg. Chem., 20 (1981) 123.
356 M.S. Haddad, W.D. Federer, M.W. Lynch and D.N. Hendrickson, Inorg. Chem., 20 (1981) 131.
357 M.D. Timken, D.N. Henrickson and E. Sinn, Inorg. Chem., 24 (1985) 3947.
358 Y. Maeda, N. Tsutsumi and Y. Takashima, Inorg. Chem., 23 (1984) 2440.
359 Y. Maeda, M. Tomokiyo, K. Kitazaki and Y. Takeshima, Bull. Chem. Soc. Jpn., 61 (1988) 1953.

360 A.K. Mahapatra, S. Datta, S. Goswami, M. Mukherjee, A.K. Mukherjee and A. Chakravorty, Inorg. Chem., 25 (1986) 1715.
361 G.K. Lahiri, S. Bhattacharya, M. Mukherjee, A.K. Mukherjee and A. Chakravorty, Inorg. Chem., 26 (1987) 3359.
362 Y. Nishida, S. Oshio and S. Kida, Bull. Chem. Soc. Jpn., 50 (1977) 119.
363 Y. Nishida, S. Oshio, S. Kida and Y. Maeda, Inorg. Chim. Acta, 26 (1978) 207.
364 H. Ohshio, Y. Maeda and Y. Takashima, Inorg. Chem., 22 (1983) 2684.
365 B.J. Kennedy, G. Brain, E. Horn, K.S. Murray and M.R. Snow, Inorg. Chem., 24 (1985) 1647.
366 B.J. Kennedy, A.C. McGrath, K.S. Murray, B.W. Skelton and A.H. White, Inorg. Chem., 26 (1987) 483.
367 H. Sakurai, K. Tsuchiya and K. Migita, Inorg. Chem., 27 (1988) 3877.
368 J.A. McCleverty, N.M. Atherton, N.G. Connelly and C.J. Winscom, J. Chem. Soc. A, (1969) 2242.
369 A.H. Maki and T.E. Berry, J. Am. Chem. Soc., 87 (1965) 4437.
370 J.W. Merkert, W.E. Geiger, M.D. Attwood and R.N. Grimes, Organometallics, 10 (1991) 3545.
371 R. Prins and F.J. Reinders, J. Am. Chem. Soc., 91 (1969) 4929.
372 R. Prins, Mol. Phys., 19 (1970) 603.
373 R. Prins and A.R. Korswagen, J. Organomet. Chem., 25 (1970) C74.
374 R. Prins and A.G.T.G. Kortbeek, J. Organomet. Chem., 33 (1971) C33.
375 R. Prins, A.R. Korswagen and A.G.T.G. Kortbeek, J. Organomet. Chem., 39 (1972) 335.
376 E. Saito, J. Chem. Phys., 50 (1969) 3539.
377 A. Horsfield and A. Wasserman, J. Chem. Soc. A, (1970) 3202.
378 A. Horsfield and A. Wasserman, J. Chem. Soc. Dalton Trans., (1972) 187.
379 O. Cowan, G.A. Candela and F. Kaufman, J. Am. Chem. Soc., 93 (1971) 3889.
380 M.D. Rowe and A.J. McCaffery, J. Chem. Phys., 59 (1973) 3786.
381 D.M. Duggan and D.N. Hendrickson, Inorg. Chem., 14 (1975) 955.
382 J.H. Ammeter and J.D. Swalen, J. Chem. Phys., 57 (1972) 678.
383 J.H. Ammeter, N. Oswald and R. Bucher, Helv. Chim. Acta, 58 (1975) 671.
384 J.H. Ammeter, Nouv. J. Chim., 4 (1980) 631; Chimia, 35 (1981) 61.
385 R.B. Materikova, V.N. Babin, S.P. Solodovnikov, I. Lyatifov, P.V. Petrovsky and E.I. Fedin, Z. Naturforsch. Teil B, 35 (1980) 1415.
386 G.A. Ozin and J. Godber, J. Phys. Chem., 93 (1989) 878.
387 U. Koelle and A. Salzer, J. Organomet. Chem., 243 (1983) C27.
388 D. O'Hare, T.P. Chadwick, J.C. Green and J.S. Miller, Organometallics, 7 (1988) 1335.
389 D. O'Hare, J.C. Green, T. Marder, S. Collins, G. Stringer, A.K. Kakkar, N. Kaltsoyannis, A. Kuhn, R. Lewis, C. Mehnert, P. Scott, M. Kurmoo and S. Pugh, Organometallics, 11 (1992) 48.
390 R.H. Magnuson, S. Zulu, W.-M. T'sai and W.P. Giering, J. Am. Chem. Soc., 102 (1980) 6887.
391 S. Javaheri and W.P. Giering, Organometallics, 3 (1984) 1927.
392 R.J. Klingler and J.K. Kochi, J. Organomet. Chem., 202 (1980) 49.
393 M.J. Therien and W.C. Trogler, J. Am. Chem. Soc., 109 (1987) 5127.
394 V. Guerchais and C. Lapinte, J. Chem. Soc. Chem. Commun., (1986) 663.
395 C. Roger, L. Toupet and C. Lapinte, J. Chem. Soc. Chem. Commun., (1988) 713.
396 J. Morrow, D. Catheline, M.-H. Desbois, J.-M. Manriquez, J. Ruiz and D. Astruc, Organometallics, 6 (1987) 2605.
397 M.-H. Desbois and D. Astruc, Angew. Chem. Intl. Ed. Engl., 28 (1989) 460.

398 N.G. Connelly, M.P. Gamasa, J. Gimeno, C. Lapinte, E. Lastra, J. Maher, N. Le Narvor, A.L. Rieger and P.H. Rieger, J. Chem. Soc. Dalton Trans., in press.
399 J. Ruiz, M. Lacoste and D. Astruc. J. Am. Chem. Soc., 112 (1990) 5471.
400 C. Elschenbroich, E. Bilger, R.D. Ernst, D.R. Wilson and M.S. Kralik, Organometallics, 4 (1985) 2068.
401 N.G. Connelly and I. Manners, J. Chem. Soc. Dalton Trans., (1989) 283.
402 J. Owen and K.W.H. Stevens, Nature (London), 171 (1953) 836.
403 J.W.E. Griffiths and J. Owen, Proc. R. Soc. London Ser. A, 226 (1954) 96.
404 E. Cipollini, J. Owen, J.H.M. Thornley and C. Windsor, Proc. Phys. Soc., 79 (1962) 1083.
405 J. Owen and J.H.M. Thornley, Rep. Prog. Phys., 29 (1966) 675.
406 S. Maniv and A. Gabay, J. Magn. Reson., 13 (1974) 148.
407 A.D. Westland, Can. J. Chem., 46 (1968) 3591.
408 A.A. Sidorov, P.N. Komozin, I.V. Miroshnichenko, V.N. Pichkov, N.M. Sinitsyn and V.P. Babaeva, Zh. Neorg. Khim., 29 (1984) 1261.
409 A.A. Sidorov, N.N. Komozin, V.N. Pichkov, I.V. Miroshnichenko, K.A. Golovin and N.M. Sinitsyn, Zh. Neorg. Khim., 30 (1985) 2595.
410 I.V. Miroshnichenko, A.A. Sidorov, P.N. Komozin, V.N. Pichkov and N.M. Sinitsyn, Zh. Neorg. Khim., 31 (1986) 2883.
411 A.L. Balch, Inorg. Chem., 6 (1967) 2158.
412 E.E. Genser, Inorg. Chem., 7 (1968) 13.
413 N.G. Connelly, J.A. McCleverty and C.J. Winscom, Nature, 216 (1967) 999; J. Chem. Soc. A, (1969) 2242.
414 A.L. Balch and R.H. Holm, J. Am. Chem. Soc., 88 (1966) 5201.
415 J. Halpern, M.S. Chan, J. Hanson, T.S. Roche and J. Topich, J. Am. Chem. Soc., 97 (1975) 1606.
416 J. Halpern, J. Topich and K.I. Zamaraev, Inorg. Chim. Acta, 20 (1976) L21.
417 J. Topich and J. Halpern, Inorg. Chem., 18 (1979) 1339.
418 N.G. Connelly, W.E. Geiger, G.A. Lane, S.J. Raven and P.H. Rieger, J. Am. Chem. Soc., 108 (1986) 6219.
419 I.N. Marov, A.T. Panfilov, A.V. Vershinin and E.K. Ivanova, Zh. Neorg. Khim., 22 (1977) 1607.
420 P.J. Toscano, E. Barren and A.L. Seligson, Organometallics, 8 (1989) 2085.
421 A.T. Nikitaev, A.L. Sigan, I. Ya. Levitin, A.A. Belyi and M.E. Vol'pin, Inorg. Chim. Acta, 1982 (64) L29.
422 G.A. Nikitaeva, A.T. Nikitaev, K.I. Zamaraev, A.L. Sigan, I. Ya. Levitin and M.E. Vol'pin, Zh. Strukt. Khim., 19 (1978) 282.
423 M.E. Vol'pin, I. Ya. Levitin, A.L. Sigan and A.T. Nikitaev, J. Organomet. Chem., 279 (1985) 263.
424 F.C. Anson, T.J. Collins, R.J. Coots, S.L. Gipson and T.G. Richmond, J. Am. Chem. Soc., 106 (1984) 5037.
425 M. Koikawa, M. Gotoh, H. Okawa and S. Kida, J. Chem. Soc. Dalton Trans., (1989) 1613.
426 R.S. Kelly and W.E. Geiger, Organometallics, 6 (1987) 1432.